Uncertainty Analysis of Phytoplankton Dynamics in Coastal Waters

Proefschrift

ter verkrijging van de graad van doctor

aan de Technische Universiteit Delft,

op gezag van de Rector Magnificus prof. ir. K. C. A. M. Luyben,

voorzitter van het College voor Promoties,

in het openbaar te verdedigen op woensdag 25 November 2015 om 12.30 uur

door

Lixia Niu

Master of Science in Hydrology and Water Resources Engineering

Hohai University, China

geboren te Puyang, China

This dissertation has been approved by the
promotors: Prof. drs. ir. J.K. Vrijling
Prof. dr. ir. P.H.A.J.M. van Gelder

Composition of the doctoral committee:

Rector Magnificus	voorzitter
Prof. drs. ir. J.K. Vrijling	Technische Universiteit Delft, promotor
Prof. dr. ir. P.H.A.J.M. van Gelder	Technische Universiteit Delft, promotor
Independent members:	
Prof. dr. ir. Z.B. Wang	Technische Universiteit Delft
Prof. ir. T. Vellinga	Technische Universiteit Delft
Dr. Y.Q. Guan	Hohai University
Dr. F.J. Los	Deltares
Dr. F. Heinis	Heinis Waterbeheer en Ecologie
Substitute member:	
Prof. dr. D.P. Solomatine	Technische Universiteit Delft/UNESCO-IHE Institute for Water Education, reservelid

This work was financially supported by the China Scholarship Council (CSC).

Printed by Ipskamp Drukkers

ISBN 978-94-6259-955-0

Author email: l.niu@tudelft.nl; xiaoxia3623@gmail.com

Summary

There is an increasing concern about the interactions between phytoplankton and coastal ecosystems, especially on the negative effects from coastal eutrophication and phytoplankton blooms. As the key indicator of the coastal ecosystem, phytoplankton plays an important role in the whole impact-effect chain. Primary production by phytoplankton forms the basic link in the food-chain. A lot of effort has been paid to the investigation of phytoplankton dynamics on the basis of literature surveys, field observations, and model predictions, providing a better understanding of the coastal ecosystem. In this thesis, the significance of phytoplankton is stressed and no discussion is given to zooplankton.

Phytoplankton dynamics (i.e. growth, loss, grazing, biomass, bloom) is closely related to environmental variables, such as light intensity, temperature, nutrients, suspended matter, wind profiles, and tidal currents. In chapter 2, factor analysis is developed to characterize the contributions of the environmental variables to the phytoplankton biomass (in terms of chlorophyll a), determined by the 10-year's historical record from 2000 through 2009 in the case study of the Frisian Inlet.

In this thesis we focus on three elements of phytoplankton dynamics: phytoplankton growth, phytoplankton biomass, and phytoplankton blooms. Based on the specific properties of the case zones, the Frisian Inlet and the Jiangsu coast, different focuses are taken. Field measurement of phytoplankton dynamics is expensive, thus we use mathematical models as the useful and convenient tool to perform the investigation. The BLOOM II model and the phytoplankton model are introduced to investigate the annual variation of the phytoplankton biomass in coastal waters (chapter 3, chapter 4, and chapter 5). The reliability of the parameter estimation largely determines the confidence of the model output. The estimate function of the phytoplankton growth rate is controlled by the variables of temperature, light intensity and nutrients, separately or comprehensively. The phytoplankton needs light to grow through the photosynthesis process, whereas the light intensity is attenuated due to the absorption by chlorophyll a, salinity, organic matter, turbid water, and background extinction. Phytoplankton consumes nutrients, in turn, phytoplankton releases nutrients back to the water bodies through its death and the subsequent decay. In this research the growth rate is estimated with the effects of light intensity and ambient water temperature. The loss rate and the grazing rate are simplified as constants in the models, but actually are varied with the environmental variables.

Moreover, the role of the vertical mixing process on the phytoplankton is significant, controlling the vertical distributions of the phytoplankton biomass and affecting the availability of light intensity and nutrients. Although a vertical phytoplankton model is discussed in chapter 4 and chapter 5, reducing the three-dimensional model to a one-dimensional model, the vertical mixing rate involved in both cases is processed with the Delft3D model. In this context, the estimation of the vertical mixing rate increases the applicability of the phytoplankton model. Chapter 4 discusses the effect of the vertical turbulent diffusivity on the variation of the phytoplankton biomass, driven by the physical and chemical conditions. Chapter 5 performs a similar study of the vertical mixing rate as described in chapter 4, but now only driven by the physical condition, as well as one driver (vertical stability threshold) of the occurrence of the phytoplankton blooms.

The model prediction is always accompanied with the simplification, overestimating or underestimating the actual status, named as *original value* $\pm$ *uncertainty*. Thus, uncertainty analysis is required to be integrated with the model output. The uncertainty arising from the model output is focused, only a short discussion is given to the uncertainty arising from the input. The Bootstrap method and the Bayesian Markov Chain Monte Carlo simulation are approached to give insight in the model prediction with a characterization of uncertainty analysis.

Samenvatting

Er is toenemende bezorgdheid over de interactie van het fytoplankton en het ecosysteem van de kust, met name met betrekking tot de negatieve effecten van eutrofiëring van de kustwateren en de algenbloei van fytoplankton. Als de belangrijkste indicator van het kust-ecosysteem, speelt de fytoplankton een belangrijke rol in de hele oorzaak-effectketen. De primaire productie van fytoplankton vormt de basis in de voedselketen. Veel aandacht is besteed aan het onderzoek van de dynamiek van fytoplankton in de literatuur, veldwaarnemingen en modelvoorspellingen, om tot een beter begrip van het kust-ecosysteem te komen. In dit proefschrift wordt de betekenis van het fytoplankton in de voedselketen benadrukt; zoöplankton wordt in dit proefschrift verder niet besproken.

De dynamiek van het fytoplankton (zoals groei, vermindering, grazen, biomassa, celgrootte, bloei) is nauw verbonden met de variabelen die zich voordoen in de natuur-lijke omgeving, zoals lichtintensiteit, temperatuur, voedingsstoffen, zwevende sedimenten, wind profielen en getijdenstromingen. In hoofdstuk 2 wordt een factoranalyse ontwikkeld om de bijdragen van de omgevingsvariabelen te karakteriseren en om de drij-vende krachten te onderscheiden, bepaald door de gegevens uit de 10-jarige historische record van 2000 tot en met 2009, in een case studie van de Friese Inlaat.

Drie aspecten van dynamiek van het fytoplankton, namelijk de groei van fytoplankton, de fytoplankton biomassa en de bloei van fytoplankton, zijn de focus van dit onderzoek. Veldmetingen van de fytoplankton dynamiek zijn kostbaar, daarom is gekozen voor het gebruik van wiskundige modellen als instrument voor de uitvoering van het onderzoek. Het BLOOM II-model en het fytoplankton model worden toegepast om de jaarlijkse variaties van de fytoplankton biomassa in de kustwateren te onderzoeken (hoofdstuk 3, hoofdstuk 4, en hoofdstuk 5). De betrouwbaarheid van de schatting van de variabelen is grotendeels bepalend voor het vertrouwen in de output van het model. De betrouwbaarheid van de bepaling van de groei van het fytoplankton op jaarbasis wordt gecontroleerd door de variabelen van temperatuur, lichtintensiteit en voedingsstoffen, afzonderlijk of geheel omvattend. Fytoplankton heeft licht nodig voor het groeiproces door middel van fotosynthese, terwijl de lichtintensiteit wordt verzwakt als gevolg van de absorptie door de chlorofyl a, het zoutgehalte, het gehalte aan organische stof, het troebele water en het uitsterven van de achtergrond. De fytoplankton verbruikt voedingsstoffen, maar de fytoplankton geeft ook weer voedingsstoffen terug aan het water door afsterving en het daaropvolgende verval. Het verlies en de begrazing van het fytoplankton zijn in het model vereenvoudigd, maar zijn in werkelijkheid meer gevarieerd onder invloed van de omgevingsvariabelen.

De rol van het verticale vermengingsproces van fytoplankton is aanzienlijk, deze is namelijk van invloed op de verticale distributies van de fytoplankton biomassa en heeft gevolgen voor de aanwezigheid van lichtintensiteit en voedingsstoffen. Hoewel in hoofdstuk 4 en hoofdstuk 5 een verticaal model van fytoplankton wordt besproken waarin het driedimensionale model van fytoplankton wordt gereduceerd tot een eendimensionaal model, wordt de mate van verticale vermenging in beide gevallen ontleend aan het Delft3D model. In deze context draagt een betrouwbare schatting van de verticale vermengingsgraad toe aan the toepasbaarheid van het fytoplankton model. In hoofdstuk 4 wordt het effect van de verticale turbulente op de variatie van de fytoplankton biomassa, gedreven door de getijde stromingen en de wind profielen, besproken. In hoofdstuk 5 wordt dezelfde studie van de mate van verticale vermenging, zoals beschreven in hoofdstuk 4, uitgevoerd, maar nu gedreven door de fysieke condities, zowel als een aanjager (de verticale stabiliteitsdrempel) van de waarschijnlijkheid van fytoplankton bloei.

De voorspelling van het model gaat gepaard met de vereenvoudiging, overschatting of onderschatting van de werkelijke situatie, genoemd *oorspronkelijke waarde* ± *onzekerheid*. Dus, de onzekerheidsanalyse dient geïntegreerd te worden met de output van het model. De onzekerheid die voortvloeit uit de output van het model is de focus, er wordt slechts een korte bespreking van onzekerheid als gevolg van de input van het model gegeven. De Bootstrap methode en de Bayesian Markov Chain Monte Carlo (BMCMC) simulatie zijn ontwikkeld om inzicht te geven in de voorspellingen van het model, met een karakterisering van de onzekerheidsanalyse.

Contents

List of Figures

List of Tables

Abbreviations

BMCMC	**B**ayesian **M**arkov **C**hain **M**onte **C**arlo
BOD_5	**B**iochemical **O**xygen **D**emand
CDF	**C**umulative **D**ensity **F**unction
Chla	**C**hlorophyll *a*
CI	**C**onfidence **I**nterval
DIN	**D**issolved **I**norganic **N**itrogen
DO	**D**issolved **O**xygen
I	**L**ight **I**ntensity
KMO	**K**aiser- **M**eyer- **O**lkin measure of sampling adequacy
ML	**M**aximum **L**ikelihood
MLD	**M**ixed **L**ayer **D**epth
NH_4	**A**mmonium
NO_3	**N**itrate
NPZ	**N**utrient-**P**hytoplankton-**Z**ooplankton
PCA	**P**rincipal **C**omponent **A**nalysis
PDF	**P**robability **D**ensity **F**unction
PO_4	**P**hosphorus
RMSE	**R**oot **M**ean **S**quare **E**rror
Si	**D**issolved **S**ilicate
SOA	**S**tate **O**ceanic **A**dministration people's republic of **C**hina
SPM	**S**uspended **P**aticulate **M**atter
T	**T**emperature
TN	**T**otal **N**itrogen
TP	**T**otal **P**hosphorus
ULS	**U**nweighted **L**east **S**quares

Symbols

c	constant coefficient (default value 0.5)	[-]
C	concentration of the state variable	$g\ m^{-3}$
C_0	phytoplankton production at the surface layer	$g\ m^{-3}$
$COV(M,D)$	covariance between predictions and observations	[-]
C_x	normalized deviation between model results	
	and observations	
$D_{x,t}$	obervations	
E_h, E_z	horizontal and vertical turbulent diffusivities	$m^2\ s^{-1}$
f	plant metabolic loss	day^{-1}
g	grazing rate by zooplankton	day^{-1}
I_{cr}	compensation light intensity	$Einstein\ m^{-2}\ day^{-1}$
		or $W\ m^{-2}$
I_0	light intensity at the surface layer	$Einstein\ m^{-2}\ day^{-1}$
		or $W\ m^{-2}$
I_z	light intensity at the water depth z	$Einstein\ m^{-2}\ day^{-1}$
		or $W\ m^{-2}$
k	net growth rate	day^{-1}
$K_{1/2}$	light intensity associated with half of	$Einstein\ m^{-2}\ day^{-1}$
	the maximum photosynthetic rate	or $W\ m^{-2}$
K_{bg}	background turbidity	m^{-1}
K_d	light attenuation coefficient	m^{-1}
l	loss rate of the phytoplankton	day^{-1}
L_0	phytoplankton loss at the surface layer	day^{-1}
$M_{x,t}$	model results	
p	significance level	

P	phytoplankton biomass	$g\ m^{-3}$
P'	photosynthetic rate	$Einstein\ m^{-2}\ day^{-1}$ or $W\ m^{-2}$
$\overline{P_H}$	depth-averaged phytoplankton biomass at Huibertgat station	$g\ m^{-3}$
$\overline{P_L}$	depth-averaged phytoplankton biomass at Lauwersoog station	$g\ m^{-3}$
P_{max}	maximum photosynthetic rate	$Einstein\ m^{-2}\ day^{-1}$ or $W\ m^{-2}$
$r\ or\ R$	correlation coefficient	
r_0	respiration rate	day^{-1}
s	mortality rate of phytoplankton	day^{-1}
sd_D	standard deviation of the observations	
sd_M	standard deviation of the model results	
μ	specific growth rate	day^{-1}
μ_{max}	maximum growth rate	day^{-1}
u_x, u_y, u_z	velocities in the x-, y- and z-direction	$m\ s^{-1}$
u_s	sinking velocity	$m\ s^{-1}$
z	water depth	m
Z	zooplankton biomass	$g\ m^{-3}$
Z_{cr}	critical depth	m

Chapter 1

Introduction

1.1 Background

1.1.1 Phytoplankton dynamics

The coastal ecosystem is facing a big challenge caused by the effects of anthropogenic activities and coastal development (Kennedy et al. [2002]; Conley et al. [2002]; Andersen [2006]). As a critical indicator of the coastal ecosystem, phytoplankton plays an important role in the whole impact-effect chain and is responsible for most of primary production. In the open ocean, the phytoplankton accounts for 80% of the marine production (Martin et al. [1987]). The coastal environment is favorable for the phytoplankton as well. The investigation of phytoplankton dynamics has provided useful insights and a better understanding of the coastal ecosystem (Cloern [1996]; Pedersen and Borum [1996]; Edelvang et al. [2005]; Fu et al. [2009]; Godrijan et al. [2013]).

Phytoplankton dynamics (i.e. growth, loss, grazing, biomass, bloom) varies with the characteristics of the environmental variables in the water column (Pedersen and Borum [1996]; Recknagel et al. [2006]; Taylor and Ferrari [2011]). The associated environmental variables are divided into three categories: physical condition, chemical condition and biological condition, displayed in figure 1.1. Take the physical condition as an example to illustrate the relation to phytoplankton dynamics: temperature and light intensity are closely related with the phytoplankton growth (Eppley [1972]; Smith [1980]; Geider et al. [1998]; Örnólfsdóttir et al. [2004]); a change of salinity has an effect on the phytoplankton

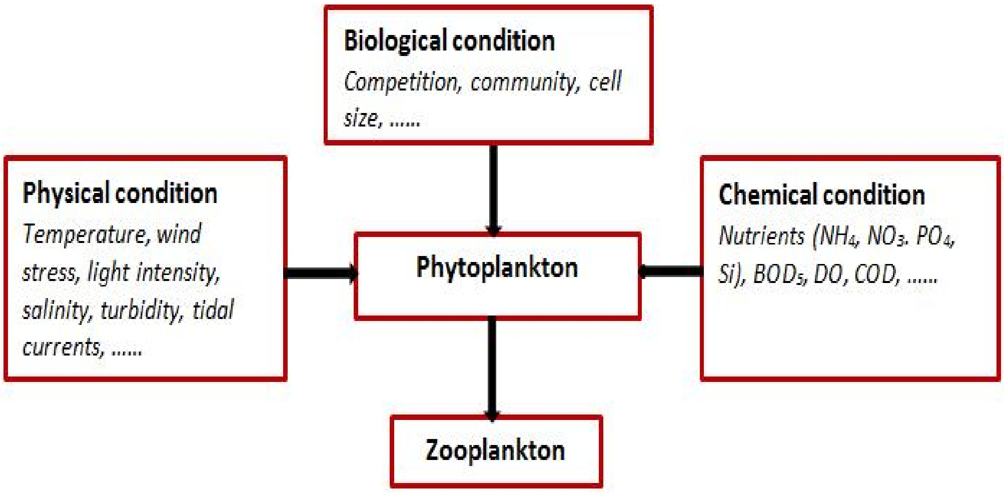

FIGURE 1.1: Contribution of the environmental variables to phytoplankton dynamics in coastal waters. The variation of the zooplankton is influenced, directly or indirectly, by the phytoplankton variability. In this thesis the research is focused on the significance of the phytoplankton, and the zooplankton remains outside the scope of the current thesis.

community (Schmidt [1999]; Lionard et al. [2005]); wind stress and tidal currents affect the turbulent mixing rate determining the vertical distributions of the phytoplankton biomass (Serra et al. [2007]; Wong et al. [2007]; Woernle et al. [2014]), and affecting the species composition due to the effects on the availability of light intensity and nutrients (Ferris and Christian [1991]); suspended sediment absorbs and scatters light intensity, implying that phytoplankton is limited by light availability in the high turbidity zone (Wild-Allen et al. [2002]).

Of all the environmental variables, phytoplankton dynamics is mainly refined by the limitations of light and nutrient availability (Eilers and Peeters [1988]; Boyer et al. [2009]).

Light intensity

Phytoplankton needs sunlight for the photosynthesis, which is averaged through the mixed layer zone. Light intensity over the water depth follows the Lambert-Beer's Law (Dennison et al. [1993]; Devlin et al. [2008]), declining exponentially with the extinction coefficient. The extinction is the sum of inorganic suspended particulate matter, organic matter, chlorophyll a, salinity and background extinction. In temperate regions, light limitation happens in winter although sufficient nutrients are available.

Nutrients

Nutrient enrichment (eutrophication) becomes a societal issue due to the increased inputs into the coastal zone and as a consequence of the phytoplankton blooms (Cloern [1999]; Andersen [2006]; Howarth and Marino [2006]). The main sources of the coastal eutrophication are the use of fertilizers in agriculture, the presence of livestock, wastewater, urban runoff, and the load of the river flow. The coastal ecosystem stores and cycles the nutrients. The nutrient fluxes in the phytoplankton processes are described in figure A.1 (Appendix A).

Three major nutrients (nitrogen, phosphorus, and silicon) are often considered as the limiting factors for phytoplankton, as well with light intensity. Nitrogen is an essential component of the light-sensitive pigments like chlorophyll a. In aquatic systems nitrogen is available as ammonium and nitrate. Compared with nitrogen, phosphorus is less sensitive to phytoplankton cells. Silicon is essential to only one phytoplankton group, diatoms, and is available as dissolved silicate.

The earlier work on the estimate function of the phytoplankton growth rate is related to the nutrients, using Michaelis-Menten kinetics to explain the uptake rate by the algal cells (Caperon [1967]; Dugdale [1967]). Diverse studies have found that nitrogen, phosphorus, or both of them control the phytoplankton growth (Haney and Jackson [1996]; Flynn and Fasham [1997]; Geider et al. [1998]; Cloern [1999]; Geider and La Roche [2002]; Smith [2003]; Örnólfsdóttir et al. [2004]; Davey et al. [2008]), the phytoplankton biomass (Cloern [2001]; Fennel [2003]; Blauw and Los [2004]; Niu et al. [2015b]; Niu et al. [2015a]; Niu et al. [2015c]), and the phytoplankton community (Mei et al. [2009]; Jin et al. [2013]).

1.1.2 Mathematical models of phytoplankton dynamics

Investigating the variations of phytoplankton dynamics could effectively elucidate the role of the coast in the biogeochemical cycling (Longhurst et al. [1995]). The behaviours of phytoplankton dynamics and the associated environmental variables can be adequately modelled with the ecological models in a site-specific station or in a broad application of the coastal and transitional water systems. A relatively large number of models has been managed as software for simulating the ecological processes (i.e. nutrient cycles, transport of substances, phytoplankton biomass, primary production), examples include BLOOM II/GEM (Hydraulics [1991]; Hydraulics [2003]), ERSEM (Baretta et al. [1995]), NORWECOM (Skogen [1993]), COHERENS (Luyten et al. [1999]), and MIKE 3 (DHI [2000]).

Moreover, the mathematical phytoplankton models are also convenient to analyze the phytoplankton processes. Generally, the characteristics of phytoplankton dynamics are coupled with a physical model (i.e. NPZ model with the advection-diffusion equation), considering the physical-chemical-biological interactions (Riley [1949]; Evans and Parslow [1985]; Franks [1997]; Franks [2002]; Murray and Parslow [1999]). With the simplifications, researchers reduce the three-dimensional phytoplankton model to a one-dimensional form to get a practical solution (Riley [1949]; Evans and Parslow [1985]; Wong et al. [2007]; Taylor and Ferrari [2011]).

1.1.3 Uncertainty of phytoplankton dynamics

When there are two or more environmental variables, there may be a variety of relationships between them. In the presence of uncertainty, the relationships are not unique. Given the values of one variable, there is a range of possible values of other variables. The relationships between the object and the associated variables thus require a probabilistic analysis (Chapman [1961]; Vrijling et al. [1998]; Van Gelder [2000]; Portielje et al. [2000]; Shukla et al. [2006]; Ang and Tang [2007]; Govaert [2009]).

The classic modelling approaches are based on the steady status with some simplifying assumptions, but the actual processes are not deterministic with respect to uncertainty. The uncertainties cannot be avoided in any of the analyses. For example, we stress the significance of the phytoplankton in this thesis, whereas the grazing rate of the zooplankton is considered as a constant value. The grazing process of the zooplankton, however, is sensitive to the phytoplankton growth, varying with the environmental factors (Steele and Henderson [1992]; Haney and Jackson [1996]). Therefore, the simplification of the model is accompanied with an overestimate or an underestimate of the real status. To give insight in the model output, uncertainty analysis is required.

In principle, uncertainty refers to a lack of knowledge, including parameter uncertainty (measurement errors, sampling errors, experimental errors, systematic errors), model uncertainty (due to the simplification of the real problems, mis-design of the model structure, model misuse), and scenario uncertainty (descriptive errors, aggregation errors, errors in the professional judgment, incomplete analysis). Tung et al. [2005] give the definition of uncertainty as following:

"Uncertainty is attributed to the lack of perfect information concerning the phenomena, processes, and data involved in problem definition and resolution. Uncertainty could simply be defined as the occurrence of events that are beyond one's control (Mays and Tung [1992]). In practical all engineering designs and operations, decisions are frequently made under uncertainty. As such, the reliability and safety of engineering projects are closely related to the level of uncertainty involved."

1.1.4 Description of the study areas

Frisian Inlet (the Netherlands)

The Frisian Inlet, as one of the case studies, is a part of the Dutch Wadden Sea located in the north of the Netherlands, with two barrier islands of Ameland (the west one) and Schiermonikoog (the east one), displayed in figure 1.2. The Frisian islands seperate the Wadden Sea from the North Sea. A large supra tidal shoal in the centre divides the inlet into two smaller ones. Three representative stations are marked out, Lauwersoog station (A), Huibertgat station (B), and Harlingen station (C). The water environment in this area is favourable for the phytoplankton (Van Beusekom et al. [2012]). In this thesis, the Frisian Inlet is addressed to three major studies. The first study is to investigate the responses of phytoplankton biomass to environmental factors, determined in the 10-year time period from 2000 through 2009 (chapter 2). The second study focuses on the application of the BLOOM II model to predict the variation of the phytoplankton biomass (in terms of chlorophyll a), determined by the dataset in 1992 (chapter 3). The third study is to develop another convenient modelling approach, a vertical phytoplankton model, to investigate the vertical distributions of the phytoplankton biomass, determined by the dataset in 2009 (chapter 4).

Jiangsu coast (China)

The Jiangsu coast is bounded by the Shandong Peninsula and is the shore of the Yellow Sea, shown in figure 1.3. In 2006, according to the historical record of the State Oceanic Administration People's Republic of China (SOA, `http://www.soa.gov.cn/`

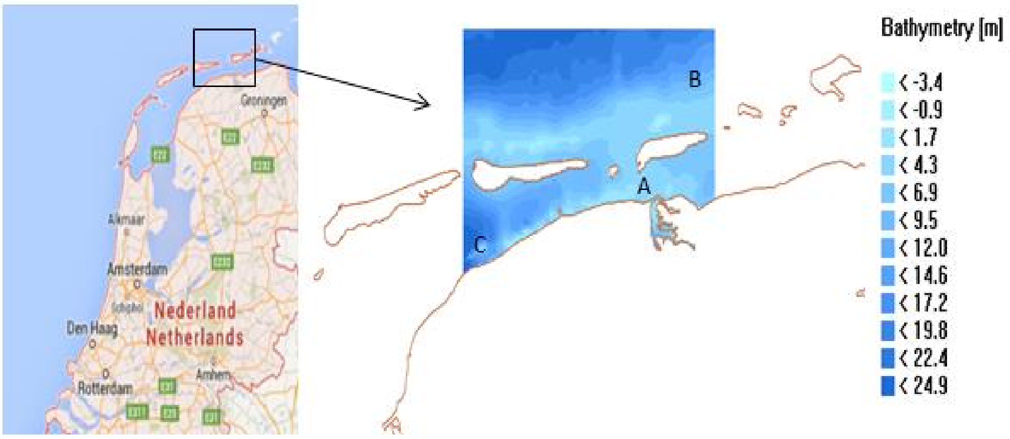

FIGURE 1.2: Case area of the Frisian Inlet and surrounding water zones. A: Lauwersoog station; B: Huibertgat station; C: Harlingen station.

zwgk/hygb/), the water was seriously polluted from the Guanhe estuary to the north branch of the Yangtze River estuary. The main pollutants are inorganic nitrogen, phosphate and oil. The average inorganic nitrogen in the Jiangsu coastal waters is 0.32 $mg\ l^{-1}$, and the average phosphate is 0.14 $mg\ l^{-1}$. The total nitrogen ranges from 0.051 $mg\ l^{-1}$ to 1.102 $mg\ l^{-1}$, and the total phosphorus ranges from 0.014 $mg\ l^{-1}$ to 0.282 $mg\ l^{-1}$. The ambient water environment provides a favourable living condition for the phytoplankton. Figure 1.4 presents the phytoplankton abundance in 2006 at the Dafeng estuary. The Radial Sand Ridges area locates in the south of the Jiangsu coast, with a complicated topography and a high suspended sediment concentration. The water masses are dominated by the Yangtze River diluted water, the Taiwan warm current and the Yellow Sea coastal water. This case study is approached to the application of the vertical phytoplankton model, and to investigate the occurrence of the phytoplankton blooms, determined by the dataset in 2006 (chapter 5).

1.2 Objectives

This research explores the following questions:

1) How does the long-term phytoplankton biomass (in terms of chlorophyll *a*) respond to the physical-chemical factors (light intensity, salinity, water temperature, suspended matter, and nutrients)? Which estimate function of the phytoplankton growth is applicable? (chapter 2)

2) How is the annual variation of the phytoplankton biomass (in terms of chlorophyll *a*)

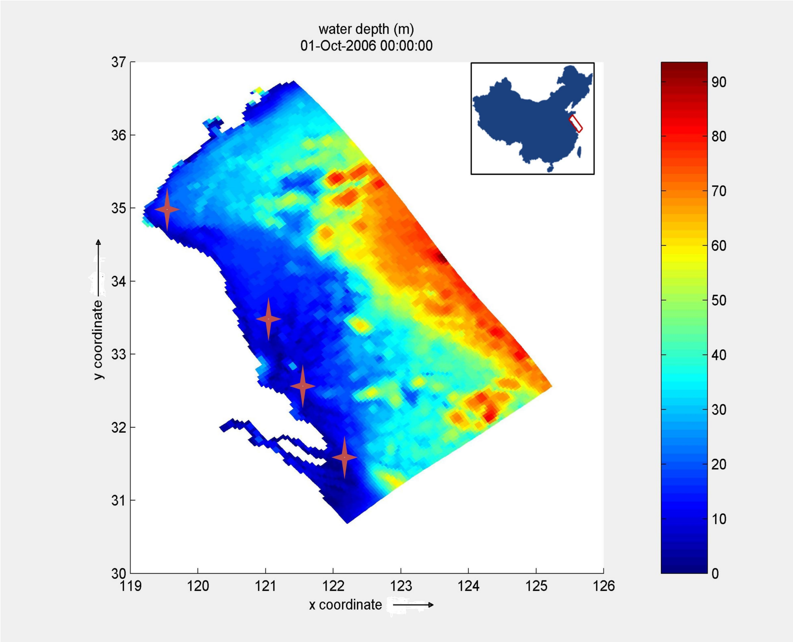

FIGURE 1.3: Case area of the Jiangsu coastal zone (from north to south, the red stars indicate Lianyungang station, Dafeng station, Yangkou station, and the north branch of the Yangtze River estuary, respectively).

FIGURE 1.4: Phytoplankton abundance at the Dafeng estuary in 2006

in a specific year of 1992? How will be the response of the phytoplankton biomass (in terms of chlorophyll a) to nutrient availability? How can we give insight in the predictions with an integration of uncertainty analysis? (chapter 3)

3) How can we investigate the annual variation of the phytoplankton biomass from physical-chemical properties in a specific year of 2009? How will the predictions fluctuate subject to uncertainty? (chapter 4)

4) How will the physical limitation contribute to the phytoplankton biomass in a specific year of 2006? How can we investigate the bloom development from the physical properties? (chapter 5)

Accordingly, the methods are introduced to solve the questions:

1) Boxplot analysis and factor analysis are convenient and flexible to process the long-term data; a reliable estimate function of the phytoplankton growth rate is developed, combined the effects of temperature and light intensity.
2) Bloom II model is able to produce the reliable prediction of chlorophyll *a*; Bayesian Markov Chain Monte Carlo simulation is used to give insight in the prediction with uncertainty.
3) A vertical phytoplankton model is developed, with the well-known simplifications, combined the analyses of Delft3D model; to give a reliable interval of the predictions, the BMCMC simulation is approached.
4) The application of the vertical phytoplankton model is performed to investigate the phytoplankton variability in coastal waters, and to extend the model application to investigate the bloom development.

These questions are motivated by issues across a range of spatial and temporal scales. The objectives of this research are described below:

1) To investigate the responses of phytoplankton dynamics to the environmental factors and to characterize the significant and non-significant factors;
2) To predict the variation of the phytoplankton biomass (in terms of chlorophyll *a*);
3) To give insight in the vertical patterns of the phytoplankton biomass;
4) To investigate the phytoplankton bloom development from the physical properties;
5) To give insight in the model output with an integration of uncertainty analysis.

1.3 Outline of the thesis

Three elements of phytoplankton dynamics are concentrated in this thesis: phytoplankton growth, phytoplankton biomass, and phytoplankton blooms. The outline of this thesis is illustrated in figure 1.5.

In chapter 1, the general descriptions of phytoplankton dynamics are introduced.

In chapter 2, the responses of phytoplankton dynamics to the environmental factors are discussed, emphasizing on the phytoplankton biomass (in terms of chlorophyll a) and the growth rate. Within this chapter, two case studies are presented, Lauwersoog station (NL) located in the north of the Dutch coast and Lianyungang station (CN) located in the north of the Jiangsu coast. For the case study of Lauwersoog station, the research aims to find out to what extent the phytoplankton biomass (in terms of chlorophyll a) responds to the environmental variables, characterizing the driving forces using factor analysis. For the case study of Lianyungang station, the research introduces a combined estimate function of the phytoplankton growth rate, incorporating the temperature-growth function with the photosynthetic light curve.

In chapter 3, the ecological model of BLOOM II is applied to predict the variation of the phytoplankton biomass (in terms of chlorophyll a) in a case of the Frisian Inlet (NL). This study is determined by the dataset in 1992. Particular attention has been paid to the phytoplankton biomass (in terms of chlorophyll a) in response to nutrient availability. Considering the uncertainty arising from the model itself, the reliable prediction of the phytoplankton biomass is derived within the 95% confidence interval using the Bayesian Markov Chain Monte Carlo (BMCMC) simulation.

In chapter 4, a vertical phytoplankton model is developed to investigate the vertical distributions of the phytoplankton biomass in the case of the Frisian Inlet. This study is determined by the dataset in 2009. To stress the uncertainty arising from the model itself, the BMCMC simulation is applied to give insight in the model output.

In chapter 5, the extended application of the vertical phytoplankton model is performed to the Jiangsu coastal waters. Skill assessment is introduced to validate the reliability of the phytoplankton model. Additionally, the physical limitation of the phytoplankton bloom is discussed: vertical stability threshold and critical depth. The vertical stability threshold is captured from the condition of $k > 0$; the critical depth is derived from the concept of the compensation light intensity, a widely used condition to distinguish the occurrence of the bloom event.

In chapter 6, various issues about phytoplankton dynamics are discussed and the suggestions for future work are elaborated.

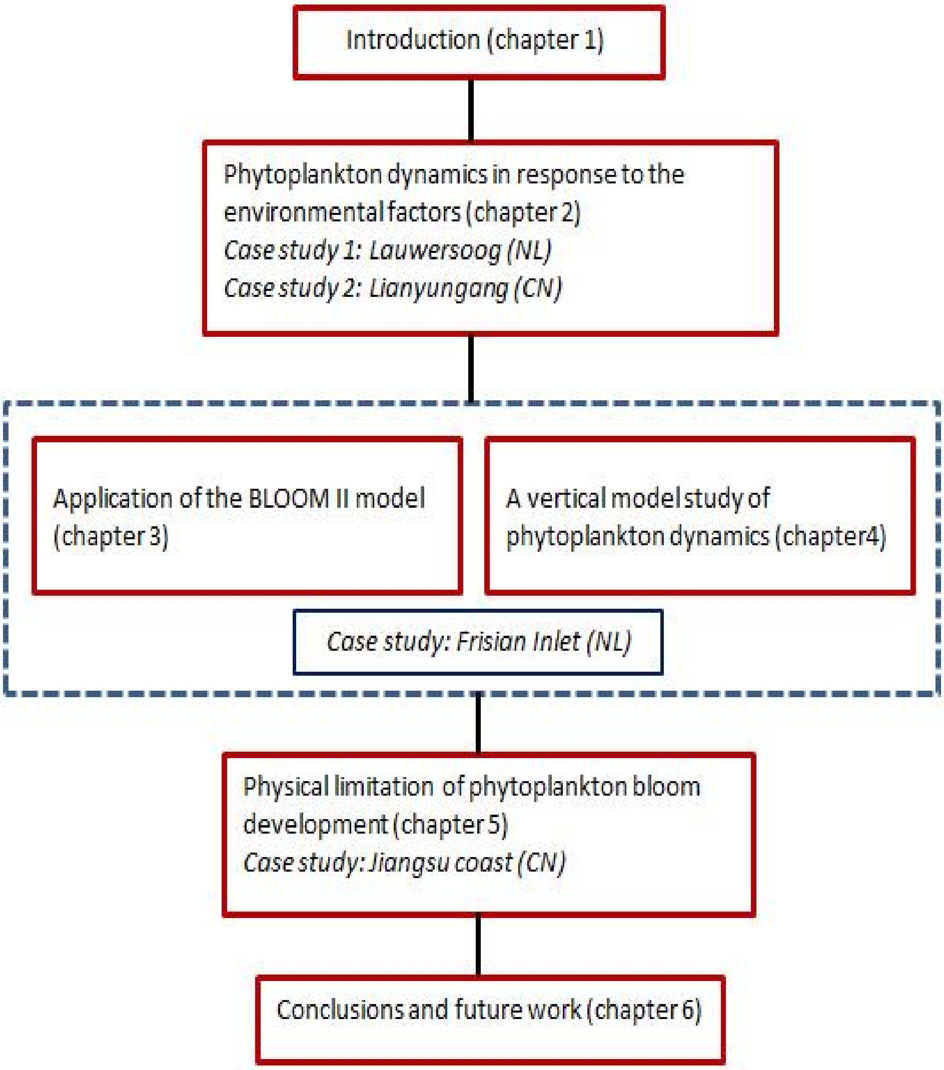

Figure 1.5: Outline of the thesis

Chapter 2

Phytoplankton dynamics in response to the environmental factors

2.1 Test case one: Statistical analysis of the phytoplankton biomass in the Wadden Sea near Lauwersoog (NL)

2.1.1 Introduction

Various research has completely accepted that chlorophyll *a* is a reliable measure of phytoplankton biomass (Voros and Padisak [1991]; Scharler and Baird [2003]; Ramírez et al. [2005]; Boyer et al. [2009]). Chlorophyll *a*, varying substantially from place to place and from time to time, has been explained as a consequence of many environmental factors, like nutrients (Margalef [1978]; Reckhow [1993]; Recknagel et al. [2006]; Paytan and McLaughlin [2007]; Struyf et al. [2010]; Jin et al. [2013]) and light intensity (Hunter and Laws [1981]; Huisman and Weissing [1994]; Moore [2009]). A multivariate analysis is needed to characterize the effects of the environmental factors to the phytoplankton biomass. There are several commonly used paths to complete the multivariate analysis, including structural analysis (Bölter et al. [1980]; Paudel and Montagna [2014]), factor analysis (Kaiser [1960]; Chau and Muttil [2007]), principal component analysis (Pedersen and Borum [1996]; Schlüter et al. [2008]; Friedrichs et al. [2009]; Primpas et al. [2010];

Marić et al. [2012]), artificial neural network analysis (Recknagel et al. [2006]), and data mining analysis (Su et al. [2013]).

This study, using the factor analysis, aims to find out to what extent the phytoplankton biomass (in terms of chlorophyll a) responds to the environmental factors in the Wadden Sea near Lauwersoog, determined in the 10-year time period dataset from 2000 through 2009. The study area of Lauwersoog station, located in the north of the Netherlands, is a part of the Frisian Inlet, shown in figure 1.2 (symbol A). The main objectives are described below: 1) to give insight in the seasonal dynamics of the phytoplankton biomass; 2) to investigate the response of phytoplankton biomass to the physical-chemical factors (light intensity, salinity, nitrate, ammonium, phosphorus, silicate, total nitrogen, total phosphorus, suspended matter, and ambient water temperature); and 3) to characterize the driving factors to the phytoplankton biomass without much loss of information.

2.1.2 Data information in 10-year time period from 2000 through 2009 at Lauwersoog station

The monitoring programme has been carried out by Rijkswaterstaat (NL), and the observations are stored in the main database of DONAR, accessible through `http://live.waterbase.nl/waterbase_wns.cfm?taal=en`. Eleven variables (chlorophyll a, $Chla$, $mg\ m^{-3}$; light intensity, I, $Einstein\ m^{-2}\ day^{-1}$; salinity, PSU; nitrate, NO_3, $mg\ l^{-1}$; ammonia, NH_4, $mg\ l^{-1}$; dissolved phosphorus, PO_4, $mg\ l^{-1}$; dissolved silicate, Si, $mg\ l^{-1}$; total nitrogen, TN, $mg\ l^{-1}$; total phosphorus, TP, $mg\ l^{-1}$; suspended matter, SPM, $g\ m^{-3}$; water temperature, T, ${}^{0}C$), monitored either biweekly or monthly, are collected for the 10-year time period from 2000 through 2009. Figure 2.1 plots the long term observations (2000-2009) of the associated variables in the Wadden Sea near Lauwersoog (NL).

2.1.3 Factor analysis

Factor analysis is a useful tool to reduce the overlapping information and to investigate the relationships between the coastal ecosystem and the environmental factors. It is often used in the data dimension-reduction to identify a small set of variables that represent most of the variance (Shukla et al. [2006]; Chau and Muttil [2007]; Friedrichs

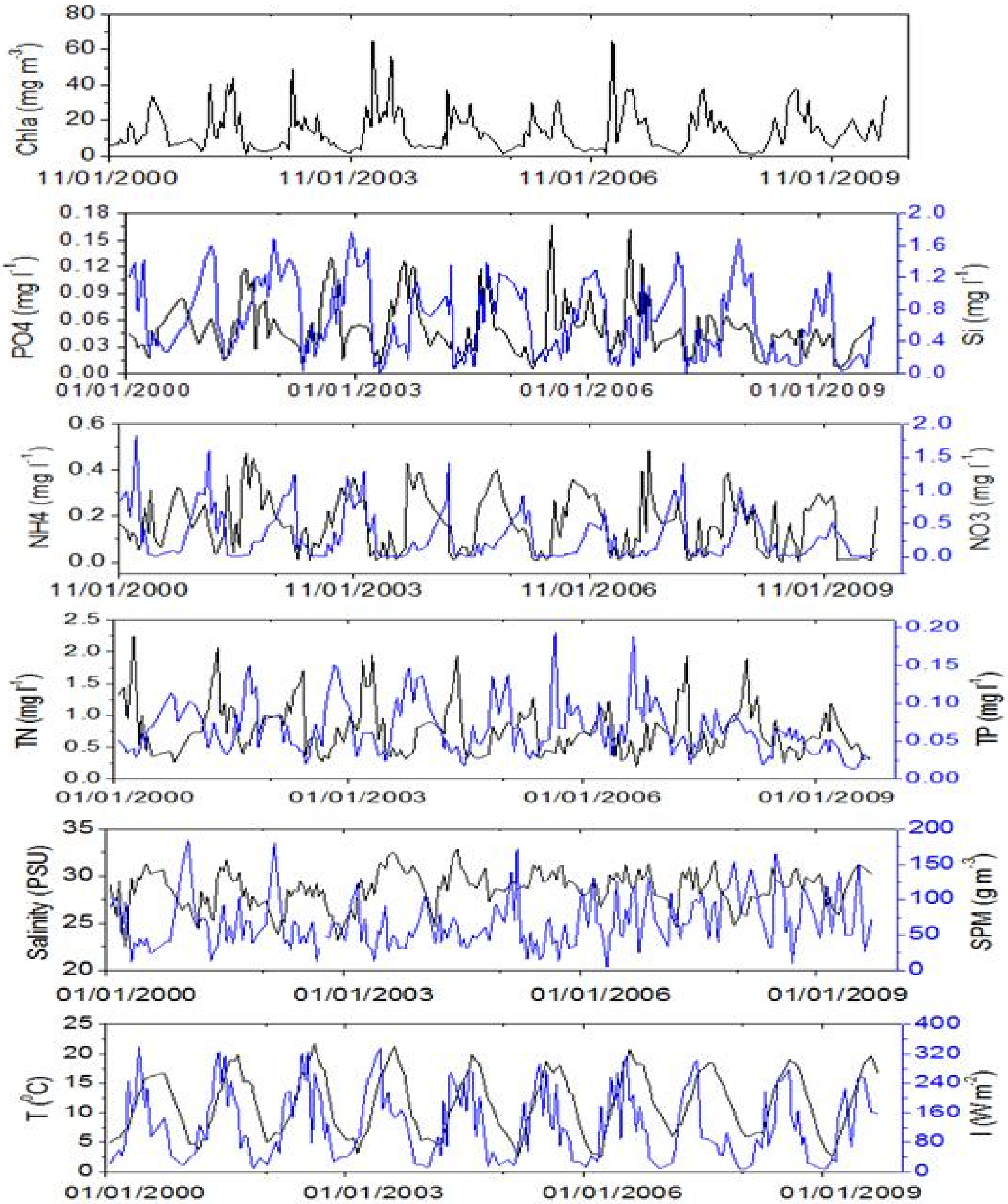

FIGURE 2.1: Observed variations in the Wadden Sea near Lauwersoog (2000-2009)

et al. [2009]). Data analysis often includes a large number of observations, and some may be unnecessary. From the factor analysis, the dominant variables could be extracted.

Factor analysis is totally dependent on correlation or covariance matrix between variables. But 90% of the factor analysis is meant to use the correlation matrix, as is applied in this study. Concerning the properties of the variables, they are divided into common variables and dependent variables in the correlation matrix. Herein, the phytoplankton biomass is set as a dependent variable, while others are set as common variables. Two types of outputs are generated, eigenvalues and fixed number of factors. The widely used is the eigenvalues. The eigenvalue analysis determines the number of the extracted components/factors. In general, it is required to satisfy the criterion of $eigenvalue > 1.0$.

Three extraction methods are introduced to perform the factor analysis: Principal Component Analysis (PCA), Maximum Likelihood (ML), and Unweighted Least Squares (ULS). It is noted that the principal component analysis could be used independently or comprehensively in the data analysis. Principal component analysis, as the basic extraction method, aims to find a linear combination of variables in a relatively simple way. Factor analysis is conducted using the statistical package IBM SPSS Statistics 20, accessible through http://www-01.ibm.com/support/docview.wss?uid=swg24029274. The detailed information of three extraction methods is described in Appendix B.

To obtain a clear pattern of the factor loadings, we can rotate the axes in any direction without any changes. There are many different types of rotations that can be applied after the initial extraction of components/factors. In this study, an orthogonal rotation method, Varimax with Kaiser normalization, is preferred to determine what the components represent.

2.1.4 Discussion

Statistics of phytoplankton biomass

Summarizing the historical dataset (2000-2009) in the Wadden Sea near Lauwersoog, the statistics of the phytoplankton biomass (in terms of chlorophyll a) are shown in table 2.1. The values of chlorophyll a vary around 15.13 ± 11.85 $mg\ m^{-3}$. Most of chlorophyll a are concentrated at a range of [0, 20], accounting for 75% of all values, followed by the ranges of [20, 40] and [40, 70] $mg\ m^{-3}$. The values larger than 60 $mg\ m^{-3}$ occur in the spring of 2003 and 2006. Fast phytoplankton growth usually appears in spring and in autumn with the favorable living conditions. The skewness of the dataset is 1.53, indicating that chlorophyll a has a long right tail. The frequency distribution is asymmetric, with some distant values in a positive direction from the center, displayed in figure 2.2A, corresponding well with the positive skewness. A Gamma model is fitted well by the observations, with a shape parameter of 1.63 mgm^{-3} and a rate parameter of 9.26 mgm^{-3}, shown in figure 2.2B. The positive skewness also states that the mean value (15.13 mgm^{-3}) is at the right of the median value (12.40 mgm^{-3}).

TABLE 2.1: Statistics of chlorophyll *a* in the Wadden Sea near Lauwersoog (2000-2009, n=187), expressed in $mg\ m^{-3}$

		Statistic	Bootstrap			
			Bias	Std. Error	95% Confidence Interval	
					Lower	Upper
Mean		15.13	-0.02	0.86	13.44	16.90
Median		12.40	-0.20	1.00	10.20	14.20
Std. Deviation		11.85	-0.05	0.94	9.97	13.54
Variance		140.47	-0.27	22.19	99.42	183.32
Skewness		1.53	-0.05	0.25	0.96	1.94
Percentiles	25	6.18	0.04	0.52	5.12	7.30
	50	12.40	-0.20	1.00	10.20	14.20
	75	20.00	0.32	1.50	18.20	24.20
	95	37.92	0.32	2.62	33.77	44.40

The Bootstrap method, based on 1000 random samples, is introduced to investigate the properties of chlorophyll *a* with a 95% confidence interval (table 2.1). In practice, there are two ways to express the degree of uncertainty of a statistical quantity, namely standard error and confidence interval. Similar to the standard deviation of a variable, the standard error measures the standard deviation of an estimated statistical quantity from a sample. On the other hand, the confidence interval of an estimated quantity is an interval that has a specified probability (confidence) to include the true values. Within the 95% confidence interval, the expected mean value varies from 13.44 to 16.90 $mg\ m^{-3}$, with a bias of -0.02 $mg\ m^{-3}$ and a standard error of 0.86 $mg\ m^{-3}$, and the expected standard deviation varies from 9.97 to 13.54 $mg\ m^{-3}$, with a bias of -0.05 $mg\ m^{-3}$ and a standard error of 0.94 $mg\ m^{-3}$. 75% of all expected values are less than 24.20 $mg\ m^{-3}$, while the observed values are less than 20.00 $mg\ m^{-3}$, accordingly.

Seasonal dynamics of phytoplankton biomass and environmental variables

In this section, the spatial variations in physical-chemical factors and phytoplankton biomass (in terms of chlorophyll *a*) are discussed, depicted in figure 2.3. The boxplot is a graphical display of the data. In which, the middle black line indicates the median, the shaded region stating the middle 50%. The lines extending out of the shaded region are the top and bottom 25% of data and the horizontal lines at the top/bottom of the boxplot are the minimum and maximum values.

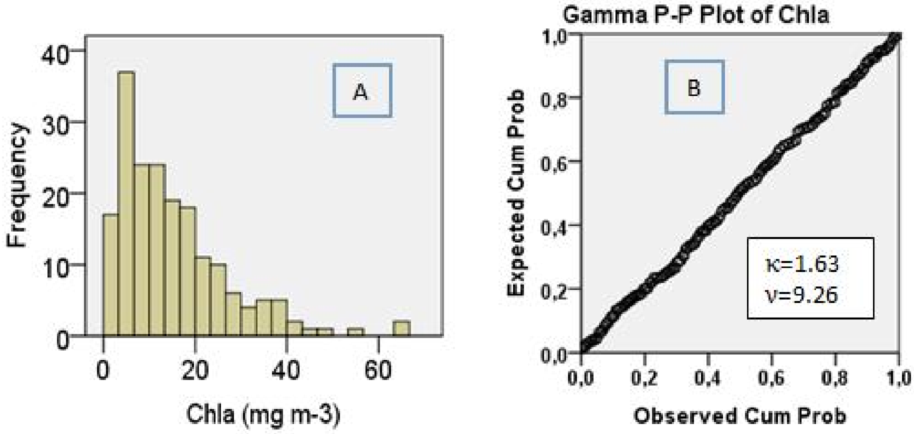

FIGURE 2.2: Historical analysis of phytoplankton biomass (in terms of chlorophyll *a*, expressed in $mg\ m^{-3}$) in the Wadden Sea near Lauwersoog, determined by the dataset from 2000 through 2009. A: frequency distribution, presented as histogram; B: goodness-of-fit test using a probability model (Gamma distribution, x-axis indicates the observed cumulative probability and y-axis indicates the expected cumulative probability, κ means the shape parameter of Gamma distribution and ν means the rate parameter)

Ammonium varies from 0.002 $mg\ l^{-1}$ to 0.485 $mg\ l^{-1}$, with a mean value of 0.16 $mg\ l^{-1}$ and a standard deviation of 0.123 $mg\ l^{-1}$. The maximum ammonium values appear in August and September, and the minimum values appear in April, June and July. Nitrate varies from 0.005 $mg\ l^{-1}$ to 1.83 $mg\ l^{-1}$, with a mean value of 0.292 $mg\ l^{-1}$ and a standard deviation of 0.373 $mg\ l^{-1}$. The maximum nitrate values appear in March and the minimum values appear in summer (from June to August) and autumn (from September to November). Compared with other nutrients, the order of phosphorus is much lower. Phosphorus ranges from 0.005 $mg\ l^{-1}$ to 0.167 $mg\ l^{-1}$, with a mean value of 0.051 $mg\ l^{-1}$ and a standard deviation of 0.031 $mg\ l^{-1}$. The maximum phosphorus values appear in July, August and September, and the minimum values appear in April.

Small difference is found in salinity, ranging from 22.55 PSU to 32.82 PSU, with a mean value of 28.75 PSU and a standard deviation of 1.95 PSU. The maximum salinity values are found in June, July and September, and the minimum values are found in March and December. Water temperature and light intensity show obvious seasonal variations, varying from 2.5 ^0C to 21.7 ^0C and from 6.37 $W\ m^{-2}$ to 337.04 $W\ m^{-2}$, respectively. The maximum temperature and light intensity appear in summer.

Chlorophyll *a* shows a significant difference, ranging from 0.86 $mg\ m^{-3}$ to 65 $mg\ m^{-3}$. The maximum chlorophyll *a* values appear in April and July, and the minimum values appear in winter.

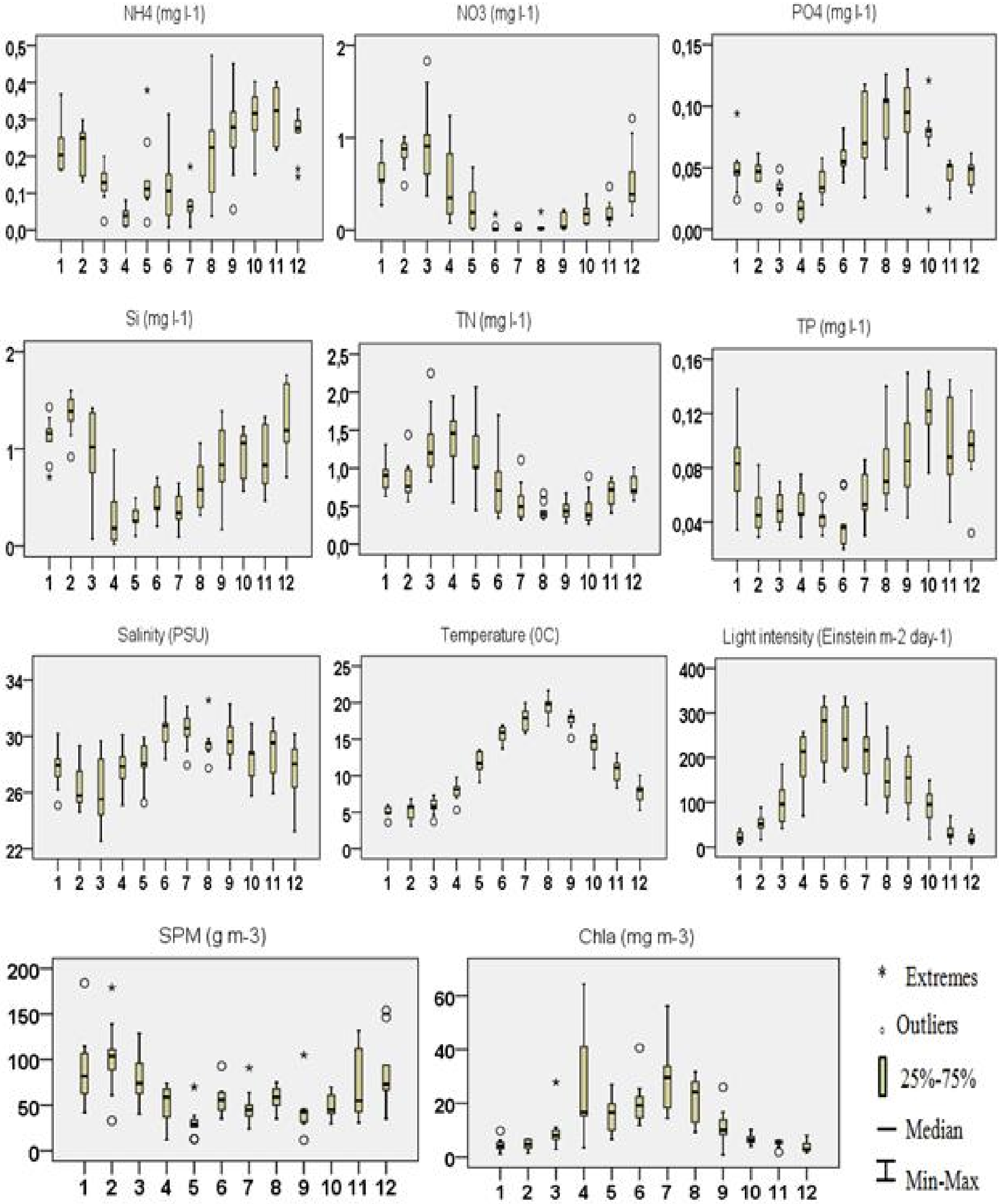

FIGURE 2.3: Seasonal dynamics of phytoplankton biomass (in terms of chlorophyll *a*) and physical-chemical conditions in the Wadden Sea near Lauwersoog (2000-2009)

Extreme values and boxplot analysis are related with each other. In this study, four extreme values are found in ammonium, two extreme values are found in nitrate, three extreme values are found in phosphorus, one extreme value is found in silicate, one extreme value is found in salinity, four extreme values are found in suspended matter, and one extreme value is found in chlorophyll *a*.

Response of phytoplankton biomass to environmental variables

As known that light intensity and nutrients contribute much to the phytoplankton. Figure 2.3 also simply presents the relationship between phytoplankton and environmental factors. The patterns of nutrients inversely follow the variation of chlorophyll *a* due to the uptake of nutrients by the phytoplankton. The maximum chlorophyll *a* is found in April, while lower nutrients are found at that time. In this section, the response of phytoplankton biomass to the effects of environmental variables is discussed, separately and comprehensively. Some variables are significant to the phytoplankton and some are non-significant.

From a comprehensive view, the regression analysis shows a good result (ANOVA). Two thirds of the variance ($r^2 = 0.684$, $F = 15.358$, $p < 0.01$) in chlorophyll *a* is explained. If we focus on the separate contribution of each variable, the correlation matrix is derived, shown in table 2.2. Chlorophyll *a* is strongly and significantly correlated with the variables of silicate, ammonium, and light intensity, and is moderately correlated with the variables of salinity, nitrate, and temperature. Additionally, temperature is correlated with salinity, nitrate, phosphorus, silicate and total nitrogen.

TABLE 2.2: Correlation matrix between the variables (187 samples for each variable) in the Wadden Sea near Lauwersoog, the Netherlands

Variables	$Chla$	Salinity	NH_4	NO_3	PO_4	Si	SPM	T
Salinity	$r = 0.333$							
	$p < 0.001$							
NH_4	$r = -0.481$	$r = -0.140$						
	$p < 0.001$	$p = 0.028$						
NO_3	$r = -0.433$	$r = -0.753$	$r = 0.107$					
	$p < 0.001$	$p < 0.001$	$p = 0.073$					
PO_4	$r = 0.124$	$r = 0.313$	$r = 0.227$	$r = -0.345$				
	$p = 0.046$	$p < 0.001$	$p < 0.001$	$p < 0.001$				
Si	$r = -0.585$	$r = -0.552$	$r = 0.657$	$r = 0.649$	$r = 0.107$			
	$p < 0.001$	$p < 0.001$	$p < 0.001$	$p < 0.001$	$p = 0.073$			
SPM	$r = -0.074$	$r = -0.237$	$r = 0.068$	$r = 0.305$	$r = -0.234$	$r = 0.306$		
	$p = 0.157$	$p < 0.001$	$p = 0.178$	$p < 0.001$	$p < 0.001$	$p < 0.001$		
T	$r = 0.375$	$r = 0.569$	$r = -0.065$	$r - 0.721$	$r = 0.656$	$r = -0.411$	$r = -0.296$	
	$p < 0.001$	$p < 0.001$	$p = 0.189$	$p < 0.001$	$p < 0.001$	$p < 0.001$	$p < 0.001$	
I	$r = 0.497$	$r = 0.260$	$r = -0.456$	$r = -0.348$	$r = 0.250$	$r = -0.510$	$r = -0.337$	$r = 0.449$
	$p < 0.001$	$p < 0.001$	$p < 0.001$	$p < 0.001$	$p = 0.002$	$p < 0.001$	$p < 0.001$	$p < 0.001$

r indicates the correlation coefficient
p indicates the significance level

Factor analysis

Factor analysis is performed to reduce the redundancy information from a set of correlated variables and to represent them with a smaller number of variables. Prior to the application of factor analysis, the reliability of the factor analysis for this dataset should be characterized with the Kaiser-Meyer-Olkin measure of sampling adequacy (KMO) and the Bartlett's test. A higher KMO (asymptotic to 1.0) and a lower significance (< 0.05) indicate a higher confidence in the factor analysis. The results of the reliability analysis (KMO=0.75, $p < 0.01$) demonstrate that factor analysis is feasible in this dataset (Chau and Muttil [2007]), displayed in table 2.3.

Table 2.3: Calculation results of the Kaiser-Meyer-Olkin Measure of Sampling Adequacy and the Bartlett's Test of Sphericity over the 10-year's chlorophyll *a* record from 2000 through 2009 in the Wadden Sea near Lauwersoog

Kaiser-Meyer-Olkin Measure of Sampling Adequacy		0.726
Bartlettis Test of Sphericity	Chi-Square	89.074
	Degree of freedom	33
	Significance level	< 0.001

The total variance explained by factor analysis is presented in table 2.4. Eleven original components/ factors are derived, which is relative to the number of the original variables. Concerning the criterion of *eigenvalue* > 1.0, the first three components/factors contribute much to this solution and form the extraction, accounting for 69.89%, 61.02% and 61.22% of the total variance using PCA, ML and ULS, respectively. PCA forms the basis of the factor analysis, and is mainly used to extract the dominant components. Compared with the proportion of the total variance by PCA, a decrease appears when using the other two extraction methods. The eigenvalues are also different using ML and ULS from those when using PCA.

From the component loadings by PCA, the first three components should be explored. However, from the factor loadings by ULS and ML, the eigenvalues of the third component are not satisfied with the criterion, so only the first two components are required to be investigated.

Table 2.4: Eigenvalues and total variance explained by the factor analysis (PCA, ULS and ML)

Component	Initial Eigenvalues			Extraction Sums of Squared Loadings by PCA		Extraction Sums of Squared Loadings by ULS		Extraction Sums of Squared Loadings by ML	
	Total	% of Variance	Cumulative %	Total	% of Variance	Total	% of Variance	Total	% of Variance
1	4.157	37.788	37.788	4.157	37.788	3.883	35.302	3.611	32.826
2	2.509	22.808	60.596	2.509	22.808	2.138	19.437	2.295	20.868
3	1.022	9.295	69.891	1.022	9.295	0.713	6.484	0.806	7.326
4	0.876	7.967	77.858						
5	0.724	6.579	84.437						
6	0.455	4.139	88.576						
7	0.401	3.649	92.225						
8	0.354	3.222	95.447						
9	0.266	2.421	97.868						
10	0.143	1.298	99.166						
11	0.092	0.834	100.000						

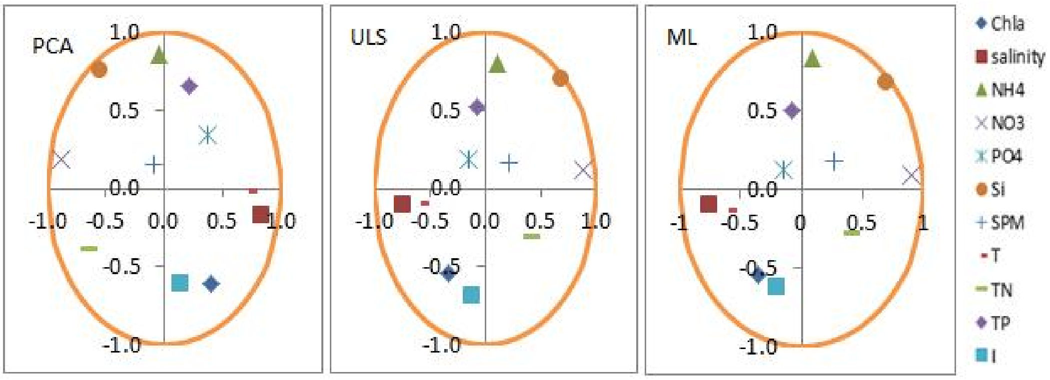

FIGURE 2.4: Target diagram for the first two rotated component/factor loading matrix from three extraction methods, determined by the 2000-2009 dataset in the Wadden Sea near Lauwersoog (x-axis: first component; y-axis: second component)

The components vary within the standard range of [-1.0, +1.0]. The closer is to the boundary value, the higher contribution is to the phytoplankton biomass, negatively or positively. In figure 2.4, the target diagrams for the first two rotated component/factor loadings from three extraction methods are displayed. From the basic extraction method of PCA, the first component, with an eigenvalue of 4.157, explains 37.8% of the total variance. In the unrotated space, it is mainly driven by the variables of NO_3 (-0.852) and T (0.815), while NO_3 denotes a high negative contribution. In the rotated space (Varimax with Kaiser normalization), it is mainly driven by the variable of NO_3 (-0.887). The second component, with an eigenvalue of 2.509, accounting for 22.8% of the total variance, is dominated by the variable of NH_4 (0.763 in the unrotated space and 0.860 in the rotated space). From the extraction method of ULS, the first factor, with an eigenvalue of 3.883, explains 35.3% of the total variance. The driving variable is NO_3 (0.881). The second factor, with an eigenvalue of 2.138, accounting for 19.4% of the total variance, is dominated by the variable of NH_4 (0.797). From the extraction method of ML, the first factor, with an eigenvalue of 3.611, explains 32.8% of the total variance. It is driven by the variable of NO_3 (0.903). The second factor, with an eigenvalue of 2.295, accounting for 20.9% of the total variance, is dominated by the variable of NH_4 (0.838).

Furthermore, the rotated component/factor score matrix is depicted in figure 2.5. This factor weight matrix is used to compute the factor scores. The contributions of the driving variables in this solution from three extraction methods correspond well with the rotated component/factor loading matrix in figure 2.4, although some changes appear in other variables.

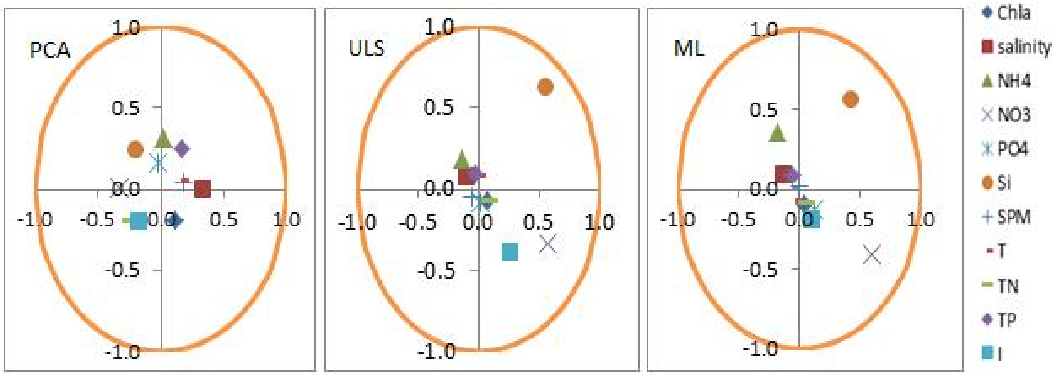

FIGURE 2.5: Target diagram for the first two rotated component/factor score matrix from three extraction methods, determined by the 2000-2009 dataset in the Wadden Sea near Lauwersoog (x-axis: first component; y-axis: second component)

2.2 Test case two: Estimate of the phytoplankton growth rate in the coastal waters of Lianyungang (CN)

2.2.1 Introduction

The commonly used estimate function of the phytoplankton growth rate is often linked with environmental variables, like nutrients (Flynn and Fasham [1997]; Geider et al. [1998]; Geider and La Roche [2002]; Örnólfsdóttir et al. [2004]; Davey et al. [2008]), temperature (Eppley [1966]; Eppley [1972]; Ratkowsky et al. [1982]; Thomann and Mueller [1987]; Bissinger et al. [2008]; Sal and López-Urrutia [2011]), light intensity (Smith [1980]), and also salinity and meteorological forcing (Marić et al. [2012]).

This case, the Lianyungang station, is located in the northeast of Jiangsu Province, China (figure 1.3). The area is a pool of the frequent blooms, with a rapid growth rate in spring and autumn (SOA: State Oceanic Administration People's Republic of China, accessing through http://www.soa.gov.cn/zwgk/hygb/). This research aims to explore a simplified estimate function of the phytoplankton growth rate, incorporating the temperature-growth function into the photosynthetic light curve.

2.2.2 Data information at Lianyungang station

Data information of the associated variables used in this study is derived from the NASA data (accessible through http://oceancolor.gsfc.nasa.gov/cms/), processed

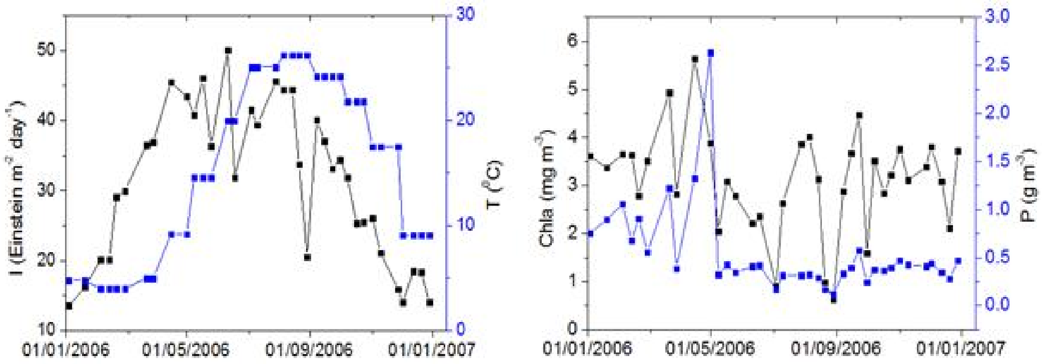

FIGURE 2.6: Time series variations of the associated variables (I, T, $Chla$, P) at Lianyungang station, monitored either weekly or biweekly over the year of 2006.

with the SeaDAS 7.0. Figure 2.6 displays the annual variations of the variables (I, T, $Chla$, P) over the year of 2006 in the Lianyungang coastal waters.

Temperature and light intensity show seasonal variations. The maximum temperature, up to 27 ^0C, appears in August, while the peak moment of the light intensity appears in June. Chlorophyll a varies from 0.63 $mg\ m^{-3}$ to 5.64 $mg\ m^{-3}$, with a mean value of 3.10 $mg\ m^{-3}$ and a standard deviation of 1.03 $mg\ m^{-3}$. The maximum chlorophyll a appears on 15th April. From the values of the chlorophyll a and the phytoplankton biomass (figure 2.6), we can distinguish that a rapid phytoplankton growth occurs in April. The frequently used estimate functions of the phytoplankton growth rate are summarized in table 2.5. In which, r' indicates growth rate constant, b' indicates the regression coefficient, and T_0 indicates a reference temperature (20 ^0C).

TABLE 2.5: Summary of the commonly used estimate of the specific growth rate

Function	Reference
$\mu = \frac{1}{\Delta t} log_2 \left(\frac{C/Chla + \Delta C/Chla}{C/Chla} \right)$	Eppley [1972]
$\mu_{max} = 0.59e^{0.0633T}$	Eppley [1972]
$\mu_{max} = 0.81e^{0.0631T}$	Bissinger et al. [2008]
$\sqrt{r'} = b' (T - T_0)$	Ratkowsky et al. [1982]
$\mu = \mu_{max}(1.066)^{T-20}$	Thomann and Mueller [1987]
$\mu = (0.0868 \frac{C}{Chla} I^{-1} + 10^{0.230-0.0275T})^{-1}$	Smith [1980]

2.2.3 Estimate function of the phytoplankton growth rate

The simplest photosynthetic light curve is described as (Steele [1962]):

$$P' = \frac{P_{max}I}{K_{1/2}+I} \tag{2.1}$$

The simple transformation of the light curve to the specific growth function is described after Huisman et al. [1999], stating that the ratio of $\frac{P'}{P_{max}}$ is asymptotic to the ratio of $\frac{\mu}{\mu_{max}}$.

Substituting the μ_{max} after Eppley [1972] into the light curve, the specific growth rate is derived as ($K_{1/2} = 30$):

$$\mu = 0.59e^{0.0633T}\frac{I}{I+30} \tag{2.2}$$

Additionally, the light intensity over the water depth follows the Lambert-Beer's Law, written as:

$$I_z = I_0 exp(-K_d z) \tag{2.3}$$

This law has been validated by the measurements after Liu et al. [2012] in the Subei Bank along the Jiangsu coast.

When the growth rate is balanced by the loss rate, the compensation light intensity I_{cr} is captured from the equation of $\mu - l = 0$, written as:

$$I_{cr} = \frac{1}{0.65exp(0.0633T) - 0.03} \tag{2.4}$$

Another important indicator, the net growth rate of the phytoplankton, is introduced (Schnoor and Di Toro [1980]; Behrenfeld [2010]), defined as an increase of the phytoplankton biomass with respect to the time interval:

$$k = ln[P(z,t_2)/P(z,t_1)]/(t_2 - t_1) \tag{2.5}$$

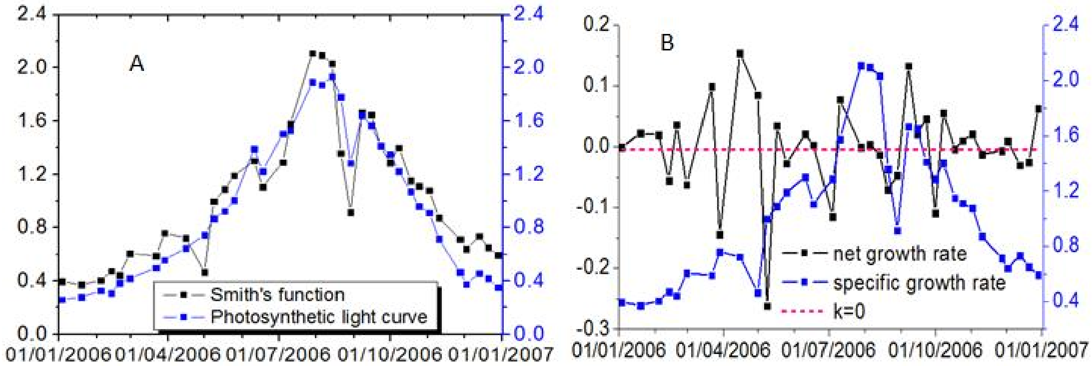

FIGURE 2.7: Estimate of the phytoplankton growth rate, expressed in day^{-1}. In which, graph A denotes the comparison of the specific growth rate between the photosynthetic light curve and Smith's function; graph B denotes the variations of the specific growth rate and the net growth rate over the year of 2006 in the Lianyungang coastal waters. The red dashed line indicates a balance of $k = 0$.

k is a comprehensive coefficient caused by the phytoplankton growth, mortality, respiration, sinking and predation. When $k = 0$ is satisfied, there is no net growth or loss from the previous time. Our concern is the condition of $k > 0$.

2.2.4 Discussion

Most of the data information is confined to the surface layer. The estimate function of the specific growth rate is obtained from equation (2.2). Compared with the estimate of Smith's function, there is no big difference between these two estimates, displayed in figure 2.7 (A). The maximum specific growth rate is around 2.0 day^{-1}, corresponding well with the view of Jorgensen [1979] and Arhonditsis and Brett [2005]. The specific growth rate also shows a seasonal variation, following the trends of I and T. But k shows a totally different fluctuation, presented in figure 2.7 (B). When the values of k are around 0, there is a balance stating that there is no net production or destruction from the previous time. Positive k values however reveal the relative increase of the phytoplankton biomass. It is noted that the variation of μ is small relative to k.

The concept of the compensation light intensity is the minimum demand of the light intensity to support the phytoplankton growth. The euphotic depth Ze is defined as a special zone in the water column. A lower I_{cr} corresponds to a deeper Ze.

In the analysis of the phytoplankton growth rate, the associated variables are not only I and T, but also the ratio of $C/Chla$, $Chla$, P, K_d, and Ze. The effects of the variables on μ and k are analyzed using regression analysis, displayed in table 2.6. When all variables are considered, the correlation coefficient r reaches the maximum, 0.975 for μ and 0.716 for k. The effects on μ are larger than that on k. The variables of I and T contribute much to the specific growth rate , but little to the net growth rate k.

TABLE 2.6: Model summary of regression analysis for the specific growth rate and the net growth rate

	Dependent variable: μ				dependent variable: k			
Model	R	R^2	Adjusted R^2	Std. Error	R	R^2	Adjusted R^2	Std. Error
1	0.891^a	0.794	0.788	0.227	0.031^a	0.001	-0.028	0.078
2	0.920^b	0.846	0.837	0.199	0.089^b	0.008	-0.052	0.078
3	0.936^c	0.875	0.864	0.182	0.064^c	0.409	0.354	0.061
4	0.967^d	0.936	0.927	0.133	0.707^d	0.5	0.436	0.057
5	0.968^e	0.937	0.926	0.134	0.708^e	0.501	0.417	0.058
6	0.973^f	0.948	0.937	0.124	0.716^f	0.513	0.412	0.058
7	0.975^g	0.95	0.937	0.123	0.716^g	0.513	0.391	0.06

a. Predictors: (Constant), T
b. Predictors: (Constant), T, I
c. Predictors: (Constant), T, I, $Chla$
d. Predictors: (Constant), T, I, $Chla$, P
e. Predictors: (Constant), T, I, $Chla$, P, K_d
f. Predictors: (Constant), T, I, $Chla$, P, K_d, Ze
g. Predictors: (Constant), T, I, $Chla$, P, K_d, Ze, $C/Chla$

With the regreesion analysis, μ is significantly correlated with T, and is moderately correlated with I, Ze, and $C/Chla$. The relationships between or among the variables of K_d, Ze, and I can be explained by the Lambert-Beer's Law. With respect to uncertainty, the Bootstrap method is introduced to describe the random effects. Within the 95% confidence interval, the correlation coefficient between μ and T varies at a range of [0.812, 0.948], while [0.376, 0.810] between μ and I, [0.056, 0.544] between μ and Ze, [-0.754, -0.411] between μ and $C/Chla$.

Chapter 3

Application of the BLOOM II model

3.1 Introduction

Concepts to describe the dynamics of phytoplankton in coastal waters are related to the effects of environmental variables, which has been discussed in chapter 2. In general, the field measurement of the phytoplankton biomass is time consuming and an expensive work. The most common issue is only a limited number of observations to explain the phytoplankton processes. The better approach is to fully analyze the limited observations and to interrogate the possible estimates of the ecological factors. Thus, there is an increasing demand of the operational tools that provide quick and inexpensive paths to investigate the phytoplankton. The BLOOM II model (one module of the Delft3D modelling suite), applied in this study, reveals the importance of coupling the hydro-sediment model with the ecological model, leading to a more realistic estimate of the phytoplankton biomass (Hydraulics [1991]; Hydraulics [2003]; Los et al. [2008]; Los [2009]).

The present study is performed to the case of the Frisian Inlet, location map shown in figure 1.2. The investigation of the phytoplankton biomass here is in terms of chlorophyll a. One objective is to predict the annual variation of the phytoplankton biomass and to pay attention to the phytoplankton biomass in response to nutrient availability, determined by the dataset in 1992. Researchers have proposed the relevant studies. Franks [1997], and Kishi and Ikeda [1986] describe the coupled physical-biological or physical-chemical-biological equations which imply the Monod-like responses of the phytoplankton to the changes of the nutrient concentrations. Villars et al. [1996] develop a model study to assess the reference conditions and the responses to the nutrient loadings in the Dutch coastal waters. Blauw and Los [2004] perform the research on the responses of the phytoplankton to the nutrient reductions in the Dutch coastal waters. The second objective of this study is to give insight in the model prediction subject to uncertainty, given that little research on uncertainty analysis of the phytoplankton biomass has been carried out in this area.

3.2 Methodology

3.2.1 Description of the BLOOM II model

BLOOM II is a multi-species ecological model, based on an optimization technique, which distributes the available resources in terms of nutrients and light intensity among the algae types (Los and Brinkman [1988]; Hydraulics [1991]; Hydraulics [2003]; Los and Wijsman [2007]; Los et al. [2008]; Los [2009]). It combines water movement and sediment fluxes. BLOOM II characterizes the species such as marine diatoms, green algae, flagellates, phaeocystis, cyanobacteria and dinoflagellates. The species have different resource demands and ecological properties. According to the classical theories, the yield of each species will be limited by only one factor at a time. Algal species living in the water column (phytoplankton) and sediment can be contained with their specific eco-physiological characteristics.

The BLOOM II model can be applied in any water body to simulate the phytoplankton processes in the water column (detailed information is shown in Appendix A).

3.2.2 Bayesian Markov Chain Monte Carlo (BMCMC)

In ecological modelling, a large amount of information on the ecological factors will be needed. The information requires us to translate the real-world into valuable information. There are two types of information: non-deterministic (probabilistic) and deterministic. The deterministic method simplifies the actual problems and tries to find a shortcut which will underestimate or overestimate the observations, while the probabilistic method provides much more reliable information because it considers the uncertainty of the natural variations or models. It is possible to take these uncertainties into account in a probabilistic approach, whereas the deterministic approach always takes a safe assumption as a beginning.

In this case, we distinguish the influences of the (uncertain) factors and processes on the final results including the uncertainty of model inputs using the Bootstrap method and the uncertainty of the model output using the BMCMC simulation.

Three situations need to be discerned in the BLOOM II model application: abundant data, only few data, or no data. The common case is the second, few but insufficient data, and hence the need is to incorporate the model results with the observations. Stressing the uncertainty of the model results, the Bayesian theory is proposed. We could estimate the parameters on the basis of the posterior distribution of the Bayesian inference. With a Bayesian approach, our understanding of the likelihood is described by a probability density function. The Bayesian theorem is composed of three parts: prior distribution, likelihood function and posterior distribution. The function is defined as:

$$\pi_1(y|x) = \frac{f(x|y)\pi_0(y)}{\int f(x|y)\pi_0(y)dy} \tag{3.1}$$

Where x is the known parameter, y is the unknown parameter of interest, $\pi_0(y)$ is the prior distribution, $f(x|y)$ is the likelihood function, and $\pi_1(y|x)$ is the posterior distribution.

The BMCMC simulation is a general purpose technique for generating fair samples from a probability in a high-dimensional space, using random numbers drawn from a uniform probability in a certain range. Two popular BMCMC algorithms are the Gibbs sampler and the Metropolis-Hastings algorithm. Bayesian inference using Gibbs sampling has been widely applied since the mid-1990s. The BMCMC simulation is a useful tool to develop a full description of the uncertainty (Kuczera [1999]; Oakley and Hagan [2004]; Reis and Stedinger [2005]; Kelly and Smith [2009]).

3.2.3 Cost-function

Undoubtedly, it is necessary before we apply the model to question: to what extent the phytoplankton biomass can be predicted with the BLOOM II model in this case? Thus, a model validation is performed. The paths for validation are conducted by graphically presenting the model output versus the observations, or the results from previous model exercises and then visually assessing the comparisons. One method called 'cost-function' is a mathematical function which provides a means of comparing the data from two different sources (Los et al. [2008]; Los [2009]; Blauw et al. [2009]). During the ASMO eutrophication modelling workshop different cost functions are put forward (Villars et al. [1996]). The use of cost-function is defined as:

$$\begin{aligned} C_x &= \frac{\sum |M_{x,t} - D_{x,t}|/12}{sd_M} \times (1-c) + c(1-r) \\ r &= \frac{COV(M,D)}{sd_M \times sd_D} \end{aligned} \tag{3.2}$$

The cost-function is classified as four standard levels: very good, good, reasonable and poor, the values defining as $[0, 1]$, $[1, 2]$, $[2, 3]$, and $[3, \infty]$ respectively.

3.3 BLOOM II model set-up at the Frisian Inlet

3.3.1 Hydrodynamic characteristics and ecological factors

The BLOOM II model is based on the hydrodynamic characteristics, the variations of which directly or indirectly influencing the distributions of the phytoplankton biomass. A refined curvilinear grid with 85×77 cells is generated in this case. For the vertical dimension, the water column is subdivided into 10 layers, 4.0%, 5.9%, 8.7%, 12.7%, 18.7%, 18.7%, 12.7%, 8.7%, 5.9%, and 4.0% (Los et al. [2008]), using a sigma-coordinated approach (Stelling and van Kester [1994]). In the BLOOM II model, three layers are integrated: the surface three integrated as the surface layer, the bottom three integrated as the bottom layer, and the middle four integrated as the middle layer. Two west boundaries, two north boundaries, and two east boundaries are set.

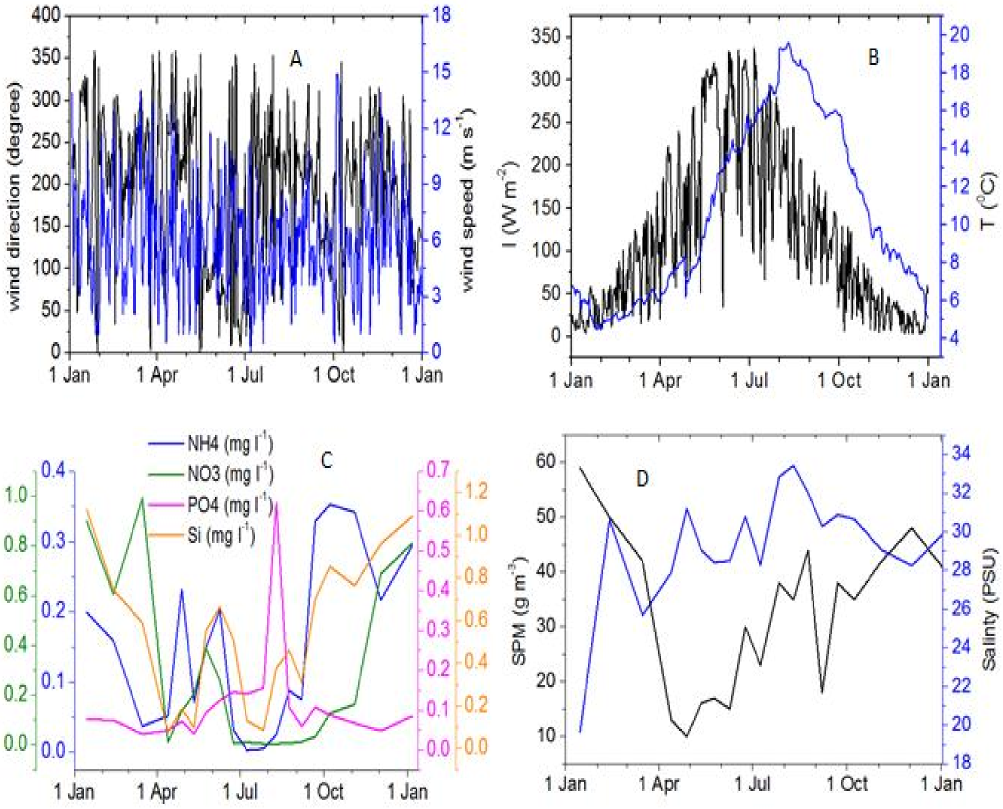

FIGURE 3.1: Observed driving forces used in the model, (A)Wind profile (speed: $m\ s^{-1}$, direction: degree), (B) I and T, (C) Annually variations of nutrients ($mg\ l^{-1}$), (D) salinity (SPU) and SPM ($g\ m^{-3}$). The sources of Figs of A and B are from the KNMI database, accessible through www.knmi.nl; Figs of C and D are from the DONAR database, at Lauwersoog station, accessible through http://live.waterbase.nl/waterbase_wns.cfm?taal=en.

Figure 3.1 displays the observed driving forces (wind profile, T, I, salinity, SPM and nutrients) in 1992. In this case, wind profile, T, and I are set as the model domain conditions, while other factors are set as the boundary inputs. I and T show seasonal variations, and the peak moments appear in the summer days. The maximum DIN ($NO_3 + NH_4$) reaches 1.0 $mg\ l^{-1}$ in winter while the target of DIN in the Wadden Sea and Wadden coast is defined as 0.46 $mg\ l^{-1}$ by the WFD (European Water Framework Directive) and 0.42 $mg\ l^{-1}$ by the OSPAR commission. Although extensive data have been collected, most of the data are confined to the surface water layer.

3.3.2 Model scenarios

The BLOOM II model aims to identify the phytoplankton processes, including light attenuation, nutrient distribution, phytoplankton growth, and transport of the substances.

Three layers are integrated in the model: surface layer, middle layer and bottom layer. Regarding the limiting factors (nutrient and light) of the phytoplankton, three phenotypes (energy type, nitrogen type and phosphorus type) are considered within the BLOOM II model (Hydraulics [1991]).

In this case, our concern is to investigate the annual variation of the phytoplankton biomass, specifically the response to nutrient availability, N-reduction (10%, 20%, 30%, 50%, 70%, and 90%), P-reduction (10%, 20%, 30%, 50%, 70%, and 90%), and both N- and P-reduction (10%, 30%, 50%, 70%, and 90%). The reference simulation is under 0% of the nutrient reduction. Specific extinction coefficients and the stoichiometric ratios of algal types used in the BLOOM II model are referred to after Los [2009].

3.4 Results

3.4.1 Observational analysis of the driving forces

Figure 3.1 has shown the variations of the major driving forces measured either biweekly or monthly. The random effects of these factors on the phytoplankton biomass are derived using the Bootstrap method, displayed in table 3.1. In chapter 2, the correlation analysis between chlorophyll a and other driving forces has been discussed, determined by the 10-year dataset from 2000 through 2009. Herein, the similar results are derived, determined by the dataset in 1992. In this study, chlorophyll a is strongly and significantly correlated with Si and NH_4, and moderately correlated with the variables of NO_3, T, I, and PO_4. We should pay more attention to these factors in further analysis. Note that 500 random samples are integrated into the Bootstrap calculation for each factor, deriving the estimate within the 95% confidence interval.

TABLE 3.1: Correlation matrix of chlorophyll a and other driving forces

					I	NH_4	salinity	NO_3	PO_4	Si	SPM	T
Chla	Pearson Correlation (r)				0.479	-0.714	0.371	-0.523	0.440	-0.732	-0.273	0.502
	Sig. (2-tailed) (p)				0.038	0.001	0.118	0.022	0.060	0.000	0.259	0.028
	Bootstrap	Bias			0.013	-0.009	-0.021	-0.017	-0.003	0.004	0.009	-0.180
		Std. Error			0.142	0.108	0.232	0.194	0.191	0.103	0.209	0.210
		95% CI	Lower		0.186	-0.877	-0.248	-0.850	-0.068	-0.892	-0.630	0.015
			Upper		0.758	-0.453	0.697	-0.132	0.720	-0.507	0.176	0.800

Table 3.2: Cost-function results of ten programs at the Frisian Inlet

programme	Harlingen	Lauwersoog	Huibertgat
salinity	1.0426	0.5637	1.1106
SPM	0.0389	0.4222	0.2859
NO_3	0.4203	0.7997	0.3016
NH_4	0.5788	0.5060	0.4493
PO_4	0.7482	0.3720	0.6185
Si	3.3355	0.4705	0.2599
BOD_5	1.3808	0.7040	0.2222
DO	1.0470	0.7786	0.2659
K_d	0.9275	1.0536	0.9917
$Chla$	1.0234	0.5736	1.7746

3.4.2 BLOOM II model output

Model validation

The more reliable model produces a better prediction of the phytoplankton biomass. Table 3.2 presents the cost-function results of ten programs (salinity, SPM, NO_3, NH_4, PO_4, Si, BOD_5, DO, K_d, and chlorophyll a) at three stations: Lauwersoog, Huibertgat, and Harlingen. It is concluded that 96.9% of the validation results have a good agreement, while only 3.1% are classified as poor. Compared with the values at Harlingen station and Huibertgat station, the model has a higher reliability at Lauwersoog station. We also can have a graphical view of the comparisons between the model results and the observations at Lauwersoog station, displayed in figure 3.2. The following discussion is explored at Lauwersoog station.

Analysis of the predicted environmental factors

As the phytoplankton biomass is strongly influenced by light intensity and light penetrates into the water column until self-shading occurs, the water property has a close relationship with K_d (Modenutti et al. [2000]; Devlin et al. [2008]). A higher turbidity corresponds to a higher K_d value. A linear relation between the predicted ($R^2 > 0.8$) or the observed ($R^2 > 0.4$) SPM and K_d exists which coincides well with the report by Devlin et al. [2008].

Secchi depth, closely related to the water turbidity in the water column, is another reliable water quality indicator (Lee et al. [2007]) and is used in the physical and biological modelling as a measure of the light penetration into the water body, inversely related

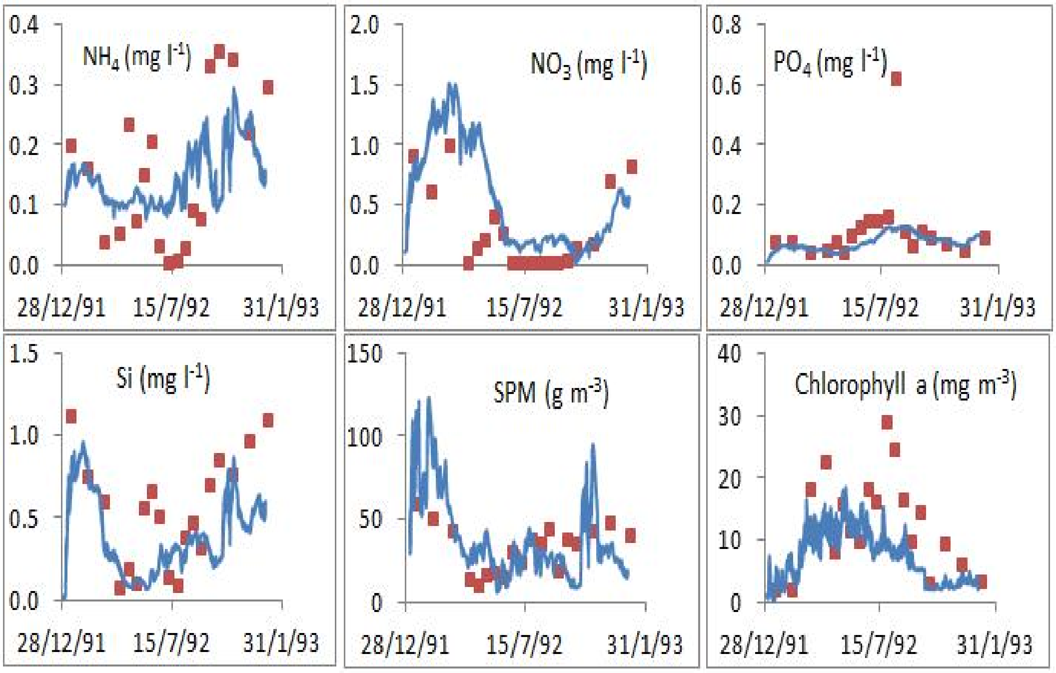

FIGURE 3.2: Graphical comparisons between the model results and the observations over the year of 1992 at Lauwersoog station. In which, the blue smooth lines indicate the model results, and the red scatters indicate the observations.

to the phytoplankton biomass. The relationships between I, K_d, and secchi depth can be explained by the Lambert-Beer's Law.

Chlorophyll a shows a large fluctuation during the whole year, with higher concentrations in spring and summer, and lower in winter. Light limitation often occurs in the winter days. In addition, the high turbidity increases the light limitation in this case until the light intensity is too low to support the phytoplankton growth.

Figure 3.3 shows the frequency distributions of two ecological factors (secchi depth and chlorophyll a) and a logarithmic relationship between them ($R^2 = 0.7113$). Chlorophyll a is fitted with a Gamma distribution, with a shape parameter of 1.605 $mg\ m^{-3}$ and a scale parameter of 0.281 $mg\ m^{-3}$. In order to better understand the ecological processes, it is necessary to have some basic understanding of the limiting factors of the phytoplankton growth. Only one limiting factor exists at a time so there is the need to know how the limiting factors vary in time and space. Light is the main limiting factor all year round especially in winter or in the higher turbidity zones.

Phytoplankton biomass in response to nutrient availability

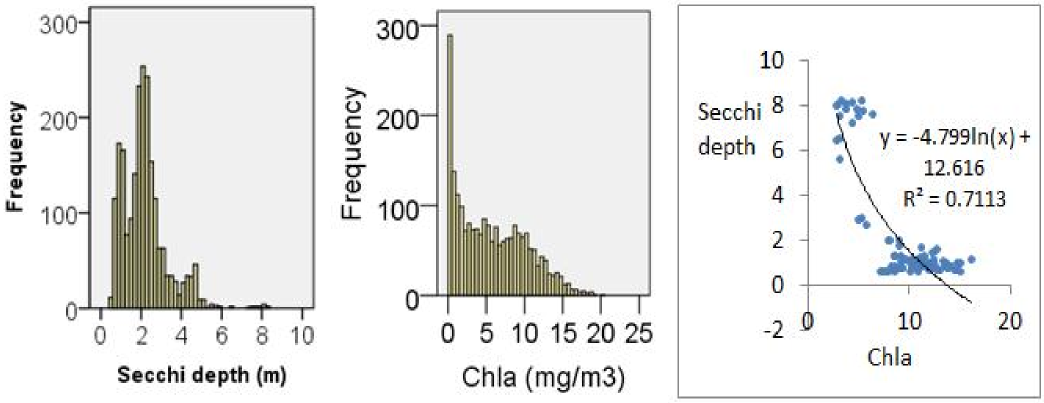

Figure 3.3: The first two graphs indicate the frequency distributions of secchi depth and chlorophyll a. The third graph indicates the secchi depth against chlorophyll a, using a non-linear function ($R^2 = 0.7113$)

As could be expected the nutrient concentrations decrease with nutrient reduction scenarios and so do the responses of chlorophyll a to a decrease of nutrients (table 3.3). If all other settings remain unchanged, chlorophyll a immediately decreases when the nutrient reduction occurs, but with a strong decrease rate at first and then tending to be relatively steady. Changes in chlorophyll a are assessed by comparing nutrient reduction results with the reference data. The maximum mean value ($\mu = 4.932\ mg\ m^{-3}$, $\sigma = 4.063\ mg\ m^{-3}$) happens at the N-90% scenario, while the minimum value ($\mu = 4.272\ mg\ m^{-3}$, $\sigma = 4.137\ mg\ m^{-3}$) is under both N- and P-90% scenario whereas there are small differences with the values of N-10%, N-50%, N-70%, and P-70%. Compared with the P-reduction (Dr: 17.4%-21.3%), the decrease rate of the N-reduction is relatively lower in this area (Dr: 16.8%-19.2%) and so phosphorus is the sensitive parameter to the phytoplankton species while the effects of chlorophyll a with both nutrient reductions are significant (Dr: 21.7%-28.0%).

Figure 3.4 illustrates the cumulative distribution functions of chlorophyll a response curve to the nutrient reductions. There are four pairs of probabilistic analysis: the reference scenario, the N-reduction scenario, the P-reduction scenario, both N- and P-reduction scenario.

3.4.3 BMCMC simulation

There is much information on the phytoplankton biomass given by the BLOOM II model although the general approximation of chlorophyll a (overestimate or underestimate) is

Table 3.3: Chlorophyll a in response to nutrient reduction (Dr: decrease rate)

Scenario	$Mean$ ($mg\ m^{-3}$)	SD ($mg\ m^{-3}$)	$Maximum$ ($mg\ m^{-3}$)	Dr
Reference	5.932	4.450	18.442	0.0%
N-10%	4.885	4.021	16.054	17.6%
N-20%	4.790	3.955	15.923	19.2%
N-30%	4.900	4.030	15.981	17.4%
N-50%	4.882	4.022	16.011	17.7%
N-70%	4.847	4.024	16.000	18.3%
N-90%	4.932	4.063	16.000	16.8%
P-10%	4.665	4.071	16.000	21.3%
P-20%	4.665	4.071	16.123	21.3%
P-30%	4.897	4.033	16.123	17.4%
P-50%	4.665	4.071	16.123	21.3%
P-70%	4.879	4.022	15.746	17.7%
P-90%	4.897	4.033	15.659	17.4%
Both-10%	4.644	4.064	15.896	21.7%
Both-30%	4.592	4.053	15.941	22.6%
Both-50%	4.556	4.077	15.924	23.2%
Both-70%	4.484	4.130	15.923	24.4%
Both-90%	4.272	4.137	15.903	28.0%

not very asymptotic to the actual data with respect to uncertainty. In this study, the uncertainty of the modelled chlorophyll a is approached using the BMCMC simulation, giving insight in the model output of the phytoplankton biomass. Bugs (Bayesian Inference Using Gibbs Sampling) is used to perform the simulation. Two Markov chains in parallel and 8000 random samples are proposed for the uncertainty analysis. The BMCMC statistics include the mean value, the standard deviation, the Monte Carlo standard error, and the 95% confidence interval. Figure 3.5 shows the probability distribution functions of the variables. Within the 95% confidence interval, the modelled chlorophyll a varies from 1.57 $mg\ m^{-3}$ to 10.11 $mg\ m^{-3}$, with a Monte Carlo error 0.04 $mg\ m^{-3}$; the prediction with uncertainty analysis varies from 0.18 $mg\ m^{-3}$ to 19.82 $mg\ m^{-3}$, with a Monte Carlo error 0.19 $mg\ m^{-3}$.

The Markov Chain Monte Carlo methods are convenient and flexible, but compare with other simpler methods, they involve two difficulties: running the Markov chains for a sufficiently long time for convergence, and having sufficient simulation draws for a suitably exact inference. Figure 3.6 displays the Gelman-Rubin convergence statistic, as introduced by Gelman and Rubin [1992] and modified by Brooks and Gelman [1998]. The Gelman-Rubin test is based on two chains and on a comparison of the within and between chain variances for variables. The normalized width of the central 80% interval

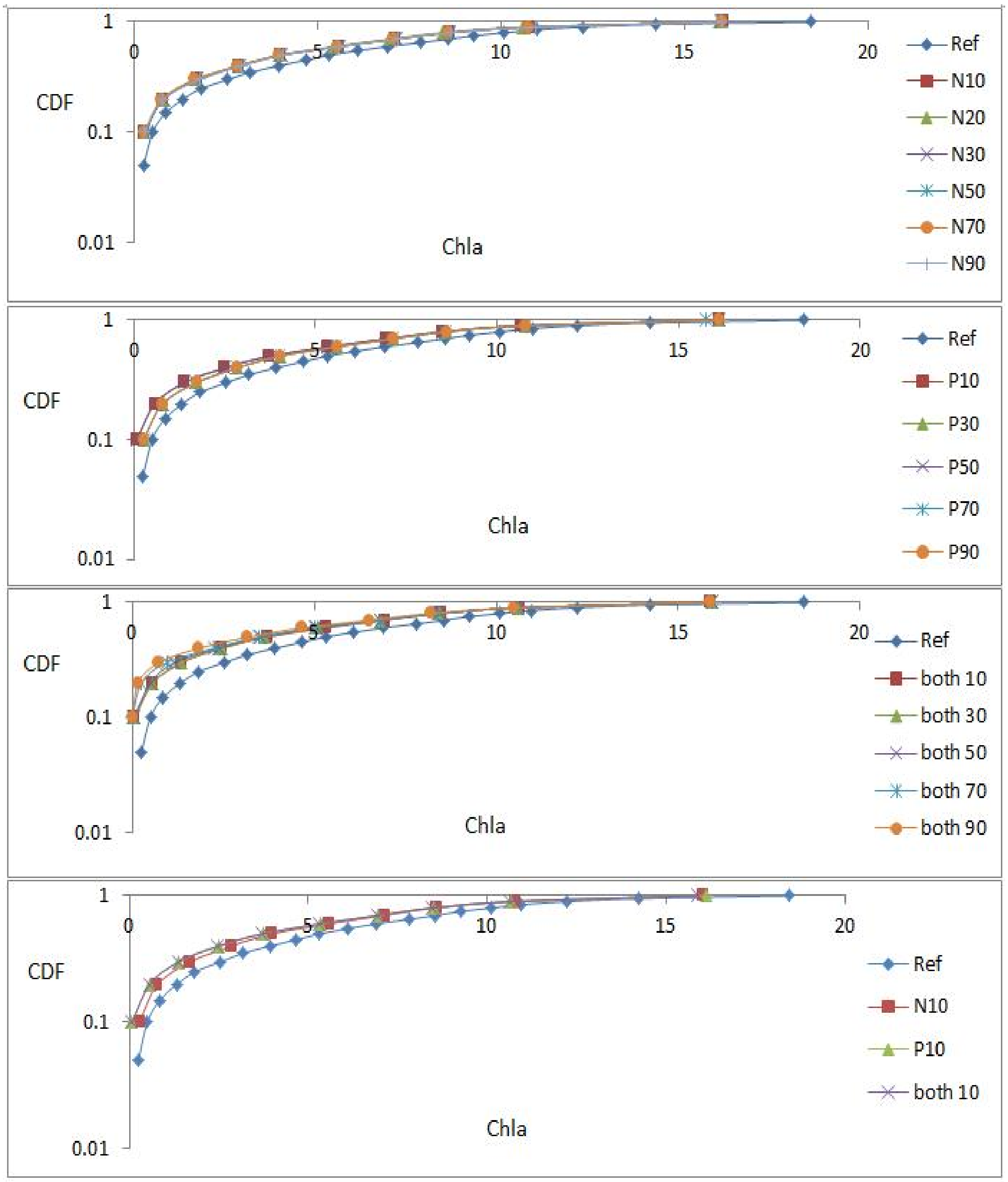

FIGURE 3.4: Cumulative density function (CDF, log scale) of chlorophyll a in response to nutrient availability

of the pooled runs is green, the average width of 80% intervals within the individual runs is blue, and their ratio R' is red; the convergence of R' should be approximately 1.

The complete trace plots of the predicted chlorophyll a of chain 1:2 are shown in figure 3.7, with 5000 random samples. They all fluctuate around a Gamma distribution, with $\mu = 5.956\ mg\ m^{-3}$ and $\sigma = 5.242\ mg\ m^{-3}$.

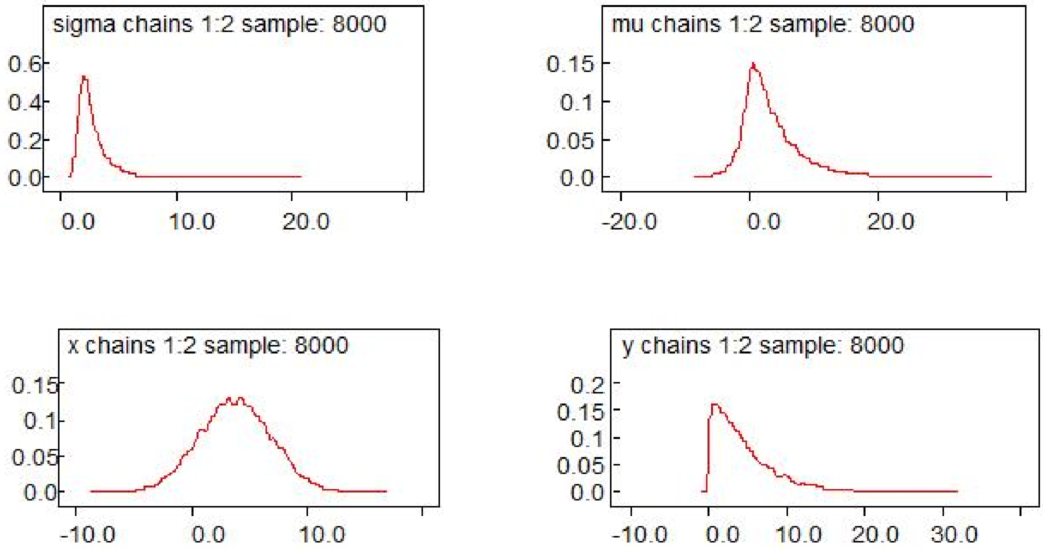

Figure 3.5: Density of chlorophyll a in the BMCMC simulation, expressed in $mg\ m^{-3}$. In which, x denotes the modelled chlorophyll a; y denotes the prediction with uncertainty analysis.

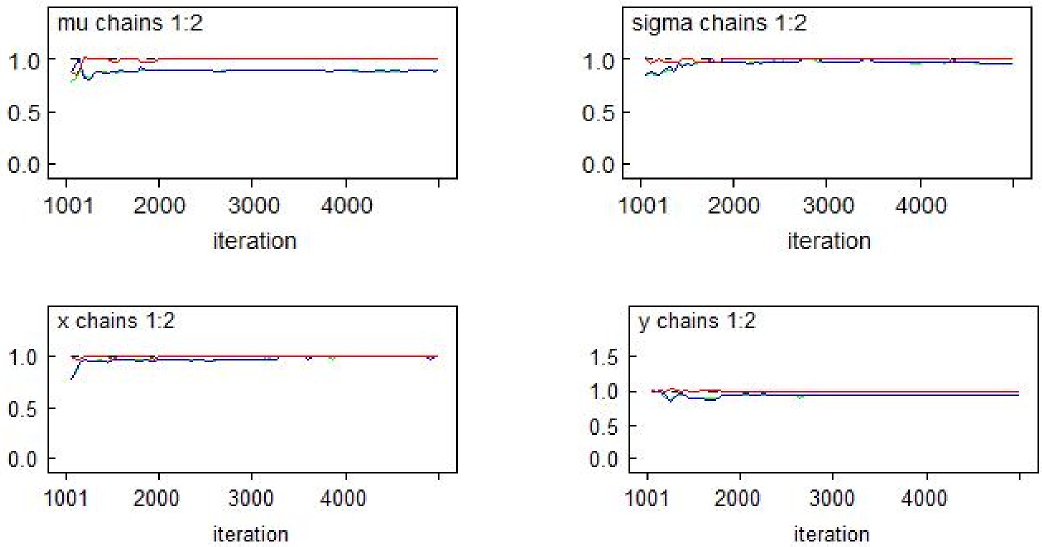

Figure 3.6: Gelman-Rubin convergence statistics in the BMCMC model. The green line indicates the normalized width of the central 80% interval of the pooled runs; the blue line indicates the average width of 80% intervals within the individual runs; the red line indicates the ratio of the green line to the blue line.

3.5 Discussion

The present study introduces the ecological model of BLOOM II which could be applied in any water system to predict the annual variation of chlorophyll a. It is a useful instrument for the coastal ecosystem management.

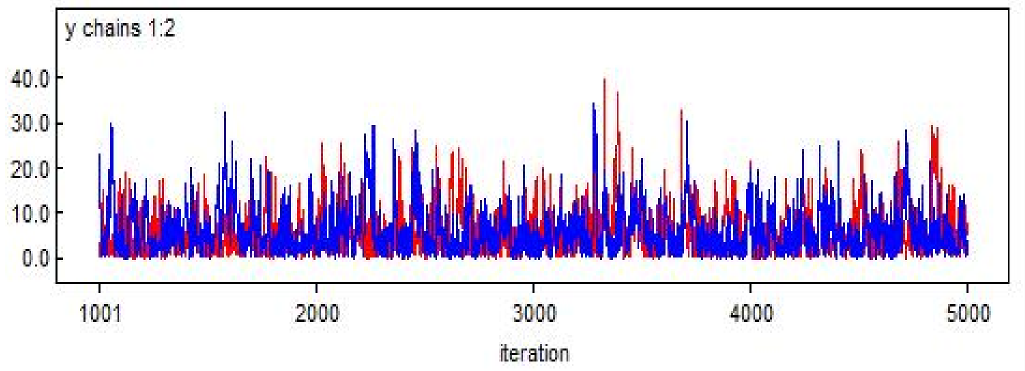

FIGURE 3.7: Trace plots of the predicted chlorophyll a, expressed in $mg\ m^{-3}$

The applicability analysis of the BLOOM II model is conducted using a 'cost-function' which has been applied for a station specific to the Dutch coast (Villars et al. [1996]; Radach and Moll [2006]; Los et al. [2008]; Los [2009]; Blauw et al. [2009]). Ten programs are involved in the validation (salinity, SPM, NO_3, NH_4, PO_4, Si, BOD_5, DO, K_d, and chlorophyll a). A smaller cost-function value indicates a better fit of the model results with the observations.

Phytoplankton biomass in response to nutrient availability is distinguished by the variations of chlorophyll a. In view of the target of the nutrients defined by the OSPAR Commission and the European Water Framework Directive (WFD), this work is especially valuable where different responses are derived with different nutrient reduction scenarios. The BMCMC simulation is to give insight in the prediction of the phytoplankton biomass, which is subject to the uncertainty. The observed chlorophyll a concentrations vary from 1.82 $mg\ m^{-3}$ to 28.9 $mg\ m^{-3}$, and the modelled values vary from 0.23 $mg\ m^{-3}$ to 18.44 $mg\ m^{-3}$ (figure 3.2 and figure 3.3), while the predictions with uncertainty vary from 0.18 $mg\ m^{-3}$ to 19.82 $mg\ m^{-3}$ within the 95% confidence interval and the maximum prediction reaches 30 $mg\ m^{-3}$ (figure 3.7).

Chlorophyll a is an important estimate of the phytoplankton biomass, however, the relationship between them, linearly or non-linearly, is not fixed but site-specific (Voros and Padisak [1991]; Felip and Catalan [2000]; Huot et al. [2007]). Therefore, the study of chlorophyll a cannot completely investigate the coastal ecosystem but also the study of phytoplankton.

Chapter 4

A vertical model study of phytoplankton dynamics

4.1 Introduction

The role of phytoplankton to a coastal ecosystem is significant and more attention has been paid to the interactions. Truscott [1995] examines the phytoplankton population in response to the environmental forcing. Franks [1997] describes the coupled physical-biological equations to examine the occurrence of the harmful algal blooms. Schmidt [1999] demonstrates the importance of the phytoplankton biomass as a key indicator of the coastal ecosystem in the western branch of the Oder-estuary. Boyer et al. [2009] discuss the nutrient limitation of the phytoplankton bloom in the Florida Bay ecosystem. Mei et al. [2009] assess how light and nutrients alter the growth rate of the phytoplankton species.

Since the BLOOM II model has been applied to investigate chlorophyll a in chapter 3, problems are still accompanied. The BLOOM II model has a higher resouce demands, including nutrients, light intensity, and species composition. The reliability of the phytoplankton biomass is hardly to be guaranteed wth the BLOOM II model when the ecological property of each species is unknown, especially when we are lack of nutrient information. As such, the mathematical phytoplankton models become available to investigate the phytoplankton. Evans and Parslow [1985] present a model to explain the annual cycle of the phytoplankton population. Skogen et al. [1995] use a coupled three-dimensional physical-chemical-biological ocean model to study the primary production. Chen et al. [1997] apply the coupled physical-biological model to study the influence of the physical forces on the shelf ecosystem. Edwards and Brindley [1996] develop the plankton model to examine the sensitivities to model complexity and to parameter values. Franks [2002] reviews the NPZ models, including the construction, coupling to a physical model, and the application in oceanography.

In this study, another convenient modelling approach, phytoplankton model, is introduced to investigate the vertical distributions of the phytoplankton biomass, reducing the three-dimensional model to a one-dimensional model (in the vertical direction). With the well-known simplification of the model, the predictions over a certain area and a certain time have a large uncertainty. Stressing the uncertainty arising from the model results, the BMCMC simulation is approached to give insight in the model output within the 95% confidence interval.

4.2 Phytoplankton model

In the general form, the characteristics of phytoplankton dynamics are coupled with a physical model (advection-diffusion equation), written as:

$$\frac{\partial C}{\partial t} + u_x\frac{\partial C}{\partial x} + u_y\frac{\partial C}{\partial y} + (u_z+u_s)\frac{\partial C}{\partial z} = E_h\left(\frac{\partial^2 C}{\partial x^2} + \frac{\partial^2 C}{\partial y^2}\right) + E_z\frac{\partial^2 C}{\partial z^2} + Phytoplankton\ dynamics \tag{4.1}$$

Further, phytoplankton dynamics has been described by researchers (Steele and Henderson [1992]; Edwards [2001]; Franks [2002]; Tian et al. [2005]) in the form of

$$\begin{aligned} \frac{\mathrm{d}P}{\mathrm{d}t} &= \mu \times P - g \times Z - l \times P \\ \frac{\mathrm{d}Z}{\mathrm{d}t} &= \gamma g \times Z - l' \times Z \end{aligned} \tag{4.2}$$

In which, γ indicates the assimilation rate and l' indicates the loss rate of the zooplankton.

Stressing the significance of the phytoplankton in the vertical direction, the vertical phytoplankton model follows the mathematical form of

$$\frac{\partial P}{\partial t} - E_z \frac{\partial^2 P}{\partial z^2} + (u_z + u_s)\frac{\partial P}{\partial z} = (\mu - l)P \tag{4.3}$$

In the coastal ecosystem, the water column is divided into three layers: surface layer, euphotic layer and non-euphotic layer. The non-euphotic layer contains available nutrients but few living algae due to little light intensity. An important notion of the euphotic zone (Ze), sufficient light intensity existing to support the phytoplankton growth, is to distinguish the dominated activity of the growth or the death (Margalef [1978], Morel and Berthon [1989]; Claustre and Marty [1995]; Aarup [2002]; Lee et al. [2007]).

The vertical model study is available to grasp the features of the phytoplankton (Riley [1949]; Schnoor and Di Toro [1980]; Evans and Parslow [1985]; Franks [1997]; Wong et al. [2007]; Taylor and Ferrari [2011]). The asymptotic solution $P(z,t) = f(z)e^{kt}$ of equation (4.3) is provided by Di Toro [1974]. The form of $f(z)$ is written as:

$$f(z) = Ae^{az}(asin\sqrt{\lambda z} + \sqrt{\lambda}cos\sqrt{\lambda z}) \quad (z < Ze) \tag{4.4}$$

$$a = (u_z + u_s)/2E_z \tag{4.5}$$

$$\lambda = [\mu - (k + l)]/E_z - (u_z + u_s)^2/4E_z^2 \tag{4.6}$$

Where A is a constant defined by the initial condition, and k is the net growth rate of the phytoplankton, written as $k = ln[P(z,t_2)/P(z,t_1)]/(t_2 - t_1)$ (Schnoor and Di Toro [1980]; Cloern [1991]; Cloern [1996]; Behrenfeld [2010]). In this case, the estimate of k is derived from the function of $k = ln(Chla_2/Chla_1)/(t_2 - t_1)$.

To explore the practical solution of the vertical phytoplankton model (equation 4.3), the transfer functions need to be investigated: E_z, u_z, u_s, μ, and l. In which, u_s and l are referred to as constants, displayed in table 4.1. The vertical mixing process E_z can be performed with the Delft3D model which has been validated in this area and the neighbouring zones (Los [2009]; Blauw et al. [2009]; Niu and Van Gelder [2013]; Niu et al. [2015b]; Niu et al. [2015a]).

TABLE 4.1: Sinking rate and the components of the loss term considered in the model

Parameters	Symbol	Value	Unit	Source
Sinking velocity	u_s	[3E-6,3E-5]	$m\ s^{-1}$	Skogen et al. [1995]
Mortality rate of phytoplankton	s	0.07	day^{-1}	Blauw et al. [2009]; Los [2009]
Respiration rate	r_0	0.06	day^{-1}	Blauw et al. [2009]
Plant metabolic loss	f	0.07	day^{-1}	Evans and Parslow [1985]

*$l = s + r_0 + f$

4.3 Case study of the Frisian Inlet

Huibertgat station and Lauwersoog station are selected as proxies to conduct the analysis. Seven variables ($Chla$, NO_3, NH_4, PO_4, Si, SPM, and salinity) over the year of 2009, measured either biweekly or monthly, are collected from the $DONAR$ database, accessible through http://live.waterbase.nl/waterbase_wns.cfm?taal=en. Another three variables of I, T, and wind profile (speed and direction), measured daily, are collected from the $KNMI$ database, accessible through www.knmi.nl. Note that the variables of T, I, and wind profile are set as domain parameters, while the others are site-specific. In addition, the monitored data of euphotic depth (Ze) and area-averaged phytoplankton biomass are derived from the $NASA$ data, processed with the SeaDAS 7.0.

4.3.1 Observational analysis

The statistics of the variables over the year of 2009 is shown in table 4.2, including the minimum value (Min), the maximum value (Max), the mean value and the standard deviation (SD). At Lauwersoog station, chlorophyll a fluctuates around a big interval, 0.64-87.89 $mg\ m^{-3}$, with the mean value of 26.92 $mg\ m^{-3}$ and the standard deviation of 25.1 $mg\ m^{-3}$. The minimum chlorophyll a appeared on 18^{th} May and the maximum appeared on 17^{th} April. The dissolved nitrate ranges from 0.01 $mg\ l^{-1}$ to 0.53 $mg\ l^{-1}$, while 0.005-0.520 $mg\ l^{-1}$ for ammonium, 0.013-0.14 $mg\ l^{-1}$ for phosphorus and 0.03-1.42 $mg\ l^{-1}$ for silicate. Most of the ratios of N/P are lower than the optimal condition of 16:1 (Brzezinski [2004]), which indicates a nitrogen deficiency relative to the phosphorus.

The nutrients show a similar pattern at two stations, increasing in winter but decreasing quickly in spring.

Table 4.2: Statistics of the observed variables over the year of 2009

	Lauwersoog station				Huibertgat station			
Variables	Min	Max	Mean	SD	Min	Max	Mean	SD
$Chla$ ($mg\ m^{-3}$)	0.64	87.89	26.92	25.1	1.11	124	12.07	25.67
I ($W\ m^{-2}$)	4.51	354.63	123.5	97.3	4.51	354.63	123.5	97.3
T (^0C)	2.1	19.8	11.27	5.59	2.1	19.8	11.27	5.59
NO_3 ($mg\ l^{-1}$)	0.01	0.53	0.15	0.16	0.01	0.72	0.19	0.2
NH_4 ($mg\ l^{-1}$)	0.005	0.52	0.147	0.16	0.005	0.3	0.08	0.08
PO_4 ($mg\ l^{-1}$)	0.013	0.14	0.051	0.03	0.008	0.043	0.021	0.01
Si ($mg\ l^{-1}$)	0.03	1.42	0.47	0.4	0.01	0.9	0.28	0.27
N/P ([−])	0.22	21.6	7.41	6.8	1.35	51.43	14.1	14.28
SPM ($g\ m^{-3}$)	27	390	105	77.3	3.6	37	17.6	8.79
Salinity (PSU)	25.9	31.7	29.56	1.81	27.4	31.9	30.2	1.35
Wind speed ($m\ s^{-1}$)	0.2	13.1	5.38	2.55	0.2	13.1	5.38	2.55

At Huibertgat station, chlorophyll a varies from 1.11 $mg\ m^{-3}$ to 124 $mg\ m^{-3}$, with the mean value of 12.07 $mg\ m^{-3}$ and the standard deviation of 25.67 $mg\ m^{-3}$. The minimum appeared on 20^{th} February and the maximum appeared on 20^{th} April. The concentrations of the nutrients are lower than that at Lauwersoog station. It is to infer that the phosphorus limits the phytoplankton growth from November to March because the ratios of N/P are larger than the optimal condition during that time period.

In the light of the definition of the euphotic depth, the condition of $I_z/I_0 \geqslant 1\%$ should be satisfied (Margalef [1978]; Morel and Berthon [1989]; Claustre and Marty [1995]; Aarup [2002]; Lee et al. [2007]). Accordingly, few light penetrates into the non-euphotic zone, stating that the death is the main activity. In this case, the Lambert-Beer's law has been validated with the observations ($R^2 = 0.8959$), displayed in figure 4.1.

Moreover, the principal component analysis (PCA) is applied to discuss the relationship between the phytoplankton biomass (in terms of chlorophyll a) and the environmental variables, and to characterize the representative variables that represent most of the variance. The first three components are required to be extracted according to the criterion of $eigenvalue > 1.0$, accounting for 77.836% of the total variance. The components vary within the standard range of [-1, +1]. The closer is to the boundary, the more contribution is to this solution. The first two rotated component loadings are displayed in figure 4.2. The first component, with an eigenvalue of 3.801, explains 38.013% of the total variance, driven by the variable of light intensity (-0.918). The second component, with

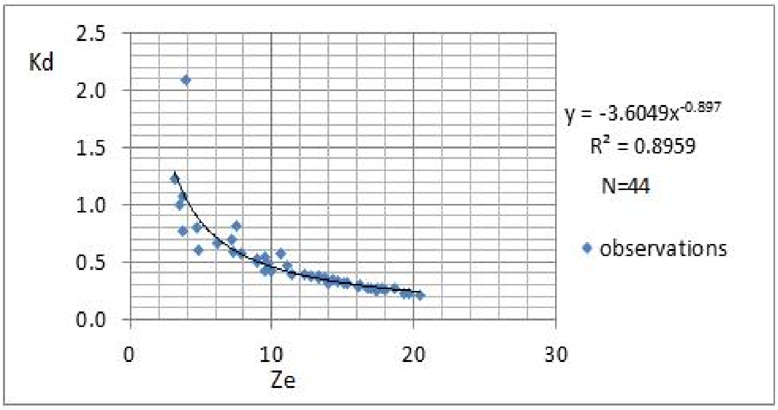

FIGURE 4.1: A function fits well with the observations ($I_z/I_0 \geqslant 1\%$) of light attenuation coefficient (K_d) and euphotic depth (Ze) at the Frisian Inlet. The light attenuation coefficient is caused by the phytoplankton growth and SPM at Lauwersoog station (high turbidity, table 4.2), but only by the phytoplankton growth at Huibertgat station.

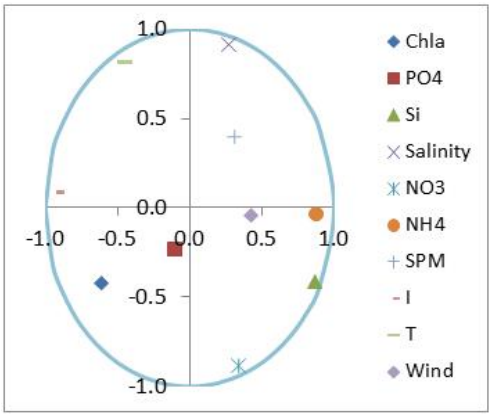

FIGURE 4.2: Component loadings in rotated space by the principal component analysis. In which, x-axis indicates the first component, and y-axis indicates the second component

an eigenvalue of 2.586, explains 25.864% of the total variance, driven by the variable of salinity (0.911). Therefore, of all the variables, light intensity and salinity contribute much to the phytoplankton biomass (in terms of chlorophyll a).

4.3.2 Parameter estimation

Estimate of the growth rate

In figure 4.3, the specific growth rate μ of the phytoplankton presents a seasonal variation over the year of 2009 (the black smooth line). Normally, the maximum value of the specific growth rate is around 2.0 day^{-1} in coastal waters (Arhonditsis and Brett [2005]). In this case, the maximum specific growth rate is 1.87 day^{-1} appeared on 18^{th} August

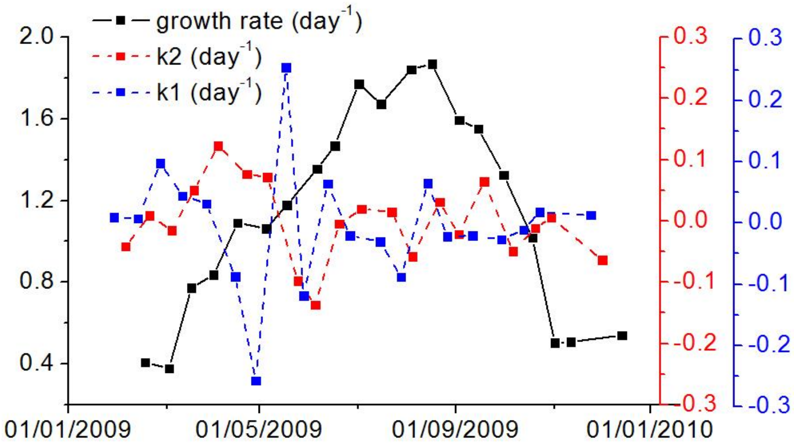

FIGURE 4.3: Annual variations of the specific growth rate (the black smooth line) and the net growth rate ($k1$: Lauwersoog station; $k2$: Huibertgat station), expressed in day^{-1}. The specific growth rate has a big potential range, varying from 0.38 day^{-1} to 1.87 day^{-1}. The net growth rate varies from -0.25 day^{-1} to 0.25 day^{-1} at Lauwersoog station, while -0.14 day^{-1} to 0.12 day^{-1} at Huibertgat station.

and the minimum is 0.38 day^{-1} appeared on 6^{th} March. The net growth rate k of the phytoplankton shows a completely different trend. The positive values of the net growth rate indicate the increased phytoplankton biomass from the previous time interval.

Estimate of the vertical turbulent diffusivity

The estimate of the vertical turbulent diffusivity is derived from the Delft3D model which has been validated in this case (Niu and Van Gelder [2013]; Niu et al. [2015a]; Niu et al. [2015b]). Graphical comparisons between Delft3D model results and observations over the year of 2009 are depicted in figure 4.4 (Niu et al. [2015a]). Figure 4.5 presents the estimated vertical turbulent diffusivity at the Frisian Inlet. In view of the specific demand, the phytoplankton species can be distinguished by the classification of Margalef (1978): the order of vertical turbulent diffusivity and nutrient availability. The order of the vertical turbulent diffusivity is 10^{-4} at Lauwersoog station, while 10^{-3} at Huibertgat station. Therefore, dinoflagellates and diatoms are equally significant at Lauwersoog station, while only diatoms are predominant at Huibertgat station.

4.3.3 Validation of the phytoplankton model

The graphical comparisons between the model output and the monitored phytoplankton biomass are displayed in figure 4.6. All of the values are confined near the surface layer in the area-averaged scale. The Delft3D model can reproduce the reliable levels

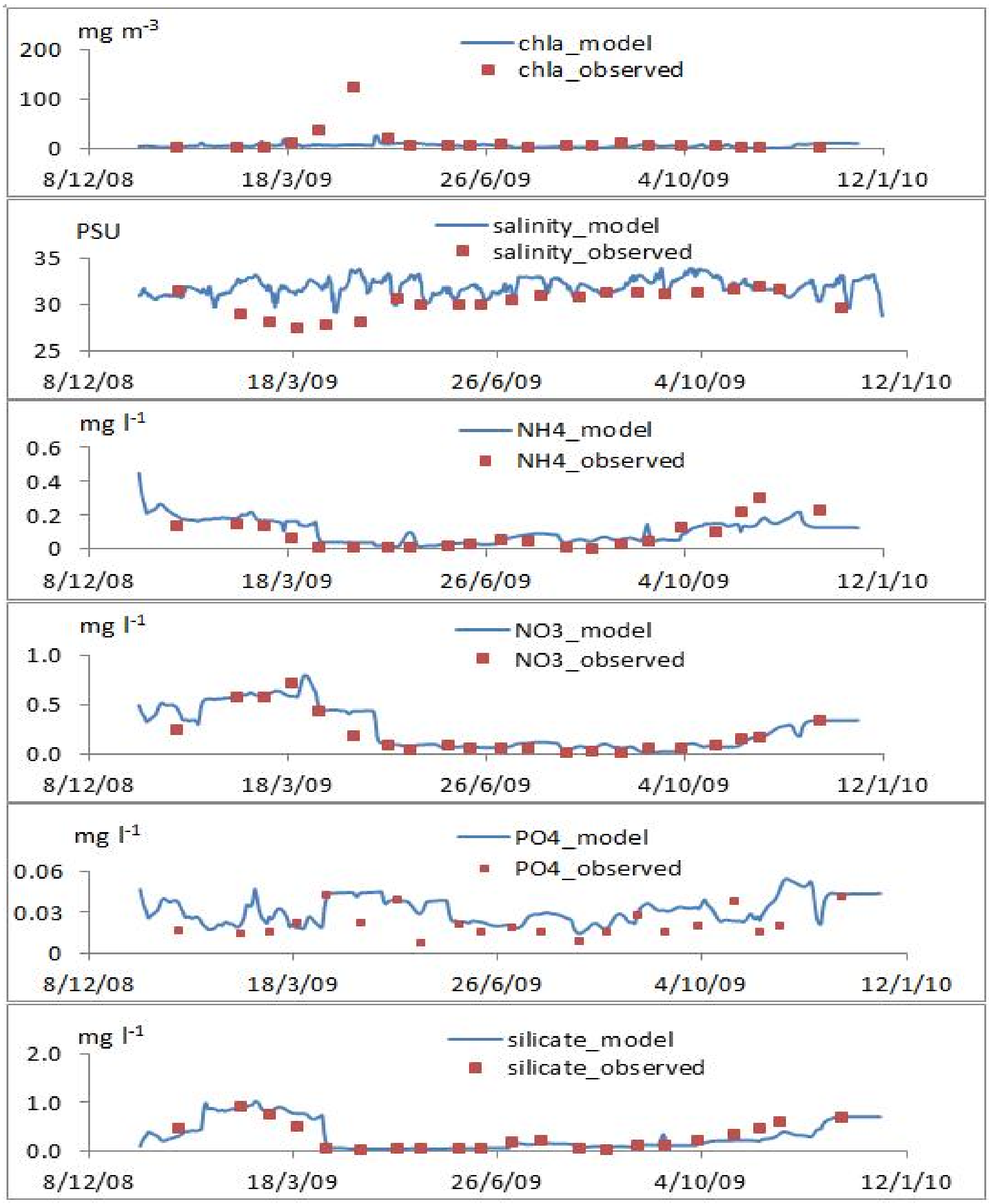

FIGURE 4.4: Graphical comparisons of chlorophyll a, salinity and nutrients between the Delft3D model output and the observations in 2009 at Huibertgat station

of chlorophyll a (figure 4.4) but only 40% agreement of the phytoplankton biomass when the properties of the species are unknown, while the vertical phytoplankton model reproduces 70% agreement. The vertical phytoplankton model is applicable in this case. The modelled phytoplankton biomass varies from 0.145 $g\ m^{-3}$ to 1.105 $g\ m^{-3}$, with the mean value of 0.44 $g\ m^{-3}$ and the standard deviation of 0.30 $g\ m^{-3}$. The monitored phytoplankton biomass varies from 0.17 $g\ m^{-3}$ to 1.40 $g\ m^{-3}$, with the mean value of 0.57 $g\ m^{-3}$ and the standard deviation of 0.26 $g\ m^{-3}$. The common disadvantage of

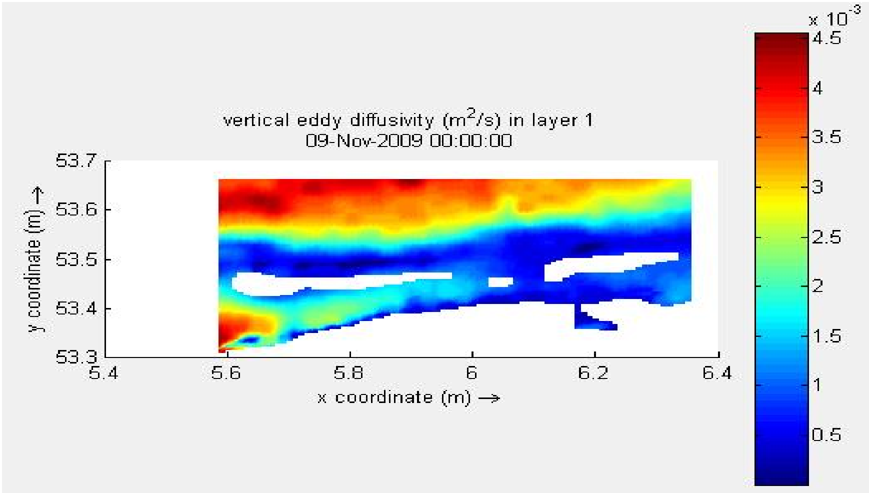

FIGURE 4.5: Estimate of the vertical turbulent diffusivity (E_z) with the Delft3D model at the Frisian Inlet, driven by the physical-chemical conditions and expressed in $m^2\ s^{-1}$. This factor is influenced by the tidal currents and the wind profile, mixing with the mass transport. The appropriate range of the vertical turbulent diffusivity can promote the phytoplankton growth (Margalef [1978]; Huisman et al. [1999]).

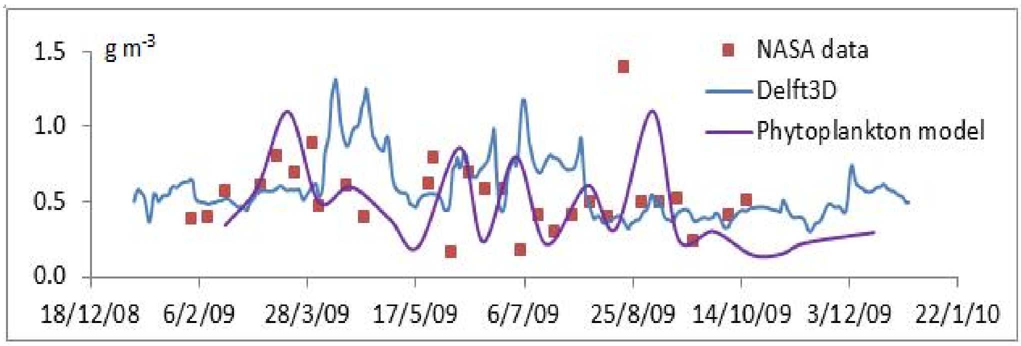

FIGURE 4.6: Graphical comparisons between model outputs (Delft3D model and vertical phytoplankton model) and monitored phytoplankton biomass in 2009 at the Frisian Inlet, expressed in $g\ m^{-3}$.

chlorophyll *a* and phytoplankton here is that they both indicate the characteristics of all the species.

4.3.4 Vertical distributions of the phytoplankton biomass

In this section, the general patterns of the phytoplankton biomass over water depth are illustrated. Table 4.3 reveals the statistical analysis of the model output for the different water depths (z=0m, 2m, 5m, 10m, and 20m) at Lauwersoog station, and gives insight in the prediction with uncertainty analysis using the Bootstrap method. At the surface layer, the phytoplankton biomass, ranging from 0.014 $g\ m^{-3}$ to 2.29 $g\ m^{-3}$, fits with chlorophyll *a* by a power function ($P = 31.43Chla^{0.67}$, $R^2 = 0.50$). In the early June, chlorophyll a rises sharply from 0.64 $mg\ m^{-3}$ to 80.27 $mg\ m^{-3}$ in the course of weeks, so does the pattern of the phytoplankton biomass increasing from 0.01 $g\ m^{-3}$ to 1.90 $g\ m^{-3}$. Higher values of the phytoplankton biomass appear in the months of March, April, July and September. Nutrients (NO_3, NH_4, PO_4, Si) show specific properties over the year. The lower values of the nutrients are in the months of May and August, accompanied with the rapid growth of the phytoplankton. Light intensity becomes limiting in winter, that constrains the phytoplankton growth regardless of sufficient nutrients (figure 4.4). Normally, the sharp decrease of nutrients happens during or before the bloom event and the followed increasing process indicates the end of the bloom event.

TABLE 4.3: Statistical analysis of the model output for the different water depths (z=0m, 2m, 5m, 10m and 20m) over the year of 2009 at Lauwersoog station, expressed in $g\ m^{-3}$

Lauwersoog		Statistic	*Bootstrap*[a]			
			Bias	Std. Error	95% CI	
					Lower	Upper
P(2)	Mean	0.291	0.003	0.066	0.179	0.438
	SD	0.294	-0.014	0.074	0.131	0.405
	Skewness	1.803	-0.315	0.709	-0.190	2.719
P(5)	Mean	0.452	0.006	0.130	0.240	0.729
	SD	0.573	-0.039	0.185	0.172	0.847
	Skewness	2.549	-0.497	0.771	0.571	3.675
P(10)	Mean	0.390	0.007	0.134	0.172	0.691
	SD	0.604	-0.036	0.178	0.190	0.871
	Skewness	2.405	-0.242	0.717	0.923	3.696
P(20)	Mean	0.569	0.009	0.128	0.348	0.851
	SD	0.578	-0.024	0.134	0.258	0.791
	Skewness	1.747	-0.216	0.555	0.550	2.831

a: unless otherwise noted, bootstrap results are based on 1000 bootstrap samples
**the object of the 95% CI in the bootstrap method is the estimate, like mean value, standard deviation, and skewness.*

For the water depth of 2m at Lauwersoog station, the phytoplankton biomass shows a relative small fluctuation, with the mean value of 0.291 $g\ m^{-3}$ and the standard deviation of 0.294 $g\ m^{-3}$. The maximum value is 1.11 $g\ m^{-3}$ appeared on 2^{nd} July. Higher values are concentrated in the months of March and July. Considering the uncertainty arising from the model, the mean value varies at a range of [0.178, 0.438] $g\ m^{-3}$ within the 95% CI. The positive skewness (1.803) indicates a long right tail in the distribution. The values follow a Gamma distribution, with a shape parameter of 0.978 $g\ m^{-3}$ and a scale parameter of 3.361 $g\ m^{-3}$.

For the water depth of 5m at Lauwersoog station, the phytoplankton biomass varies from 0.013 $g\ m^{-3}$ to 2.406 $g\ m^{-3}$, with the mean value of 0.452 $g\ m^{-3}$ and the standard deviation of 0.573 $g\ m^{-3}$. The maximum value occurred on 19^{th} March. Take the uncertainty into account, the mean value fluctuates at a range of [0.240, 0.729] $g\ m^{-3}$ within the 95% CI. For the water depth of 10m, the maximum value is 2.331 $g\ m^{-3}$ appeared on 19^{th} March, the same day as the depth of 5m. The average phytoplankton biomass is 0.390 $g\ m^{-3}$, varying at a range of [0.172, 0.691] $g\ m^{-3}$ within the 95% CI. For the water depth of 20m, the phytoplankton biomass varies from 0.007 $g\ m^{-3}$ to 2.260 $g\ m^{-3}$, with the mean value of 0.569 $g\ m^{-3}$. 80% of the values are less than 1.0 $g\ m^{-3}$.

Table 4.4 presents the statistical analysis of the model output for the different water depths (z=0m, 2m, 5m, 10m and 20m) at Huibertgat station. The values are smaller than that at Lauwersoog station. At the surface layer, the phytoplankton biomass, varying from 0.03 $g\ m^{-3}$ to 0.96 $g\ m^{-3}$, fits with chlorophyll a by a logarithmic function ($P = 0.2ln(Chla) - 0.05$, $R^2 = 0.70$)). In April, although chlorophyll a and the phytoplankton biomass all reach the peak values, the nutrients are decreasing sharply from 1.63 $mg\ l^{-1}$ to 0.22 $mg\ l^{-1}$.

TABLE 4.4: Statistical analysis of the annual cycles of the phytoplankton biomass for the different water depths (z=0m, 2m, 5m, 10m and 20m) over the year of 2009 at Huibertgat station, expressed in $g\ m^{-3}$.

Huibertgat		Statistic	*Bootstrap*[a]			
			Bias	Std. Error	95% CI	
					Lower	Upper
P(2)	Mean	0.215	0.000	0.576	0.105	0.338
	SD	0.263	-0.011	0.049	0.144	0.337
	Skewness	1.411	-0.012	0.586	0.411	2.823
P(5)	Mean	0.179	0.001	0.040	0.106	0.259
	SD	0.182	-0.008	0.035	0.099	0.234
	Skewness	1.427	-0.047	0.537	0.489	2.596
P(10)	Mean	0.163	0.002	0.039	0.088	0.245
	SD	0.182	-0.007	0.037	0.076	0.230
	Skewness	1.565	-0.006	0.624	0.471	3.102
P(20)	Mean	0.138	0.000	0.030	0.085	0.198
	SD	0.139	-0.006	0.026	0.079	0.177
	Skewness	1.394	-0.054	0.534	0.474	2.554

a: unless otherwise noted, bootstrap results are based on 1000 bootstrap samples

For the water depth of 2m at Huibertgat station, the mean value of the phytoplankton biomass is 0.215 $g\ m^{-3}$, varying at a range of [0.105, 0.338] $g\ m^{-3}$ within the 95% CI.

The maximum value of 0.678 $g\ m^{-3}$ occurred on 20^{th} March, while the minimum of 0.012 $g\ m^{-3}$ appeared on 19^{th} May. For the water depth of 5m, the phytoplankton biomass varies from 0.014 $g\ m^{-3}$ to 0.648 $g\ m^{-3}$, with the mean value of 0.178 $g\ m^{-3}$ and the standard deviation of 0.182 $g\ m^{-3}$. The maximum value appeared on 2^{nd} September and the minimum appeared on 16^{th} September. The model output for the water depth of 10m is similar to the water depth of 5m. For the water depth of 20m, the phytoplankton biomass varies from 0.008 $g\ m^{-3}$ to 0.497 $g\ m^{-3}$, with the mean value of 0.138 $g\ m^{-3}$ and the standard deviation of 0.139 $g\ m^{-3}$.

4.3.5 Depth-averaged phytoplankton biomass

In this section, the depth-averaged phytoplankton biomass at the Frisian Inlet is discussed, shown in table 4.5. At Lauwersoog station, the phytoplankton biomass fluctuates at a range of [0.009, 1.902] $g\ m^{-3}$. The mean value is 0.459 $g\ m^{-3}$, varying from 0.284 $g\ m^{-3}$ to 0.695 $g\ m^{-3}$ within the 95% CI. The phytoplankton biomass follows a Gamma distribution, with a shape parameter of 0.936 $g\ m^{-3}$ and a scale parameter of 2.037 $g\ m^{-3}$. At Huibertgat station, the phytoplankton biomass fluctuates at a range of [0.019, 0.663] $g\ m^{-3}$. The average phytoplankton biomass is 0.197 $g\ m^{-3}$, varying from 0.123 $g\ m^{-3}$ to 0.238 $g\ m^{-3}$ within the 95% CI. The values also follow a Gamma distribution, with the shape parameter of 1.099 $g\ m^{-3}$ and the scale parameter of 5.573 $g\ m^{-3}$.

Table 4.5: Statistical analysis of the depth-averaged phytoplankton biomass at the Frisian Inlet over the year of 2009, expressed in $g\ m^{-3}$

Depth-averaged		Statistic	*Bootstrap*[a]			
			Bias	Std. Error	95% CI Lower	95% CI Upper
$\overline{P_L}$	Mean	0.459	0.007	0.106	0.284	0.695
	SD	0.475	-0.024	0.124	0.163	0.668
	Skewness	2.053	-0.208	0.651	0.642	3.317
$\overline{P_H}$	Mean	0.197	0.001	0.041	0.123	0.280
	SD	0.188	-0.008	0.034	0.103	0.238
	Skewness	1.285	-0.059	0.512	0.344	2.422

a: unless otherwise noted, bootstrap results are based on 1000 bootstrap samples
$\overline{P_L}$*: the depth-averaged phytoplankton biomass at Lauwersoog station;*
$\overline{P_H}$*: the depth-averaged phytoplankton biomass at Huibertgat station;*

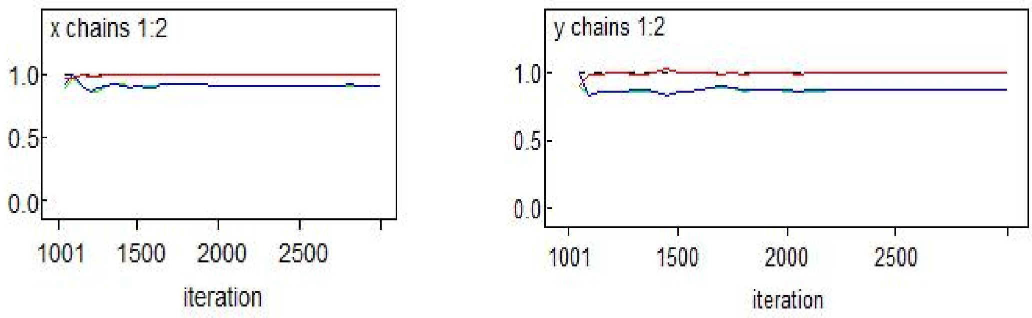

FIGURE 4.7: Gelman-Rubin convergence statistics. x denotes the model output; y denotes the prediction with uncertainty analysis. The normalized width of the central 80% interval of the pooled runs is green, the average width of the 80% intervals within the individual runs is blue, and their ratio R' is red.

4.3.6 Uncertainty analysis

Prior to the approaching of the BMCMC simulation in this case, the convergence is needed to be tested. Figure 4.7 displays the widely used Gelman-Rubin convergence statistics. Two chains are designed, and 2000 random samples are distributed to each chain. As described in chapter 3, the rule of the convergence is to keep the red line tended to 1. The BMCMC simulation is reliable in this case.

We stress the uncertainty of the model and perform the BMCMC simulation to give insight in the prediction with uncertainty analysis. Table 4.6 shows the important BMCMC statistics, including the mean value, the standard deviation, the Monte Carlo standard error (MC error) and the 95% CI. Compared with the 95% CIs in the BMCMC simulation and the Bootstrap method, we find out that there is a big difference between the values. Worth to point out that the object of the 95% CI in the Bootstrap method is for the estimates (like the mean value, the standard deviation, the skewness), while the object in the BMCMC simulation is for the whole dataset. Therefore, the 95% CI in the two methods has a different meaning. At Lauwersoog station, the modelled phytoplankton biomass varies from 0.010 $g\ m^{-3}$ to 1.721 $g\ m^{-3}$ within the 95% CI, with a MC error of 0.007 $g\ m^{-3}$; the prediction with uncertainty analysis varies from 0.006 $g\ m^{-3}$ to 1.526 $g\ m^{-3}$, with a MC error of 0.004 $g\ m^{-3}$. At Huibertgat station, the modelled phytoplankton biomass varies from 0.011 $g\ m^{-3}$ to 0.677 $g\ m^{-3}$ within the 95% CI, with a MC error of 0.002 $g\ m^{-3}$; the prediction with uncertainty analysis varies from 0.008 $g\ m^{-3}$ to 0.708 $g\ m^{-3}$, with a MC error of 0.001 $g\ m^{-3}$. Figure 4.8 shows

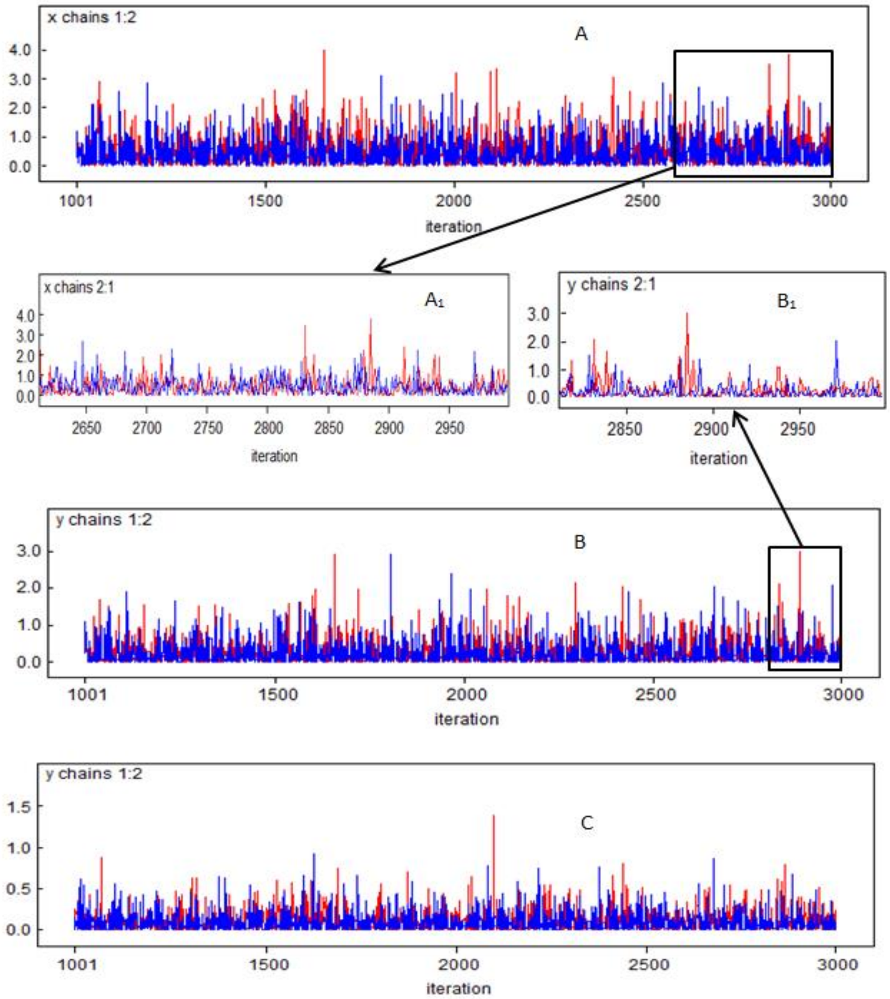

FIGURE 4.8: Trace plots of the phytoplankton biomass at the Frisian Inlet, expressed in $g\ m^{-3}$. Graph A displays the model output of the phytoplankton biomass at Lauwersoog station. Graph B displays the prediction with uncertainty analysis at Lauwersoog station. A_1 and B_1 are to zoom out the iterations of the prediction. Graph C displays the prediction with uncertainty analysis at Huibertgat station.

the completely trace plots of the model output with uncertainty analysis, based on 4000 samples.

TABLE 4.6: Node statistics of the depth-averaged phytoplankton biomass in the BMCMC simulation

	Node	Mean	SD	MC error	2.5%	Median	97.5%
Lauwersoog	x	0.459	0.475	0.007	0.010	0.299	1.721
	y	0.332	0.308	0.004	0.006	0.116	1.526
Huibertgat	x	0.200	0.188	0.002	0.011	0.145	0.677
	y	0.198	0.116	0.001	0.008	0.157	0.708

**the object of the 95% CI in the BMCMC simulation is the whole dataset*

4.4 Discussion

In this case, there is a low vertical mixing rate due to the semi-enclosed inlet position. The slow exchange between the tidal inlet and the North Sea also increases the water residence time, which promotes the phytoplankton growth. The vertical mixing process, playing an important role in the investigation of phytoplankton dynamics, is performed with the Delft3D model.

Comparing the model output with the monitored phytoplankton biomass, the application of the vertical phytoplankton model in this case is reliable. Higher values of the phytoplankton biomass appear in spring and in autumn, followed by the rapid reduction of the nutrients. The phytoplankton biomass at Lauwersoog station is higher than that at Huibertgat station. One reason is closely related to the concentration of the nutrients (figure 4.4). Another reason is that water exchange with the North Sea or the Wadden Sea is slower at Lauwersoog station, so longer residence time encourages the phytoplankton growth (figure 4.5).

The model output of the phytoplankton biomass are non-deterministic, which is subject to the uncertainty. In this case, we stress the uncertainty arising from the model results. The BMCMC simulation, as a useful tool to fully describe the uncertainty, is proposed to give insight in the prediction with an integration of uncertainty analysis, fluctuating at a reliable range within the 95% CI.

Chapter 5

Physical limitation of phytoplankton bloom development

5.1 Introduction

The notion of the phytoplankton bloom is in the forefront of the coastal ecosystem in the Chinese marginal seas, and has been better understood since 2000 (Tang et al. [2003]; Tang et al. [2006a]; Tang et al. [2006b]; Son et al. [2012]; Jin et al. [2013]). Phytoplankton bloom events are often visible and caused by population explosions in the course of days to weeks, the pigments of water colours showing the characteristics of the phytoplankton species (Smayda [1997]; Allen et al. [2008]; Allen and Wolfe [2013]). The major causes of the blooms are eutrophication (nutrient enrichment), an unbalanced ratio of N/P, and a favourable living environment. Phytoplankton blooms have become a common issue in coastal waters, frequently occurring in spring and in autumn, as well as occasionally in winter (Allen and Wolfe [2013]). The bloom events are thought to be globally increasing and have turned out to be a great threat to the coastal ecosystem, especially the so-called harmful algal blooms (Falkowski et al. [1991]; Van Dolah [2000]; Anderson et al. [2002]). Although most of the blooms are not poisonous, they can block the sunshine penetration into the water column and consume large amounts of oxygen, which can threaten the marine life. Therefore, it is necessary to be aware of the phytoplankton bloom development in coastal waters. Within the course of a year, the bloom events follow an annual cycle, accompanied with the cycles of phytoplankton and zooplankton (Evans and Parslow [1985]; Steele and Henderson [1992]; Behrenfeld [2010]).

This study proposes the modelling approach, as described in chapter 4, to give insight in the phytoplankton variability and to extend the application to investigate the bloom development. The trigger of the phytoplankton blooms is not a single factor. Critical factors contribute much to the occurrence of the bloom events, like light availability (Sverdrup [1953]; Huisman et al. [1999]), nutrient availability (Margalef [1978]; Jamart et al. [1979]; Wong et al. [2007]; Jin et al. [2013]), vertical mixing rate (Margalef [1978]; Huisman et al. [1999]; Wong et al. [2007]; Taylor and Ferrari [2011]) and meteorological forcing (Henson et al. [2006]; Taylor and Ferrari [2011]). A case study of the Jiangsu coastal waters is performed. The physical-ecological samples in the Jiangsu coastal waters are derived from two sources: the NASA monitoring data (the Ocean Color web, accessible through `http://oceancolor.gsfc.nasa.gov/cms/`) and in situ observations. Suppose in this case the nutrients are saturated. Seven variables are extracted from the NASA data, including chlorophyll a, ambient water temperature, light intensity, light attenuation coefficient, euphotic depth, mixed-layer depth, and phytoplankton biomass. Five variables are taken from in situ observations, including salinity, wind stress, suspended sediment, water turbidity, and water level.

5.2 Phytoplankton model

The phytoplankton model is described as the same form as equation 4.3:

$$\frac{\partial P}{\partial t} - E_z \frac{\partial^2 P}{\partial z^2} + (u_z + u_s)\frac{\partial P}{\partial z} = (\mu - l)P \tag{5.1}$$

5.2.1 Vertical stability theory

We assume that no mass crosses the air-water interface, so the eigenvalue condition of the vertical phytoplankton model requires the initial condition of $C(z, 0) = 0$ to be satisfied. Then we can derive the function of $f(z) = 0$.

So,

$$asin\sqrt{\lambda z} + \sqrt{\lambda}cos\sqrt{\lambda z} = 0, \quad (0 < z < Ze) \qquad (5.2)$$

Then,

$$tan\sqrt{\lambda z} = -\frac{\sqrt{\lambda}}{a} \qquad (5.3)$$

In the non-euphotic zone, the water environment is unfavourable for the phytoplankton species, mostly the species die off due to little light penetration into this layer.

Given insight in the asymptotic solution, $P(z,t) = f(z)e^{kt}$, attention should be paid to the transfer functions: k , μ, l, u_z, u_s , and E_z. Reliability of the parameter estimation largely determines the applicability of the model. In which, the functions of l and u_s are referred to as constants ($l = 0.05$ after Wei et al. [2004]; the order of u_s is 10^{-6} after Blauw et al. [2009] and Skogen et al. [1995]). Estimates of vertical turbulent diffusivity and phytoplankton growth rate are equally significant in the phytoplankton model.

The vertical mixing process is performed with the Delft3D model which has been validated in this area (He et al. [2015]). Figure 5.1 plots the graphical comparisons of the water level between the model results and the observations at Dafeng station and Yangkou station, from 6^{th} September to 14^{th} September in 2006.

To incorporate the ratio of $(u_z + u_s)/E_z$ into equation (5.3), the asymptotic function of $tan\sqrt{\lambda Ze} \approx 0$ is obtained. Following this derivation, when the condition of $k > 0$ is satisfied, we can get the lower boundary of the vertical turbulent diffusivity, $E_z > (u_z+u_s)^2/4(\mu-l)$, which corresponds to the view of Riley [1949]. Consider the reciprocal transformation of equation (5.3), $cot\sqrt{\lambda Ze} = -\frac{a}{\sqrt{\lambda}}$, then the upper boundary of the vertical turbulent diffusivity can be derived, $E_z < 4(\mu - l)Ze^2/\pi^2$.

5.2.2 Critical depth

The critical depth concept is commonly used as one critical condition to distinguish the phytoplankton blooms from the physical properties (Sverdrup [1953]; Platt et al.

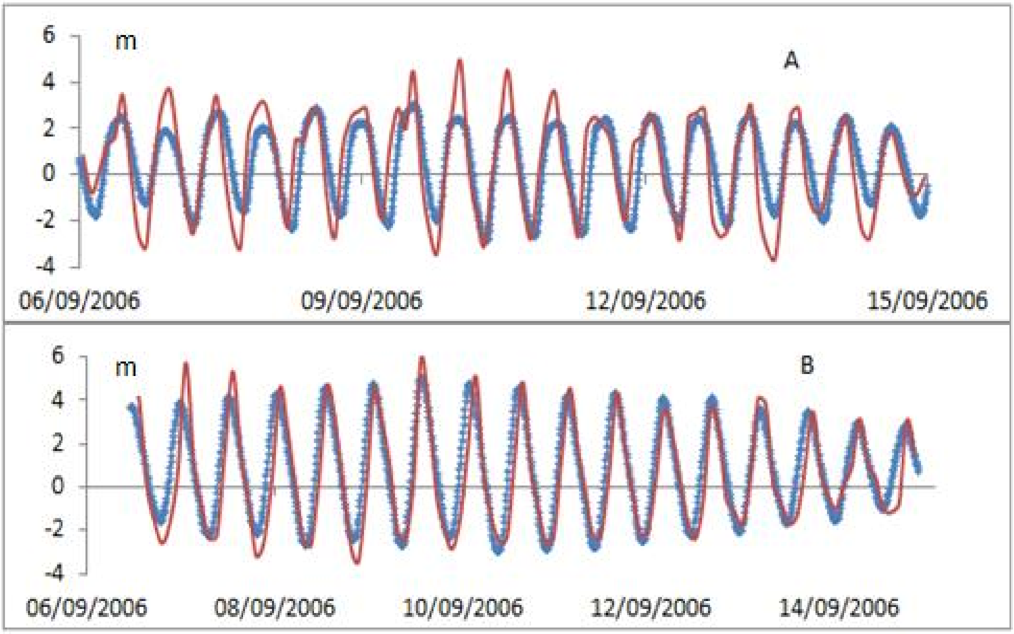

FIGURE 5.1: Graphical comparisons of the water level between the model results (the red smooth line) and the observations (the blue markers) at Dafeng station (A) and Yangkou station (B) in the Jiangsu coastal zone, expressed in m. Most of the model results are consistent with the observations.

[1991]; Huisman et al. [1999]; Schloss et al. [2002]; Taylor and Ferrari [2011]). When the mixed layer depth (MLD) is shallower, the light condition for the phytoplankton growth will be favourable, so the density of the phytoplankton will increase. When the density reaches a critical level, the bloom events will be initiated. The critical density corresponds to a critical depth.

From the concept of the compensation light intensity, a simplified estimate of the critical depth is introduced (Sverdrup [1953]; Huisman et al. [1999]), written as $Z_{cr} = ln(I/I_{cr})/K_{bg}$. Additionally, Siegel et al. [2002] define the critical depth as a function of $Z_{cr} = ln(C_0/L_0)/K_d$, C_0 and L_0 indicating the production and the loss at the surface layer. We can see that Siegel's view is related to Huisman's report.

In this case, the values of MLD are extracted from the Ocean Productivity of the NASA data (accessible through http://www.science.oregonstate.edu/ocean.productivity/index.php), processed by the SeaDAS (http://seadas.gsfc.nasa.gov/).

5.2.3 Parameter estimation

Specific growth rate

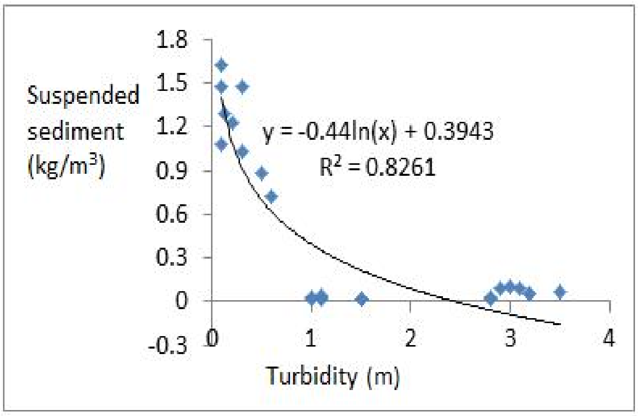

FIGURE 5.2: A logarithm function fits with the observations of suspended sediment (expressed in $kg\ m^{-3}$) and turbidity (expressed in m^{-1}) in the coastal waters of Jiangsu ($R^2 = 0.8261$)

The estimate function of the specific growth rate has been discussed in chapter 2. There is no big difference between the Smith's estimate and the simplified estimate on the basis of temperature-function with the light curve. Smith's curve is selected as the estimate of the growth rate in this study, integrating the effect of the ratio of carbon/chlorophyll a ($C/Chla$) into the phytoplankton growth.

Estimate of turbidity

The Jiangsu coastal waters with high turbidity block the sunlight penetration into the water column. A relationship between the turbidity and the suspended sediment has been investigated (Lewis [1996]; Holliday et al. [2003]). A logarithmic function fits with the observations of suspended sediment and turbidity in the Jiangsu coastal zone ($R^2 = 0.8261$), shown in figure 5.2.

The samples of the suspended sediment are separately monitored at spring tide and neap tide. The vertical distributions of the suspended sediment are displayed in figure 5.3. The variations of the suspended sediment show specific characteristics at four stations. The highest suspended sediment is found at Dafeng station, 2.5 $kg\ m^{-3}$. Estimates of the water turbidity vary at the ranges of [1.0, 1.5] m^{-1}, [0.143, 1.256] m^{-1}, [0.323, 2.06] m^{-1}, and [0.53, 1.90] m^{-1} at Lianyungang station, Dafeng station, Yangkou station and the north branch of the Yangtze River estuary, respectively.

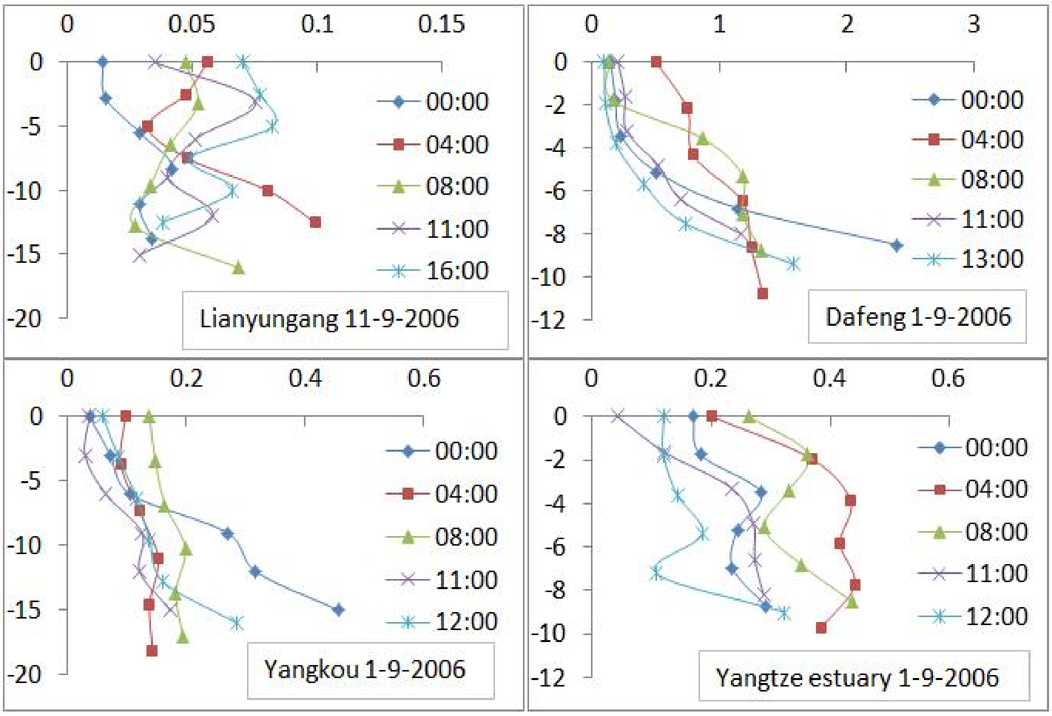

FIGURE 5.3: Vertical distribution of the observed suspended sediment over the water depth in September at four stations (x-: sediment concentration, expressed in $kg\ m^{-3}$; y-: water depth, expressed in m).

5.2.4 Skill assessment

In order to get the practical solution of the phytoplankton model, the estimates of the key parameters have to be captured. The quality of the estimates determines the reliability of the model output. To make sure getting relatively better model output, we should test the applicability of the phytoplankton model in this case. Skill assessment measures the difference between the model results and the observations. The Root Mean Square Error (RMSE), summed over data points, provides a reliable comparison of the models.

In principle, the form of RMSE is defined as:

$$RMSE = (\tfrac{1}{N} \textstyle\sum_{i=1}^{N} \Delta^2)^{\frac{1}{2}} \qquad (5.4)$$

The use of Δ is defined as:

$$\Delta = P_m - P_d \qquad (5.5)$$

In which, P_m is the modelled phytoplankton biomass, P_d is the monitored data.

The bias provides a measure of the mean values, defined as:

$$Bias = \overline{P_m} - \overline{P_d} \qquad (5.6)$$

If $Bias < 0$, P_m is underestimating P_d; if $Bias > 0$, P_m is overestimating P_d .

The unbiased RMSE (RMSE') is defined as:

$$RMSE'^2 = RMSE^2 - Bias^2 \qquad (5.7)$$

Normalized Bias (Bias*) by standard deviation (σ_d):

$$Bias* = Bias/\sigma_d \qquad (5.8)$$

And the normalized RMSE' (RMSE'*) is defined as:

$$RMSE'* = \frac{RMSE'}{P_{dmax} - P_{dmin}} \qquad (5.9)$$

Equations (5.6-5.9), $\overline{P_m}$ and $\overline{P_d}$ indicate the mean value of the model output and the monitored data; σ_d indicates the standard deviation of the monitored data; Bias* states the normalized Bias; RMSE' states the unbiased root mean square error; RMSE'* states the normalized unbiased root mean square error. If the values of Bias* and RMSE'* are out of the standard range [-1, 1], the model results are less reliable.

5.2.5 Bloom forecast

This research is intended to investigate the physical limitation of the bloom development in the coastal waters of Jiangsu. Critical factors mentioned above contribute much to the trigger of the blooms, but only the physical control is concentrated in this case.

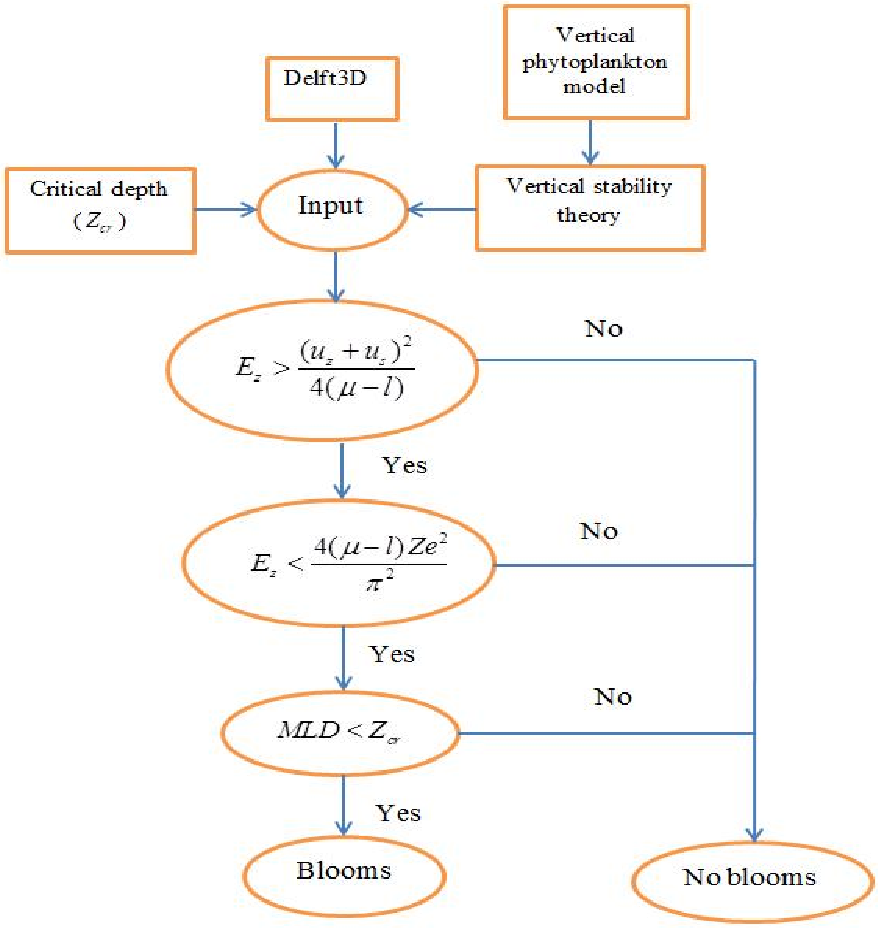

FIGURE 5.4: Work-flow of the bloom forecast from the physical limitation in the Jiangsu coastal waters

The vertical stability theory has been discussed under the condition of $k > 0$ over the water depth, which is closely related to the specific growth rate, the loss rate and the euphotic zone depth. Several transfer functions need to be investigated. Our concern is on the descriptions of the vertical turbulent diffusivity, the specific growth rate and the net growth rate. The vertical stability provides a favourable living condition for the phytoplankton, while the shallower mixed layer depth promotes the accumulation of the phytoplankton density in the water volume. The work-flow of the bloom forecast is depicted in figure 5.4.

5.3 Results

5.3.1 Statistical analysis of the monitored data

The statistical analysis of the associated variables is displayed in table 5.1, including $Chla$ $(mg\ m^{-3})$, T (^0C), I $(Einstein\ m^{-2}\ day^{-1})$, Ze (m), K_d (day^{-1}), and P $(g\ m^{-3})$. Note that all the samples are confined at the surface layer, monitored either 8-day or biweekly.

TABLE 5.1: Statistical analysis of the monitored samples in 2006 at four stations along the Jiangsu coast

		Lianyungang	Dafeng	Yangkou	North branch of the Yangtze River estuary
$Chla$	Mean	3.10	3.91	3.68	5.50
	SD	1.03	0.46	1.20	5.29
	Min	0.63	3.30	2.45	3.24
	Max	5.64	5.20	7.79	25.71
P	Mean	0.54	0.37	0.34	0.38
	SD	0.45	0.02	0.04	0.06
	Min	0.11	0.32	0.28	0.33
	Max	2.63	0.41	0.45	0.58
K_d	Mean	0.23	0.27	0.26	0.41
	SD	0.06	0.03	0.08	0.48
	Min	0.09	0.24	0.19	0.23
	Max	0.38	0.35	0.53	2.25
I	Mean	30.85	30.06	30.41	30.94
	SD	10.99	11.31	11.84	12.12
	Min	10.72	10.78	6.85	7.11
	Max	50.08	49.88	54.39	55.40
Ze	Mean	17.34	7.44	7.49	6.11
	SD	7.96	2.89	2.73	2.23
	Min	5.61	3.17	3.46	3.00
	Max	39.51	15.61	14.10	11.69
T	Mean	15.1	16.5	17.0	17.3
	SD	8.1	8.0	7.8	7.8
	Min	4.0	5.3	6.3	6.3
	Max	26.2	28.4	28.3	28.6

The annual variations of the two seasonal variables, light intensity and water temperature, show a small difference at four stations. In other words, these two variables can be set as domain parameters. An extreme value of chlorophyll a (25.71 $mg\ m^{-3}$) appeared on 4^{th} August at the north branch of the Yangtze River estuary, while the maximum phytoplankton biomass (2.63 $g\ m^{-3}$) appeared on 30^{th} April at Lianyungang station. Significant correlations ($R = 0.74-0.90$) are established between phytoplankton biomass and chlorophyll a in this case, described as $P = Ae^{BChla}$ ($P = 0.1166e^{0.4291Chla}$ and $R^2 = 0.5458$ at Lianyungang station, $P = 0.2238e^{0.1193Chla}$ and $R^2 = 0.6047$

at Dafeng station, $P = 0.2527e^{0.0768Chla}$ and $R^2 = 0.8139$ at Yangkou station, and $P = 0.3268e^{0.0241Chla}$ and $R^2 = 0.7154$ at the north branch of the Yangtze River estuary). Accordingly, the coefficients of A and B also follow a non-linear function ($B = 2.2547e^{-13.61A}$, $R^2 = 0.9933$).

Another important variable of euphotic depth Ze, ranging from 5.61 m to 39.51 m at Lianyungang station, is higher than that at other three stations. Within the layer of Ze, sufficient light intensity exists to support the phytoplankton growth. Light is one of the limiting factors for the phytoplankton, especially in winter. Light attenuation coefficient K_d has a close link with Ze, which can be explained by the Lambert-Beer's law (Sverdrup [1953]; Huisman et al. [1999]; Devlin et al. [2008]). This law has been validated by the observations in the Jiangsu coastal zone ($y = 900.96e^{1.333x}$ and $R^2 = 0.9307$, in which, y indicates the incident light intensity; x indicates the water depth), and the data sources are after Liu et al. [2012].

In table 5.2, the correlation matrix between the phytoplankton biomass and the physical conditions is discussed. Considering the random effects, the Bootstrap method is applied to derive the reliable range of the correlation coefficient within the 95% confidence interval. The phytoplankton biomass is significantly correlated with T, K_d, and Ze.

Table 5.2: Correlation matrix between the phytoplankton biomass and the physical conditions in 2006

				I	K_d	Ze	T
P	Pearson Correlation (r)			0.284	0.591**	-0.630**	0.706**
	Sig. (2-tailed) (p)			0.104	0.000	0.000	0.000
	Bootstrap^a	Bias		-0.004	-0.012	-0.004	-0.001
		Std. Error		0.152	0.113	0.073	0.077
		95% CI	Lower	0.008	0.307	-0.752	0.555
			Upper	0.587	0.758	-0.472	0.845

***. Correlation is significant at the 0.01 level (2-tailed);*
a. Unless otherwise noted, bootstrap results are based on 500 bootstrap samples;
r: Correlation coefficient;
p: Significant level;
Note: The object of the bootstrap is the estimate of Pearson Correlation.

5.3.2 Specific growth rate and net growth rate

A general function of the specific growth rate is used in this study, integrating the temperature-function into the light curve. In figure 5.5, the specific growth rate μ shows

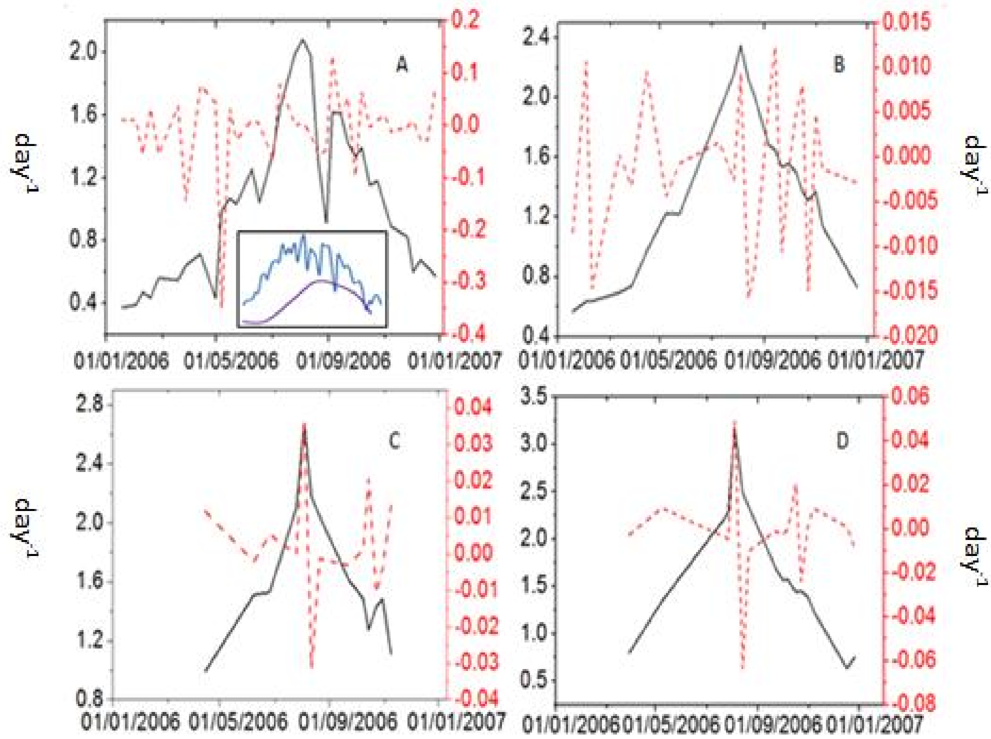

FIGURE 5.5: Time series variations of the specific growth rate μ (the black smooth line) and the net growth rate k (the red dash line) at four stations along the Jiangsu coastal zone (A: Lianyungang, B: Dafeng, C:Yangkou, D: the north branch of the Yangtze River estuary), both expressed in day^{-1}. The specific growth rate is estimated from the combined effects of temperature and available light intensity, while the net growth rate is derived from the increase of the phytoplankton biomass with respect to time interval (8-day or biweekly). The area-averaged patterns of light intensity (the blue smooth line, expressed in $Einstein\ m^{-2}\ day^{-1}$) and water temperature (the purple smooth line, expressed in ^{0}C) are presented in the first graph (A).

a seasonal variation, fluctuating with light intensity and temperature. The patterns of the specific growth rate at four stations are similar. The values continually increase in winter and peak in the summer days, and then gradually decrease until winter. But at Lianyungang station, an abnormal situation happens, the specific growth rate μ decreasing sharply after the maximum value (figure 5.5A). The abnormal process is probably caused by the special variation of light intensity, reducing sharply from 34 to 20 $Einstein\ m^{-2}\ day^{-1}$ during that time period.

In this case, the maximum growth rate is 3.17 day^{-1} appeared on 4^{th} August at the north branch of the Yangtze River estuary (figure 5.5D). The relative temperature and light intensity are all very high, 28.6 ^{0}C and 52.89 $Einstein\ m^{-2}\ day^{-1}$, respectively. The followed maximum value is 2.67 day^{-1} appeared at Yangkou station (figure 5.5C), with a high temperature of 28.3 ^{0}C and sufficient light intensity of 54.39 $Einstein\ m^{-2}\ day^{-1}$.

Compared with the variation of the specific growth rate, the net growth rate presents a totally different pattern both in spatial and temporal dimensions. The positive values of the net growth rate state that the phytoplankton production is higher than the loss with respect to time interval. Furthermore, the bloom events may be triggered when the sharp increase of the net growth rate happens, like the day of 4^{th} August both at Yangkou station and the north branch of the Yangtze River estuary (figure 5.5C and figure 5.5D).

Although the phytoplankton species have a large growth potential (μ=0.37-2.08 day^{-1}, 0.55-2.34 day^{-1}, 0.67-2.67 day^{-1}, and 0.63-3.17 day^{-1} at Lianyungang station, Dafeng station, Yangkou station, and the north branch of the Yangtze River estuary, respectively), the net growth rate k varies within $\pm$0.1 day^{-1}, $\pm$0.015 day^{-1}, $\pm$0.03 day^{-1}, and $\pm$0.06 day^{-1} over the 8-day interval at four stations along the Jiangsu coast accordingly. When the values of k fluctuate around 0, there is no obvious increase or loss of production during that time period.

5.3.3 Validation of the phytoplankton model

To test the applicability of the phytoplankton model in this case, skill assessment is performed to compare the model output with the monitored data, displayed in table 5.3. Figure 5.6 presents the graphical comparisons.

At Lianyungang station, the monitored phytoplankton biomass varies around 0.54 ± 0.45 $g\ m^{-3}$, while the modelled phytoplankton biomass varies around 0.48 ± 0.55 $g\ m^{-3}$. At Dafeng station, the monitored data varies around 0.37 ± 0.02 $g\ m^{-3}$, while the modelled data varies around 0.37 ± 0.10 $g\ m^{-3}$. At Yangkou station, the monitored phytoplankton biomass varies around 0.34 ± 0.03 $g\ m^{-3}$, while the modelled phytoplankton biomass varies around 0.31 ± 0.07 $g\ m^{-3}$. At the north branch of the Yangtze River estuary, the monitored phytoplankton biomass varies around 0.38 ± 0.07 $g\ m^{-3}$, while the modelled phytoplankton biomass varies around 0.34 ± 0.11 $g\ m^{-3}$. The index of $RMSE$ denotes the difference between the model output and the monitored data. The modelled phytoplankton biomass underestimates the monitored data ($Bias < 0$) at Lianyungang, Yangkou, and the north branch of the Yangtze River estuary, while the modelled values overestimate the monitored data at Dafeng station ($Bias > 0$). The normalized $Bias$ and unbiased $RMSE$ are used to characterize the skill assessment, 90% being inside the

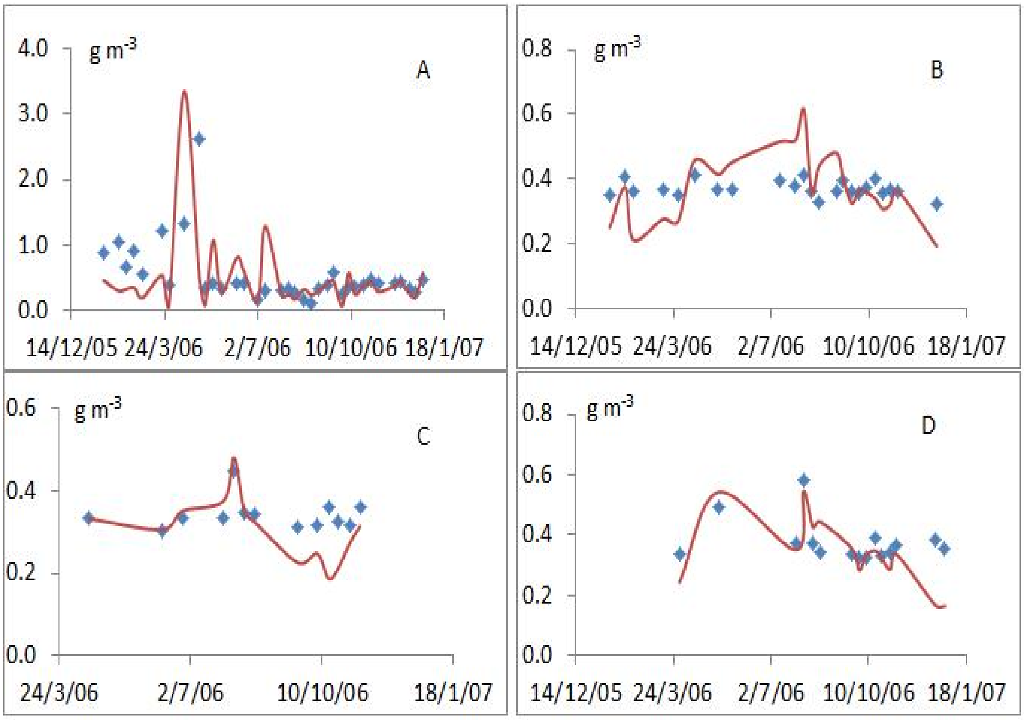

FIGURE 5.6: Graphical comparisons of the modelled phytoplankton biomass and the monitored data in the Jiangsu coastal zone (A: Lianyungang station; B: Dafeng station; C: Yangkou station; D: the north branch of the Yangtze River estuary), determined by the samples over the year of 2006 at the surface layer. The red smooth lines indicate the model output and the blue markers indicate the monitored data, expressed in $g\ m^{-3}$.

standard range of [-1, 1]. It is concluded that the vertical phytoplankton model is able to reproduce reliable predictions of the phytoplankton biomass in this case.

TABLE 5.3: Skill assessment of the vertical phytoplankton model at four stations along the Jiangsu coast

	$\overline{P_d}$	$\overline{P_m}$	σ_d	Bias	Bias*	RMSE	RMSE'	RMSE'*
Lianyungang	0.54	0.48	0.45	-0.06	-0.14	0.59	0.59	0.23
Dafeng	0.37	0.37	0.02	0.00	0.17	0.09	0.09	1.06
Yangkou	0.34	0.31	0.03	-0.03	-0.88	0.07	0.06	0.38
North branch of the Yangtze River estuary	0.38	0.34	0.07	-0.03	-0.51	0.09	0.08	0.32

5.3.4 Vertical distributions of the phytoplankton biomass

To investigate the vertical distributions of the phytoplankton biomass, the phytoplankton model is developed over the water depth, shown in figure 5.7. In spring, the phytoplankton biomass is higher at Lianyungang station than that at other three stations. A decrease of the phytoplankton biomass corresponds to a deeper water depth, excluding the case of Yangkou station.

Figure 5.7A displays the annual variation of the phytoplankton biomass for the water depth of 2m in the Jiangsu coastal waters. At Lianyungang station, the minimum value is 0.01 $g\ m^{-3}$, appeared on 30^{th} April. And the maximum is 3.07 $g\ m^{-3}$, appeared on 14^{th} April. Higher values are in spring and in autumn. The average value is 0.36 $g\ m^{-3}$ and the standard deviation is 0.51 $g\ m^{-3}$. At Dafeng station, the annual fluctuation is relatively steady, with the mean value of 0.28 $g\ m^{-3}$ and the standard deviation of 0.15 $g\ m^{-3}$. The minimum value is 0.03 $g\ m^{-3}$, appeared on 10^{th} February. And the maximum is 0.57 $g\ m^{-3}$, appeared on 26^{th} July. At Yangkou station, the phytoplankton biomass varies at a range of [0.01, 0.28] $g\ m^{-3}$. The minimum appeared on 19^{th} August and the maximum appeared on 4^{th} August. At the north branch of the Yangtze River estuary, the phytoplankton biomass varies around 0.21 ± 0.16 $g\ m^{-3}$. Higher values appear in August.

Figure 5.7B displays the annual cycle of the phytoplankton biomass for the water depth of 5m. Similar to the water depth of 2m, the phytoplankton biomass varies with a big difference at Lianyungang station, ranging from 0.02 $g\ m^{-3}$ to 3.34 $g\ m^{-3}$. At Dafeng station, the phytoplankton biomass varies at a range of [0.03, 0.57] $g\ m^{-3}$, with the mean value of 0.27 $g\ m^{-3}$ and the standard deviation of 0.14 $g\ m^{-3}$. While at Yangkou station and the north branch of the Yangtze River estuary, the values of the phytoplankton biomass are relatively smaller, varying at the ranges of [0.02, 0.35] $g\ m^{-3}$ and [0.002, 0.51] $g\ m^{-3}$, respectively.

Figure 5.7C displays the annual variation of the phytoplankton biomass for the water depth of 10m. At Lianyungang station, the phytoplankton biomass varies at a range of [0.005, 2.95] $g\ m^{-3}$, with the mean value of 0.41 $g\ m^{-3}$ and the standard deviation of 0.53 $g\ m^{-3}$. The minimum appeared on 6^{th} May and the maximum appeared on the same day as other water depths. Higher values appear in the months of April, May and July. The phytoplankton biomass fluctuates with 0.26 ± 0.13 $g\ m^{-3}$, 0.15 ± 0.11 $g\ m^{-3}$, and 0.22 ± 0.18 $g\ m^{-3}$ at Dafeng station, Yangkou station and the north branch of the Yangtze River estuary, respectively.

Figure 5.7D shows the time series variation of the phytoplankton biomass for the water depth of 20m. At Lianyungang station, the minimum value appeared on 1^{st} July. The values become smaller with the deeper water depth. At Dafeng station, the phytoplankton biomass varies at a range of [0.007, 0.57] $g\ m^{-3}$, with the mean value of

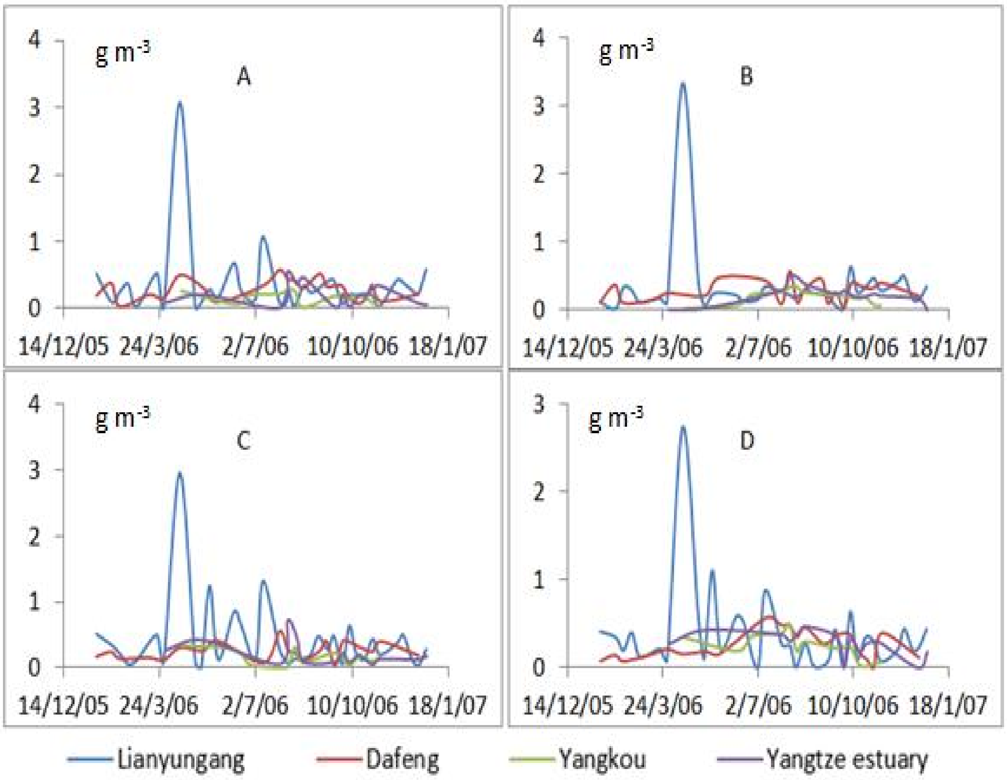

FIGURE 5.7: Annual distributions of the phytoplankton biomass for the different water depths over the year of 2006 in the Jiangsu coastal waters, expressed in $g\ m^{-3}$. In this graph, A, B, C and D denote the annual variations of the phytoplankton biomass for the water depths of 2m, 5m, 10m and 20m, respectively.

0.26 $g\ m^{-3}$ and the standard deviation of 0.15 $g\ m^{-3}$. At Yangkou station, the values become higher with the deeper water. The phytoplankton biomass ranges from 0.01 $g\ m^{-3}$ to 0.50 $g\ m^{-3}$, with the mean value of 0.22 $g\ m^{-3}$ and the standard deviation of 0.14 $g\ m^{-3}$. At the north branch of the Yangtze River estuary, the phytoplankton biomass ranges from 0.002 $g\ m^{-3}$ to 0.47 $g\ m^{-3}$, with the mean value of 0.27 $g\ m^{-3}$ and the standard deviation of 0.13 $g\ m^{-3}$.

5.3.5 Depth-averaged phytoplankton biomass

In this section, the annual variation of the depth-averaged phytoplankton biomass in the Jiangsu coastal waters is discussed, shown in table 5.4. At Lianyungang station, the depth-averaged phytoplankton biomass varies at a range of [0.05, 2.76] $g\ m^{-3}$, with the mean value of 0.49 $g\ m^{-3}$ and the standard deviation of 0.71 $g\ m^{-3}$. At Dafeng station, the depth-averaged phytoplankton biomass varies around 0.28 ± 0.09 $g\ m^{-3}$, while 0.20 ± 0.06 $g\ m^{-3}$ and 0.28 ± 0.09 $g\ m^{-3}$ at Yangkou station and the north branch of the Yangtze River estuary, respectively.

In order to get a practical solution of the phytoplankton model, we have simplified the real problems. With respect to the random effects, the Bootstrap method is used to derive the 95% confidence interval of the estimate, shown in table 5.4. At Lianyungang station, the mean value varies from 0.23 $g\ m^{-3}$ to 0.91 $g\ m^{-3}$ within the 95% confidence interval, with a bias of -0.007 $g\ m^{-3}$. At Dafeng station, the mean value varies from 0.23 $g\ m^{-3}$ to 0.33 $g\ m^{-3}$ within the 95% confidence interval, with a bias of -0.001 $g\ m^{-3}$. At Yangkou station, the mean value varies from 0.17 $g\ m^{-3}$ to 0.23 $g\ m^{-3}$ within the 95% confidence interval, with a bias of 0.001 $g\ m^{-3}$ and a standard error of 0.015 $g\ m^{-3}$. At the north branch of the Yangtze River estuary, the mean value varies from 0.23 $g\ m^{-3}$ to 0.33 $g\ m^{-3}$ within the 95% confidence interval.

From the index of skewness, the distributions of the depth-averaged phytoplankton biomass have a long right tail at Lianyungang station (3.091) and at the north branch of the Yangtze River estuary (1.866), deviating largely from the centre. The potential extreme values of the phytoplankton biomass may appear at these two stations resulting from the boxplot analysis, shown in figure 5.8. The open dots indicate the higher values of the phytoplankton biomass (non-extreme), and the black star indicates the extreme value. The probability distribution model of Weibull is explored to perform the good-of-fit test at Lianyungang station and at the north branch of the Yangtze River estuary, presented as figure 5.9A and figure 5.9D, respectively. The values of skewness are relatively smaller at Dafeng station (0.054) and Yangkou station (0.639), revealing that the symmetric distribution can fit with the data. Figure 5.9B and figure 5.9C display the good-of-fit test of Normal distribution at these two stations.

5.3.6 Vertical stability threshold

As mentioned above, there is a suitable range of the vertical turbulent diffusivity for the phytoplankton, which promotes the growth. When the vertical turbulent diffusivity is outside that boundary, the phytoplankton biomass will show a negative increase. The vertical stability is determined by the condition of $k > 0$, depending on the specific growth rate, the loss rate and the euphotic zone depth, shown in figure 5.10 (the blue

TABLE 5.4: Statistical analysis of the depth-averaged phytoplankton biomass in the Jiangsu coastal waters over the year of 2006

Statistic		Statistic	*Bootstrap*[a]			
			Bias	Std. Error	95% CI	
					Lower	Upper
Lianyungang	Mean	0.496	-0.007	0.194	0.232	0.911
	Std. Deviation	0.712	-0.132	0.330	0.110	1.102
	Skewness	3.091	-1.114	1.031	-0.090	3.470
Dafeng	Mean	0.279	-0.001	0.025	0.230	0.331
	Std. Deviation	0.095	-0.005	0.014	0.060	0.118
	Skewness	0.054	-0.088	0.466	-0.992	0.998
Yangkou	Mean	0.197	0.001	0.015	0.169	0.229
	Std. Deviation	0.059	-0.004	0.010	0.035	0.075
	Skewness	0.639	-0.190	0.563	-0.747	1.643
North branch of the Yangtze River estuary	Mean	0.280	0.001	0.027	0.236	0.336
	Std. Deviation	0.097	-0.009	0.029	0.037	0.140
	Skewness	1.866	-0.479	0.690	0.071	2.776

a: Unless otherwise noted, bootstrap results are based on 500 bootstrap samples;
Note: the object of the bootstrap method is the estimate of the mean vaue, the standard deviation, and the skewness.

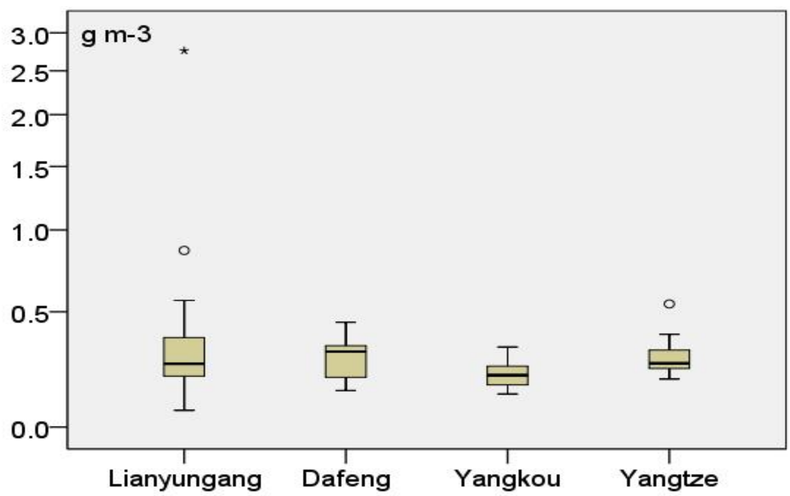

FIGURE 5.8: Boxplot of the depth-averaged phytoplankton biomass in the Jiangsu coastal waters. In which, the middle black line indicates the median, the shaded region stating the middle 50%. The lines extending out of the shaded region are the top and bottom 25% of the data and the horizontal lines at the top/bottom of the boxplot are the minimum and maximum values (non-extreme). One case is classified as the extreme value at Lianyungang station (2.76 $g\ m^{-3}$).

smooth line). In winter, the smaller values of the euphotic depth and the specific growth rate reduce the vertical stability threshold.

The vertical mixing process can influence the vertical distributions of the phytoplankton biomass, driven by the effects of the hydrodynamics. The strong turbulence appears in winter. The average estimate of the vertical turbulent diffusivity is $9.99 \pm 2.78\ cm^2\ s^{-1}$ in the Jiangsu coastal zone ($8.07 \pm 3.64\ cm^2\ s^{-1}$ at Lianyungang station, $7.21 \pm 2.70\ cm^2\ s^{-1}$ at Dafeng station, $14.40 \pm 8.00\ cm^2\ s^{-1}$ at Yangkou station, $10.3 \pm 4.13\ cm^2\ s^{-1}$

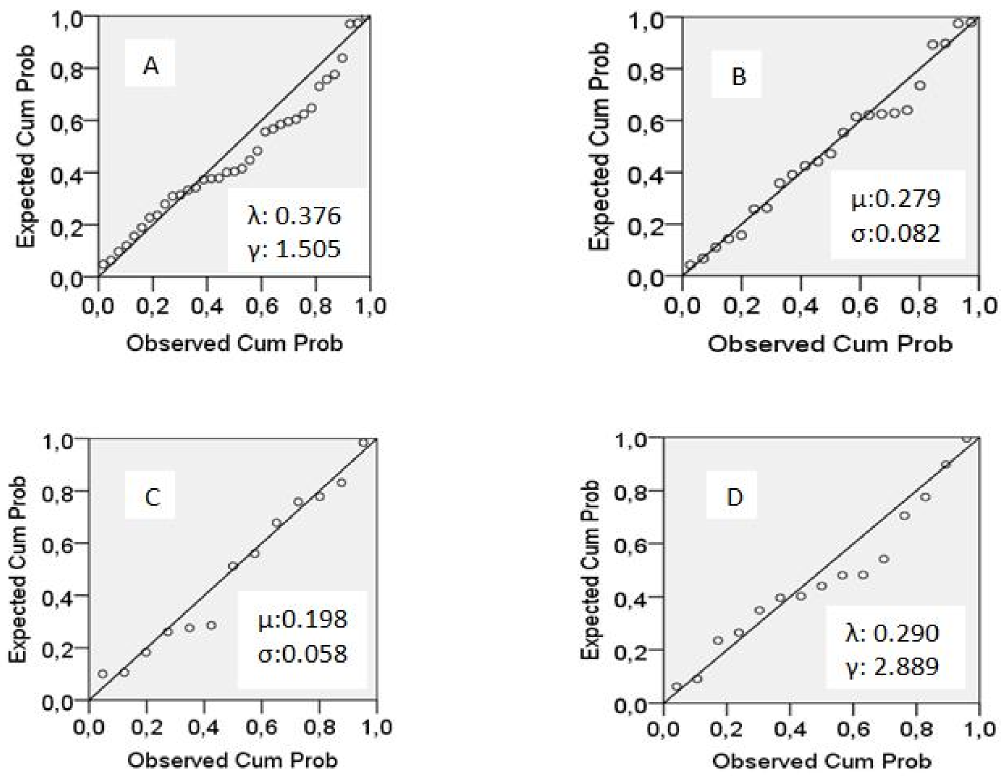

FIGURE 5.9: Good-of-fit test using the probability distribution models of Weibull and Normal, determined by the depth-averaged phytoplankton biomass over the year of 2006 in the Jiangsu coastal waters. In which, x-axis indicates the cumulative probability of the model output and y-axis indicates the cumulative probability of the predictions with the random effects. λ: shape parameter for Weibull distribution, γ: scale parameter for Weibull distribution. μ: mean value for Normal distribution, σ: standard deviation for Normal distribution. A: Lianyungang station (Weibull distribution); B: Dafeng station (Normal distribution); C: Yangkou station (Normal distribution); D: the north branch of the Yangtze River estuary (Weibull distribution).

at the north branch of the Yangtze River estuary). The order of the vertical turbulent diffusivity coincides with the report after Su et al. [2013]. By the classification of Margalef [1978], diatoms are the dominant species in this zone.

From the condition of the vertical turbulent diffusivity within the threshold (the purple rectangles in figure 5.10), the phytoplankton bloom events potentially occur in the months of March, May, August and October at Lianyungang station, while in the months of April, June and August at Dafeng station, in the months of June and August at Yangkou station, and in the months of May and August at the north branch of the Yangtze River estuary.

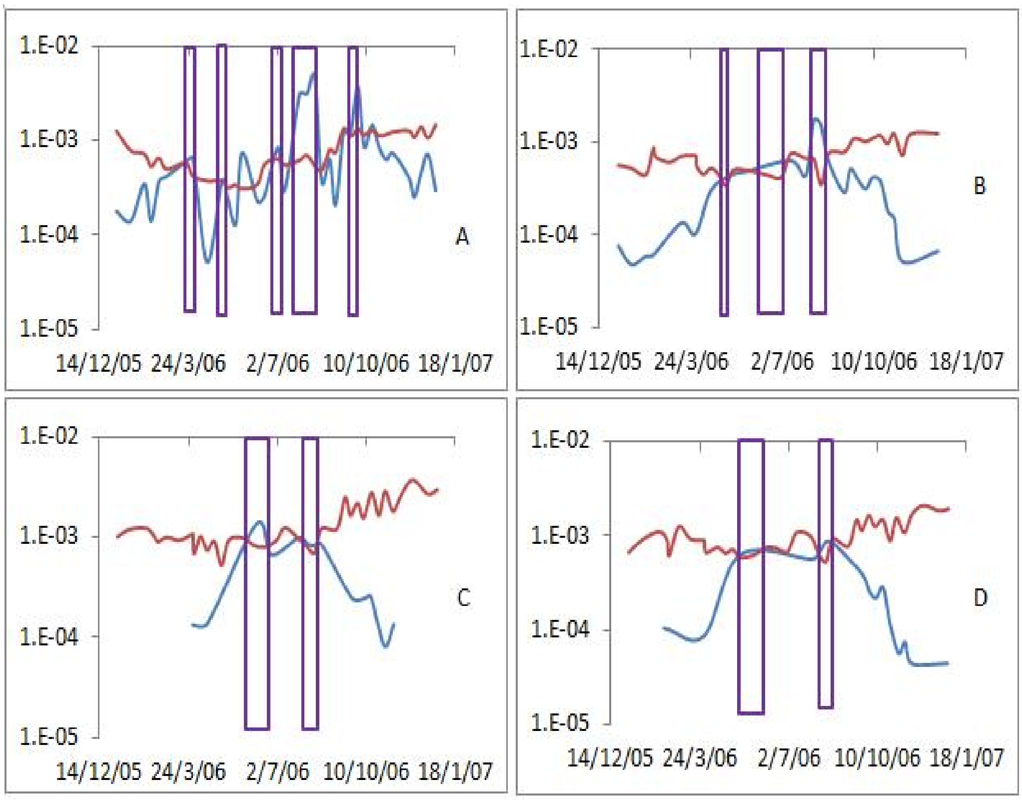

FIGURE 5.10: Vertical stability threshold (the blue smooth line) and the vertical turbulent diffusivity (the red smooth line) at four stations (A: Lianyungang; B: Dafeng; C: Yangkou; D: the north branch of the Yangtze River estuary), expressed in $m^2\ s^{-1}$. The purple rectangles mark the moments that the vertical turbulent diffusivity is within the vertical stability threshold.

5.3.7 Critical depth and mixed layer depth

Regardless of the concepts of the critical depth, the euphotic depth or the mixed layer depth, all have a link with light availability, following the Lambert-Beer's Law. To be exact, the critical depth varies with the compensation light intensity derived from a balanced interface of $\mu - l = 0$.

One frequently used condition of characterizing the blooms is to compare the mixed layer depth with the critical depth. The mixed layer depth is the layer between the water surface and a depth, where there is little variation in temperature, salinity and phytoplankton density over the water depth. Similar with the vertical turbulent diffusivity, the mixed layer depth mostly depends on the stability of water and the effects of wind stress and tidal currents. When the mixed layer depth is shallower than the critical depth, the light intensity will be more favourable for photosynthesis. On the contrary, when the mixed layer depth is deeper than the critical depth, the phytoplankton growth will be limited by light intensity despite sufficient nutrients may be available.

In figure 5.11, the critical depth varies with a similar trend but with different ranges at four stations, [8.58, 16.15]m at Lianyungang station, [5.84, 12.01]m at Dafeng station, [7.55, 18.07]m at Yangkou station, and [8.92, 14.89]m at the north branch of the Yangtze River estuary. The average critical depth is 12.32m, 9.21m, 13.67m and 12.13m at Lianyungang, Dafeng, Yangkou and the north branch of the Yangtze River estuary, respectively. The minimum critical depth appeared on 19^{th} January at Lianyungang station, while it appeared on 2^{nd} February at Dafeng station, on 4^{th} August at Yangkou station and on 17^{th} November at the north branch of the Yangtze River estuary. The maximum critical depth appeared on 27^{th} June, while on 20^{th} August at Dafeng station, on 8^{th} June at Yangkou station and on 8^{th} October at the north branch of the Yangtze River estuary. Compared with other three stations, the critical depth at Dafeng station shows a relatively stable state over the year of 2006.

All of the mixed layer depths are less than 50m in the Jiangsu coastal waters. The deeper mixed layer depth occurs in winter and in the early spring, which may be caused by the wind stress and the weak stratification. The mixed layer depth ranges from 10.69m to 40m at Lianyungang station, while 10.81-50m at Dafeng station, 10.79-50m at Yangkou station, and 10.93-50m at the north branch of the Yangtze River estuary. The shallowest mixed layer depth appeared on 21^{st} August at four stations.

From the condition of the mixed layer depth being shallower than the critical depth (the purple rectangles in figure 5.11), the phytoplankton bloom events probably happen in the months of May, July, September and October at Lianyungang station, while in August at Dafeng station, from May to October at Yangkou station and in the months of May, August and October at the north branch of the Yangtze River estuary.

5.3.8 Phytoplankton bloom

The phytoplankton bloom events have been predicted based on the discussion of the physical limitation, shown in figure 5.12 (the blue column); the observed bloom events are also shown (the red arrow).

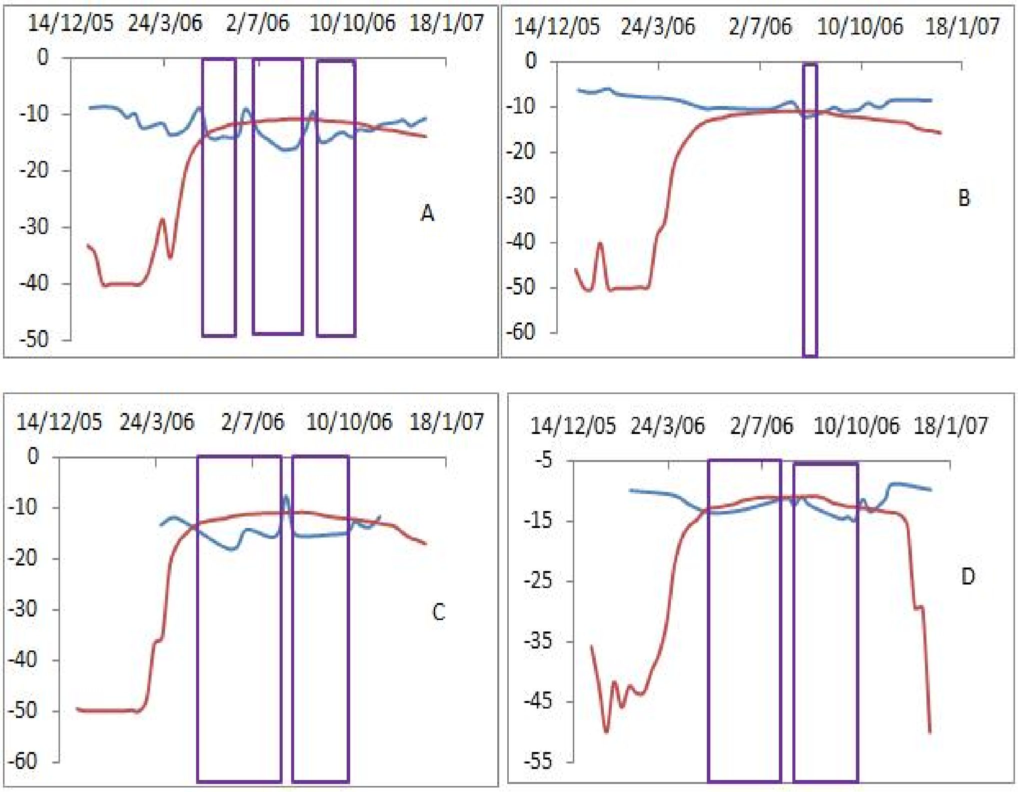

FIGURE 5.11: Time series variation of the critical depth (the blue smooth line) and the mixed layer depth (the red smooth line) over the year of 2006 at four stations (A: Lianyungang; B: Dafeng; C: Yangkou; D: the north branch of the Yangtze River estuary), expressed in m. The mixed layer depth starts to be shallower in March. The purple rectangles mark the moments that the mixed layer depth is shallower than the critical depth, corresponding to a higher phytoplankton density.

At Lianyungang station (figure 5.12A), the predicted timings of the phytoplankton bloom events are from 23^{rd} May to 25^{th} May, 26^{th} July to 12^{th} August, and 30^{th} September to 7^{th} October, while the observed bloom event occurs on 2^{nd} October till 8^{th} October, which is mainly caused by *Eucampia zodiacus Ehrenberg* and *Gymnodinium catenatum*, covering an area of 600 km^2 (the observed information from SOA, accessible through http://www.soa.gov.cn/zwgk/hygb/). At Dafeng station (figure 5.12B), the phytoplankton bloom event happens from 10^{th} August till 18^{th} August. At Yangkou station (figure 5.12C), the predictions of the bloom events happen from 4^{th} June to 17^{th} June and 4^{th} August to 13^{th} August. While no observed data is collected at Dafeng and Yangkou station. At the north branch of the Yangtze River estuary (figure 5.12D), the predicted bloom events appear from 8^{th} May to 23^{rd} May and 2^{nd} August to 18^{th} August, while the observed blooms occur on 14^{th} May and 4^{th} August.

Unfortunately, we don't have much in situ information on the small scale bloom events,

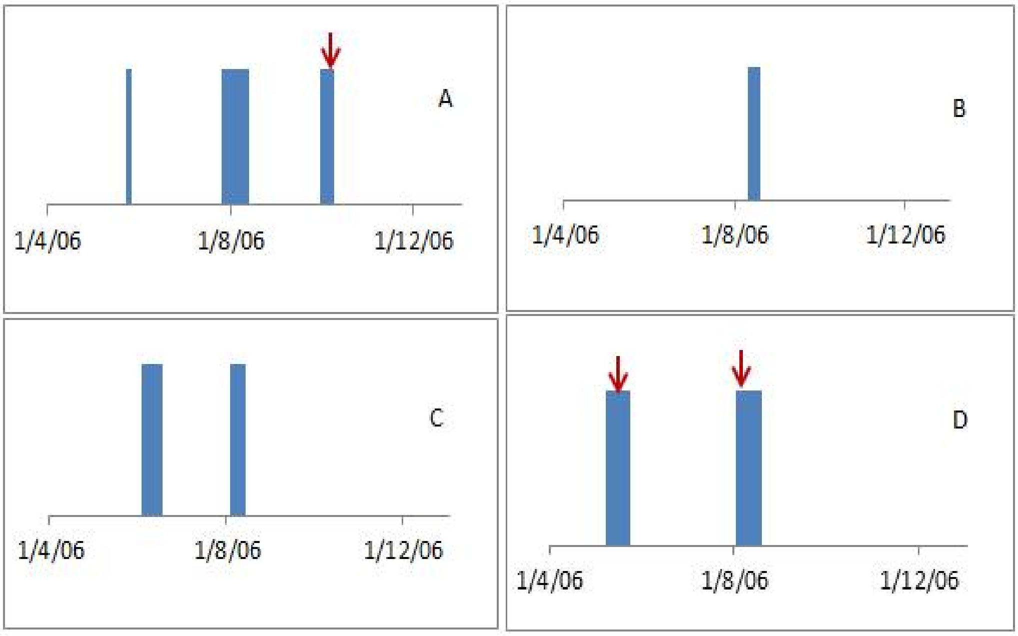

FIGURE 5.12: Comparisons of the predicted blooms (the blue column) and the observations (the red arrow) in the Jiangsu coastal zone (A: Lianyungang; B: Dafeng; C: Yangkou; D: the north branch of the Yangtze River estuary). The red arrow at Lianyungang station indicates the timing of the bloom occurrence, 2^{nd} to 7^{th} October, while the other two red arrows at the north branch of the Yangtze River estuary indicate the timings of 14^{th} May and 4^{th} August, respectively.

only having collected the large scale blooms which cover an area more than 100 km^2. Most likely, more smaller blooms have occurred around the observed timings. From the comparisons of the predictions and the limited observations, the physical control of the blooms is applicable in this case.

As is already known, chlorophyll a can be a measure of the phytoplankton biomass. Researchers also have found out that critical chlorophyll a or critical phytoplankton concentrations can be the condition to distinguish the bloom events (Xuan et al. [2011]). In this case, for chlorophyll a, when the bloom events occur, the values vary from 3.01 to 4.01 $mg\ m^{-3}$ at Lianyungang station, while 3.56-3.74 $mg\ m^{-3}$ at Dafeng station, 3.37-7.79 $mg\ m^{-3}$ at Yangkou station and 6.59-27.51 $mg\ m^{-3}$ at the north branch of the Yangtze River estuary. For the phytoplankton biomass, when the blooms occur, the values vary from 0.32 to 0.37 $g\ m^{-3}$ at Lianyungang station, while 0.33-0.36 $g\ m^{-3}$ at Dafeng station, 0.30-0.44 $g\ m^{-3}$ at Yangkou station and 0.49-0.58 $g\ m^{-3}$ at the north branch of the Yangtze River estuary. Therefore, we can simply conclude that chlorophyll a should be larger than 3 $mg\ m^{-3}$ or the phytoplankton biomass should be larger than 0.3 $g\ m^{-3}$ when the phytoplankton bloom events occur.

5.4 Discussion

The investigation of the phytoplankton has provided useful insights in the coastal ecosystem. The typical subject regarding phytoplankton is the bloom development. The trigger of the blooms is not a single event but is linked with environmental factors. This study develops a vertical phytoplankton model and extends the application to investigate the blooms from the physical properties. Due to the semi-enclosed location, the Jiangsu coastal waters have a slow exchange with other water systems. In other words, the horizontal effects are less sensitive to the phytoplankton. Among all the transfer functions, our concern is on the descriptions of specific growth rate and vertical turbulent diffusivity.

Only when the condition of $k > 0$ is satisfied, the phytoplankton blooms may occur. The vertical stability threshold is obtained from the asymptotic transformation of the trigonometric functions, $[(u_z + u_s)^2/4(\mu - l)\ ,\ 4(\mu - l)Ze^2/\pi^2\ ]$, which corresponds with the view of other researchers (Riley [1949]; Wong et al. [2007]). The vertical mixing process is driven by the effects of tidal currents and wind stress, performed with the Delft3D model. From the concept of the compensation light intensity, the critical depth is introduced after Sverdrup [1953] and Huisman et al. [1999]. When the mixed layer depth is shallower than the critical depth, the phytoplankton density will increase rapidly, which may trigger the bloom events (figure 5.11).

It is noted that a combination of environmental factors will improve the application of the phytoplankton model. However, more field samples are required. In this study, only the physical control of the bloom development is stressed, but no consideration is given to the chemical conditions (like nutrient availability, DO, COD and BOD_5), especially nutrient availability. In future work, we will further research these issues.

Chapter 6

Conclusions and future work

Phytoplankton is recognized as a basic component of the coastal ecosystem. Primary production by phytoplankton forms the first link in the food chain. The interactions between the phytoplankton and the water properties are concerned. Shallow water zones (i.e. coasts, lakes, and estuaries) are the hot spots for the phytoplankton owing to sufficient nutrients originating from the lands and the oceans (Schmidt [1999]; Cloern et al. [2014]). The studies of the phytoplankton have frequently been proposed (Cloern [1996]; Edelvang et al. [2005]; Godrijan et al. [2013]). Within the course of a year, the features of phytoplankton dynamics will move forward to a steady state (Evans and Parslow [1985]; Steele and Henderson [1992]; Behrenfeld [2010]). The annual cycles of phytoplankton dynamics are driven by the cycles of the physical characteristics in coastal waters. We stress the significance of the phytoplankton in this thesis without the discussions of the zooplankton or the higher level species.

To capture the key point of this thesis is to completely understand the interrelations between chlorophyll a, phytoplankton, and coastal ecosystems. The relationship between phytoplankton and coastal ecosystems has been explained above. Chlorophyll a is a reliable estimate of phytoplankton, so the investigation of phytoplankton is often explained by the study of chlorophyll a. However, the relation between chlorophyll a and phytoplankton is not fixed but site-specific. It is not acceptable to give a better vision in the coastal ecosystem only through the research of chlorophyll a but also phytoplankton.

In this thesis, different focuses are taken in the four body chapters (chapter 2 to chapter 5). Chapter 2 investigates the response of chlorophyll a to the environmental factors (temperature, salinity, suspended particulate matter, nutrients, and light intensity) from 2000 through 2009, and characterizes the significant factors. Chapter 3 discusses the annual variation of chlorophyll a over the year of 1992, with a case study of the Frisian Inlet, and the attention is also paid to the response of chlorophyll a to the environmental factors. Chapter 4 describes the vertical distributions of phytoplankton biomass over the year of 2009. Chapter 5 discusses the annual variation of the phytoplankton biomass and investigates the bloom development from the physical properties over the year of 2006, with a case study of the Jiangsu coast.

This section concludes the main study, and gives a few recommendations and future directions.

6.1 Conclusions

6.1.1 Statistical analysis of the phytoplankton biomass in response to the environmental variables

In chapter 2, the factor analysis is developed to reduce the redundant information from a set of correlated variables and to represent with a smaller set of variables in a case of Lauwersoog station (NL), determined by the 10-year's historical dataset from 2000 through 2009. Summarizing the historical dataset of the chlorophyll a (187 samples), 75% of the values fluctuate at a range of [0, 20] $mg\ m^{-3}$, and a Gamma model fits well by the observations (k = 1.63 , ν = 0.11) (figure 2.2). From a comprehensive view, two thirds of the total variance in the phytoplankton biomass can be explained by the physical-chemical conditions. The phytoplankton biomass is positively correlated with the physical conditions (salinity, light intensity, and temperature), and is negatively correlated with the nutrients (ammonium, nitrate, and silicate).

Factor analysis identifies the driving variables from a set of correlated variables to the phytoplankton biomass. The first two components/factors are concerned in the analysis. Of all the variables, dissolved nitrate is characterized as the driving variable in the first rotated component/factor (-0.887 by PCA, 0.881 by ULS, and 0.903 by ML), and ammonium is the driving variable in the second rotated component/factor (0.860 by PCA, 0.797 by ULS, and 0.838 by ML). Moreover, nitrate is higher correlated with other variables than ammonium, accounting for 37.8%, 35.3%, and 32.8% of the total variance by PCA, ULS, and ML, respectively (figure 2.5 and figure 2.6).

6.1.2 Validation of the mathematical models

In chapter 3, prior to the application of the BLOOM II model, the validation is performed using the graphical comparisons and a cost-function as proposed in ASMO eutrophication modelling workshop. 96.9% of all the comparisons are classified as in good agreement, while only 3.1% as in poor (table 3.2).

In chapter 4, the graphical comparisons of the model output and the monitored phytoplankton biomass are displayed (figure 4.4), demonstrating that the phytoplankton model can produce reliable predictions of the phytoplankton biomass in this case.

In chapter 5, skill assessment is introduced to discuss the reliability of the phytoplankton model. The normalized Bias and unbiased RMSE, 90% being inside the standard range of [-1, 1], indicate that the phytoplankton model is applicable in the Jiangsu coastal waters (table 5.3).

6.1.3 Application of the mathematical models

In chapter 3, the ecological model of BLOOM II is applied to the Frisian Inlet to investigate the dynamics of chlorophyll a. Attention is paid to the response of chlorophyll a to nutrient availability, including N-reduction, P-reduction and both N-and P-reduction (table 3.3). The effect from both N- and P-reduction scenario is larger than that from N-only and P-only reduction scenarios.

In chapter 4, a vertical phytoplankton model is developed. This study aims to better understand the vertical distributions of the phytoplankton biomass. Higher values of the phytoplankton biomass appear in spring and autumn, followed by the rapid reduction of the nutrients (figure 4.5).

In chapter 5, the extended application of the vertical phytoplankton model is apllied to the Jiangsu coastal waters, emphasizing on the phytoplankton biomass and the phytoplankton blooms from the physical properties. Normally, the occurrence of the bloom event is triggered by the critical conditions. Our concern is focused on the physical limitation, vertical stability threshold and critical depth. At Lianyungang station, the predicted timings of the phytoplankton bloom events are from 23^{rd} May to 25^{th} May, 26^{th} July to 12^{th} August, and 30^{th} September to 7^{th} October, while the observed bloom event occurs on 2^{nd} October till 8^{th} October. At Dafeng station, the phytoplankton bloom event happens on 10^{th} August till 18^{th} August. At Yangkou station, the bloom events happen from 4^{th} June to 17^{th} June and 4^{th} August to 13^{th} August. While no observed data is collected at Dafeng and Yangkou station. At the north branch of the Yangtze River estuary, the predicted bloom events appear from 8^{th} May to 23^{rd} May and 2^{nd} August to 18^{th} August, while the observed blooms occur on 14^{th} May and 4^{th} August (figure 5.12).

6.1.4 Uncertainty analysis of phytoplankton dynamics

The simplfiication of the models is accompanied with uncertainty, which cannot be avoided in any of analyses. To get insight in the model prediction, uncertainty analysis is required. The Bayesian Markov Chain Monte Carlo simulation, a full description of uncertainty, is approached to perform uncertainty analysis, processed with WinBugs. Prior to the application, the commonly used Gelman-Rubin convergence test is explored. The prediction varies at a range within the 95% confidence interval, with a small Monte Carlo error. The Bootstrap method is also used in the study to get the 95% confidence interval of the estimate.

6.2 Suggestions for future work

Possible future directions for this research extend to four categories.

Firstly, testing of the models in other cases may result in a broad reflection. Meanwhile, we may in the future introduce other widely used models applied to coastal waters, like SMS (Surface Water Modelling System, accessible through `http://www.scientificsoftwaregroup.com/pages/detailed_description.php?products_id=119`) and MIKE (accessible through `http://www.mikepoweredbydhi.com/`).

Secondly, more field samples should be collected to improve the models. For the BLOOM II model (in chapter 3), the physical and chemical factors are observed, but the effects of the biological features also should be studied, like species composition, cell size, and predation. For the phytoplankton model (in chapter 5), only the physical condition is considered, other chemical-biological factors should still be measured. The common weakness of the BLOOM II model and the phytoplankton model is that chlorophyll *a* or the phytoplankton biomass indicates all the species due to the unknown properties of the species. The specific properties of the species should be distinguished, like diatoms, flagellate, dinoflagellate, and phaeocystis.

Thirdly, a comprehensive understanding of the impact-effect chain of the coastal ecosystem is required. In this thesis, only the significance of the phytoplankton is stressed. The interactions between the phytoplankton and the zooplankton, even the fish and the benthic organisms, need to be investigated in future analysis.

Fourthly, it is valuable to link the phytoplankton model to the bloom forecasting system. One subject of phytoplankton dynamics concerns the bloom development, but is only briefly discussed in chapter 5. Although most of the blooms are not poisonous, the phytoplankton blooms would block the light intensity penetration into the water and affect the marine life. The impacts of these blooms show up in many ways: water is seriously polluted; human health is placed at risk; coastal ecosystems are destroyed; marine life is dying; and overall, economic loss is immense. To reduce the impacts of the bloom events, it is required to regulate the phytoplankton bloom dynamics. A bloom event is defined as a sharp increase of the phytoplankton population within a short time period. The problem is that there is no officially recognized threshold level of the increased population to define a bloom. Researchers have developed the trigger conditions of the blooms, like critical nutrients, critical depth, and vertical stability threshold. In this thesis, the theories of vertical stability threshold and critical depth are discussed. Phytoplankton blooms result from a complex interaction between the environmental variables (hydrographic, meteorological, biological and chemical conditions), of which only a few can be controlled. Without essential nutrients, principally nitrates and phosphates, algae will usually not reach the bloom proportions. The need of the nutrient reduction measures has been recognized as essential for controlling the blooms. We should pay much more attention to these issues in future work.

To manipulate bloom events is a combined work, all the associated actors should involve and cooperate with each other.

- Government

The role of the government is to draft the practical measures to control the wastewater which include a large amount of nutrients.

- Public

On the one hand, the public should reduce the use of fertilizers in agriculture. On the other hand, the public are responsible for informing the relevant departments when they encounter abnormal water colours.

- Industry

The role of the industry is to comply with the emission standards of the sewage and to control the water quality.

- Scientific researchers

The role of the scientific researchers is to provide accurate and timely information on the prediction of the bloom events, finding out the main causes and offering reasonable suggestions.

Appendix A

BLOOM II model

BLOOM II model could be applied in fresh water, transitional water or coastal water to calculate the growth of algae species and transport of substances in the water column. The objective is to maximize the total biomass concentration of phytoplankton species at equilibrium in a certain time period given a set of environmental conditions. The following ecological processes are concentrated:

Phytoplankton processes: growth and mortality;
Attenuation of light;
Decomposition of particulate organic matter in water and sediment;
Reaeration of oxygen;
Nitrification and denitrification of nitrogen;
Settling;
Burial;
Competition processes: grazing, excretion and respiration.

Figure A.1 considers the physical-chemical-biological interactions, and the mathematical formulations required are described after Blauw et al. [2009].

A.1 Nutrient cycling

Nutrient (N, P, and Si) is one of the main limiting factors for the phytoplankton species. The nutrient cycle has three major pools: dissolved inorganic nutrients, living organic

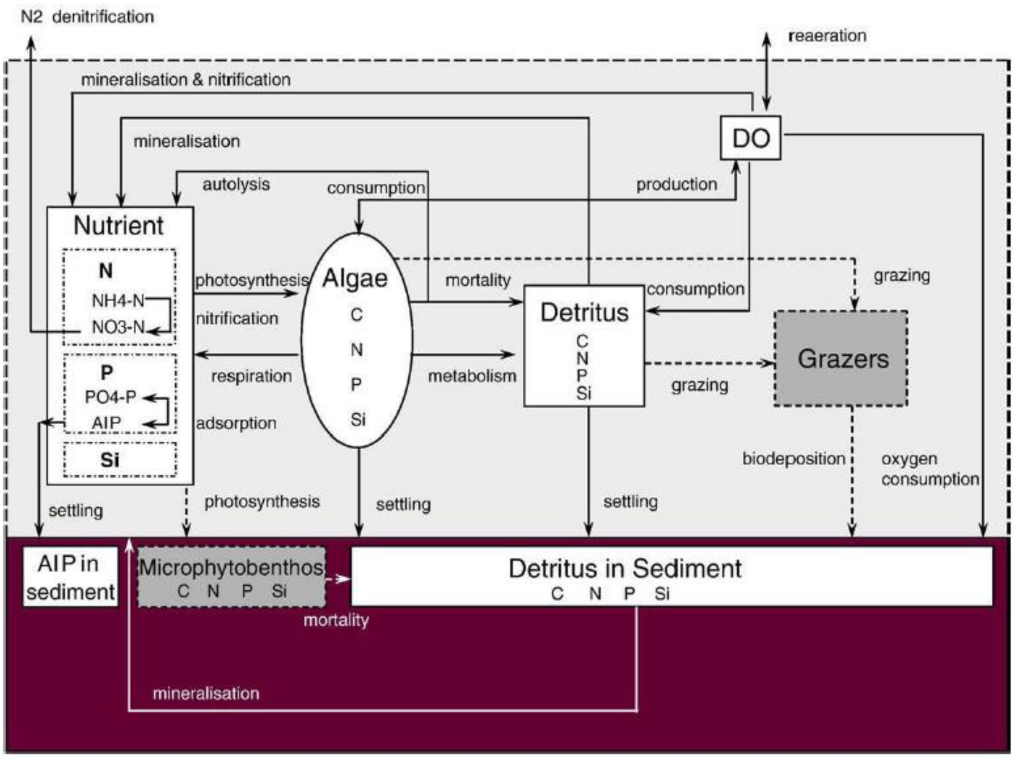

FIGURE A.1: Ecological processes in BLOOM II (after Los et al. [2008])

matter and dead organic matter. Dissolved inorganic nutrients are uptake by primary producers. A number of nutrients are released as dissolved inorganic nutrients within the processes which are called autolysis by the mortality of algae, mineralisation by detritus and nitrification by algae. Some are released from the respiration by the algae. Processes for nitrogen are denitrification (N_2) and nitrification. Nitrate (NO_3^-) is subjected to denitrification in anaerobic zones of the water system: the sediment and deep water in stratified water systems. The microbial process reduces nitrate into elementary nitrogen, which may escape from water system as nitrogen gas. The opposite process is possible by means of the fixation of nitrogen into ammonium by algae.

Living organisms require phosphorus for energy transfer within the cell, for several enzyme systems, and as ingredients of DNA and RNA (Ishige et al. [2003]). In the water column, all phosphorus forms are transformed to more bio-available forms at various rates dependent on microbial actions and environmental conditions. In the sediment layer, phosphorus affects the concentration in the water column when it occurs P-release from the sediment (Nurnberg [1988]; Sas [1989]).

Silicon is only available for phytoplankton in the form of dissolved silicate which just exists in diatoms.

A.2 Light attenuation

The energy constraint concerns the energy obtained from light intensity. It is expressed as the maximal extinction by phytoplankton when the light intensity is reduced to a level where the growth rate equals to the respiration rate. Extinction is modelled as an exponential decrease of light intensity with water depth according to the Lambert-Beer formula. The total extinction coefficient is the sum of the extinction by inorganic suspended particulate matter, organic matter, chlorophyll a, salinity and background extinction. Primary production is strongly influenced by light intensity.

A.3 Growth and mortality

The growth of phytoplankton has been concerned many years ago (Goldman et al. [1979]; Eppley [1981]; Stockner and Antia [1986]). The researchers also explored the relationships between growth rate and cell size (Banse [1976]), nutrient (Skogen et al. [1995]; Los et al. [2008]), temperature (Goldman and Carpenter [1974]) and light (Langdon [1988]).

A.4 Reaeration of dissolve oxygen

Algae can produce and consume oxygen. The process of reaeration of oxygen is to exchange the oxygen with atmosphere and this activity can result in the gain or loss of oxygen in the water column (Hydraulics [2003]).

A.5 Competition between species

Two (or more) plants may influence each other by means of competition and coexistence. Different species of vegetation compete for nutrients, space, light etc. For vegetation the competition is mostly governed by local processes, but for animals the competition takes place over larger domains. In a model this process often implemented as a formulation limited by the interaction of a relatively small number of computational segments in space and time.

Appendix B

Factor analysis

B.1 Principal Component Analysis (PCA)

Let X be the (n,p) matrix of observations $x_{i,j}$, for $i = 1, 2, ..., n,\ j = 1, 2, ..., p$.

$$X = \begin{pmatrix} x_{11} & ... & x_{1p} \\ ... & & ... \\ x_{n1} & ... & x_{np} \end{pmatrix}$$

Where x_{ij} is the value of individual i for variable j which is defined with a vector of n components $(x_{1j}, ..., x_{nj})'$. In the same way, an individual i is identified to a vector x_i of p components with $(x_{i1}, ..., x_{ip})'$.

Let $\overline{x}$ be the vector of arithmetic means of each of the p variables,

$$\overline{x} = (\overline{x_1}, ..., \overline{x_p})'$$

Where

$$\overline{x_j} = \sum_{i=1}^{n} p_i x_{ij}$$

However, it can be useful for some applications to use weight p_i varying from one individual to another as grouped data. These weights, which are positive numbers summing to 1, can be viewed as frequencies and are stored in a diagonal matrix of size n,

$$D_p = \begin{pmatrix} p_1 & & \\ & ... & \\ & & p_n \end{pmatrix}$$

The method consists of projecting the data cloud in order to minimize the shrinkage of the distances which are inherent to the projection. This is equivalent to choosing the projection space F which maximizes the criterion:

$$\sum_{i=1}^{n} \sum_{j=1}^{n} p_i p_j d^2(i,j)$$

Where, $d(i,j)$ indicates the distance between two individual x_i and x_j.

One dimension subspace is defined by a unit vector $u = (u_1, ..., u_p)'$. The projection, or coordinate c_i , is defined by $c_i = \sum_{j=1}^{p} x_{ij} u_j = Xu$. It is a linear combination of the original variables. The variance is then:

$$Var(c) = \sum_{i}^{n} p_i c_i^2 = c' D_p c = u' X' D_p X u$$

The solution of this quadratic maximization problem is the eigenvector u_1 associated with the largest eigenvalue ω_1. We then search for the vector u_2 orthogonal to u_1. Similarly, it is shown that u_2 is the eigenvector associated with the second largest eigenvalue ω_2.

Vectors u_j are called principal factors. They contain the coefficients to be applied to the original variables in the linear combination $c = Xu$. Principal components are artificial variables defined by principal factors $c_j = Xu_j$.

B.2 Maximum Likelihood (ML)

This method determines the values of parameters of a distribution model that maximizes the likelihood of the sample data. The maximum solutions are obtained by minimizing

$$F = tr[(\Lambda\Lambda' + \Psi^2)^{-1}R] - log|(\Lambda\Lambda' + \Psi^2)^{-1}R| - p$$

Where, Λ is the factor loading matrix, Ψ^2 is the diagonal matrix of variances.

Firstly, the conditional minimum of F for a given y is found. This gives the function $f(\Psi)$, which is minimized using the Newton-Raphson procedure. Let x_s be the column vector including the logarithm of the diagonal elements of y at the s^{th} iteration, then

$$x_{s+1} = x_s - d_s$$

In which, d_s is the solution to the system of linear equations,

$$H_s d_s = h_s$$

and

$$H_s = \frac{\partial^2 f(\Psi)}{\partial x_i \partial x_j}$$

h_s is the column vector. The starting point x_1 is,

$$x_j^1 = log[(1 - m/2p)/r_{ij}]$$

Where m is the number of factors and r_{ij} is the j^{th} diagonal element of R^{-1}.

The function of $f(\Psi)$ can be expressed in terms of the eigenvalues $\omega_1 \leq \omega_2 \leq ... \leq \omega_p$. That is,

$$f(\Psi) = \sum_{k=m+1}^{p} (log\omega_k + \omega_k^{-1} - 1)$$

B.3 Unweighted Least Squares (ULS)

The same basic theory is used in ULS as in ML, except the form of function $f(\Psi)$.

$$f(\Psi) = \sum_{k=m+1}^{p} \frac{(w_k - 1)^2}{2}$$

Appendix C

Critical depth

This concept is introduced after Sverdrup [1953], and is referred to after Huisman et al. [1999] here.

Consider a well-mixed water column. Let ω denote the phytoplankton population density, with dimension being number of phytoplankton per unit volume. The growth rate of the phytoplankton population depends on the balance between production and loss:

$$\frac{\mathrm{d}\omega}{\mathrm{d}t} = \frac{1}{H}\int_0^H p[I(z)]\omega dz - L\omega$$

where $p[I]$ is the specific rate of production as an increasing function of light intensity, $I(z)$ is the light intensity as a decreasing function of depth, H is the total depth of the water column, and L is the loss rate imposed by dilution.

The light intensity, I, decreases with depth according to Lambert-Beer's law:

$$I(z) = I_{in}e^{-(K_d\omega z + K_{bg}z)}$$

Where I_{in} is the incident light intensity, K_d is the specific light attenuation coefficient of the phytoplankton, and K_{bg} is the total background turbidity due to non-phytoplankton components. The light intensity at the bottom of the water column, I_{out}, is given by $I_{out} = I(H)$.

Combining the two equations mentioned above gives the following dynamical system (Huisman and Weissing [1994]; Weissing and Huisman [1994]; see also Bannister [1974]):

$$\frac{\mathrm{d}\omega}{\mathrm{d}t} = \frac{1}{H}\frac{K_d\omega}{K_d\omega+K_{bg}}\int_{I_{out}}^{I_{in}}\frac{p[I)]}{K_dI}dI - L\omega$$

$$I_{out} = I_{in}e^{-(K_d\omega z+K_{bg}z)}$$

This model predicts that there is a critical value of I_{out} which we have called the critical light intensity, at which the phytoplankton population should remain stationary. Because the critical light intensity is independent of mixing depth, the population density at steady state should be inversely proportional to mixing depth:

$$\omega* = \frac{1}{K_dH}ln(I_{in}/I_{out}*) - \frac{K_{bg}}{K_d}$$

Where $I_{out}*$ is the critical light intensity, and $\omega*$ indicates that ω is evaluated at steady state. Then we can get the critical depth ($\omega* = 0$):

$$z* = \frac{ln(I_{in}/I_{out}*)}{K_{bg}}$$

Appendix D

Commonly used probability distributions

D.1 Normal distribution

The best known and most widely used probability distribution is undoubtedly the normal distribution (Gaussian distribution). Its PDF for a continuous random variable X, is given by

$$f_X(x) = \frac{1}{\sigma\sqrt{2\pi}} exp[-\frac{1}{2}(\frac{x-\mu}{\sigma})^2] \qquad -\infty < x < \infty$$

Where, μ and σ indicate the mean and standard deviation of X , respectively. It is well known that the normal distribution is bell-shaped and symmetrical with respect to the mean μ. Therefore, the skewness coefficient of a normal random variable is zero.

D.2 Lognormal distribution

The lognormal distribution is also a popular probability distribution for positively valued random variables. Its PDF for a random variable X is defined as:

$$f_X(x) = \frac{1}{\varsigma x\sqrt{2\pi}} exp[-\frac{1}{2}(\frac{lnx-\eta}{\varsigma})^2] \qquad x \geqslant 0$$

Where, $\eta = E(lnX)$ and $\varsigma = \sqrt{Var(lnX)}$ indicate the mean and standard deviation of lnX , respectively. Lognormal random variables are closely related to normal random variables by a transform $Y = ln(X)$.

D.3 Gamma distribution

The Gamma distribution is a versatile continuous distribution associated with a positive-valued random variable. The Gamma distribution for a random variable X has the following PDF,

$$f_X(x) = \frac{\nu(\nu x)^{\kappa-1}}{\Gamma(\kappa)} exp(-\nu x) \qquad x \geqslant 0$$

In which, ν and κ are the rate parameter and shape parameter of Gamma distribution, respectively, and $\Gamma(\kappa)$ is the Gamma function defined as:

$$\Gamma(\kappa) = \int_0^\infty x^{\kappa-1} e^x dx \qquad \kappa > 1$$

The mean and variance of Gamma distribution are,

$$\mu_X = \frac{\kappa}{\nu}$$

and

$$\sigma_X^2 = \frac{\kappa}{\nu^2}$$

D.4 Weibull distribution

The Weibull distribution for a random variable X is defined as:

$$f_X(x) = \frac{\gamma}{\lambda}(\frac{x}{\lambda})^{\gamma-1}exp[-(\frac{x}{\lambda})^{\gamma}] \qquad\qquad x \geqslant 0$$

In which, γ and λ indicate the scale parameter and shape parameter of Weibull distribution, respectively.

Appendix E

Statistical properties of random variables

E.1 Mean, median, and quartiles

The central tendency of a random variable is the so-called mean μ_X, which is the first order moment.

$$\mu_X = E(X) = \int_{-\infty}^{\infty} x f_X(x) dx$$

The median of a random variable is the value that splits the distribution into two equal halves. Mathematically, the median of a continuous random variable satisfies the following equation.

$$F_X(x_{md}) = \int_{-\infty}^{x_{md}} f_X(x) dx = 0.5$$

Therefore, the median is the 50^{th} percentile of a random variable X. A quantity x_p satisfies

$$p = P(X \leqslant x_p) = F_X(x_p)$$

E.2 Variance and standard deviation

The variance is the second order central moment, defined as

$$Var[X] = \sigma_x^2 = E[(X - \mu_X)^2] = \int_{-\infty}^{\infty} (x - \mu_X)^2 f_X(x) dx$$

The positive squared root of variance is the standard deviation, which is often used as the measure of the degree of uncertainty.

E.3 Skewness coefficient and kurtosis

Another property of a random variable is the symmetry or asymmetry of its PDF or PMF, and the associated degree of asymmetry. Skewness is the third central moment,

$$\gamma_x = E(X - \mu_X)^3 = \sum_{x_i} (x_i - \mu_X)^3 P_X(x_i) \quad \text{for discrete } X$$

and

$$\gamma_x = E(X - \mu_X)^3 = \int_{-\infty}^{\infty} (x_i - \mu_X)^3 P_X(x_i) \quad \text{for continuous } X$$

If $\gamma_x = 0$, the distribution is symmetric about its mean value μ_X; if $\gamma_x > 0$, the distribution has a long tail to the right; if $\gamma_x < 0$, the distribution has a long tail to the left.

A convenient dimensionless measure of the degree of asymmetry can be defined as

$$\theta = \frac{\gamma_x}{\sigma^3}$$

Kurtosis is a measure of the peakedness of the underlying distribution. It is the fourth central moment of a random variable.

$$\kappa_x = E(X - \mu_X)^4 = \sum_{x_i} (x_i - \mu_X)^4 P_X(x_i) \qquad \text{for discrete } X$$

and

$$\kappa_x = E(X - \mu_X)^4 = \int_{-\infty}^{\infty} (x_i - \mu_X)^4 P_X(x_i) \qquad \text{for continuous } X$$

E.4 Covariance and correlation coefficient

When there are two dependent random variables, there may be a relationship between them. The correlation coefficient is defined by the covariance to standard deviations of the two random variables.

$$\rho_{x,y} = Corr(X, Y) = \frac{Cov(X,Y)}{\sigma_x \sigma_y}$$

Where $Cov(X, Y)$ is the covariance defined as

$$Cov(X, Y) = E[(X - \mu_X)(Y - \mu_Y)] = E(XY) - \mu_X \mu_Y$$

$\rho_{x,y}$, a dimensionless number, ranges between -1.0 and +1.0.

Bibliography

MIKE 3: environmental hydraulics. Technical report, 2000.

T. Aarup. Transparency of the North Sea and Baltic Sea – a Secchi depth data mining study. *Oceanologia*, 44(3):323–327, 2002.

J.I. Allen, Timothy J. Smyth, John R. Siddorn, and Martin Holt. How well can we forecast high biomass algal bloom events in a eutrophic coastal sea? *Harmful Algae*, 8(1):70–76, 2008.

S.E. Allen and M.A. Wolfe. Hindcast of the timing of the spring phytoplankton bloom in the Strait of Georgia, 1968–2010. *Progress in Oceanography*, 115:6–13, 2013.

J.H. Andersen. Coastal eutrophication: recent developments in definitions and implications for monitoring strategies. *Journal of Plankton Research*, 28(7):621–628, 2006.

D.M. Anderson, P.M. Glibert, and J.M. Burkholder. Harmful Algal Blooms and Eutrophication Nutrient Sources , Composition , and Consequences. *Estuaries*, 25:704–726, 2002.

A.H.S. Ang and W.H. Tang. Probability concepts in engineering: emphasis on applications to civil and environmental engineering, 2007.

G.B. Arhonditsis and M.T. Brett. Eutrophication model for Lake Washington (USA). *Ecological Modelling*, 187(2-3):140–178, 2005.

T.T. Bannister. Production equations in terms of chlorophyll concentration, quantum yield and upper limit to production. *Limnology and Oceanography*, 19:1–12, 1974.

K. Banse. Rates of growth, respiration and photosynthesis of unicellular algae as related to cell size- a review. *Phycology*, 12:135–140, 1976.

J.W. Baretta, W. Ebenhöh, and P. Ruardij. The European regional seas ecosystem model, a complex marine ecosystem model. *Journal of Sea Research*, 33(3-4):233–246, 1995.

M.J. Behrenfeld. Abandoning Sverdrup's Critical Depth Hypothesis on phytoplankton blooms. *Ecology*, 91:977–989, 2010.

M.J Behrenfeld and P.G. Falkowski. Photosynthetic rates derived from satellite-based chlorophyll concentration. *Limnology and Oceanography*, 42(1):1–20, 1997.

J.E. Bissinger, D.J.S Montagnes, and J. Sharples. Predicting marine phytoplankton maximum growth rates from temperature : Improving on the Eppley curve using quantile regression. *Limnology and Oceanography*, 53(2):487–493, 2008.

A. Blauw and F.J. Los. Analysis of the response of phytoplankton indicators in Dutch coastal waters to nutrietnt reduction scenarios. Technical report, 2004.

A. Blauw, F.J. Los, M. Bokhorst, and P.L. Erftemeijer. GEM: a generic ecological model for estuaries and coastal waters. *Hydrobiologia*, 618:175–198, 2009.

M. Bölter, M. Meyer, and B. Probst. A statistical scheme for structural analysis in marine ecosystems. *Ecological Modelling*, 9:143–151, 1980.

J.N. Boyer, C.R. Kelble, P.B. Ortner, and D.T. Rudnick. Phytoplankton bloom status: Chlorophyll a biomass as an indicator of water quality condition in the southern estuaries of Florida, USA. *Ecological Indicators*, 9(6):S56–S67, 2009.

S.P. Brooks and A. Gelman. Alternative methods for monitoring convergence of iterative simulations. *Journal of Computational and Graphical Statistics*, 7:434–455, 1998.

M.A. Brzezinski. The Si:C:N ratio of marine diatoms: interspecific variability and the effect of some environmental variables. *Journal of Phycology*, 21(3):347–357, 2004.

J. Caperon. Population growth in micro-organisms limited by food supply. *Ecology*, 48: 715–722, 1967.

G.C. Chang. Coastal ocean optical influences on solar transmission and radiant heating rate. *Journal of Geophysical Research*, 109:C01020, 2004.

D.G. Chapman. Statistical problems in dynamics of explited fisheries populations, 1961.

K.W. Chau and N. Muttil. Data mining and multivariate statistical analysis for ecological system in coastal waters. *Hydroinformatics*, 9:305–317, 2007.

C. Chen, D.A. Wiesenburg, and L. Xie. Influences of river discharge on biological production in the inner shelf. A coupled biolgical and physical model of the Louisiana-Texas shelf. *Marine Research*, 55:293–320, 1997.

H. Claustre and J.C. Marty. Specific phytoplankton biomasses and their relation to primart production in the tropical North Atlantic. *Deep Sea Research Part I: Oceanographic Research Papers*, 42(8):1475–1493, 1995.

J.E. Cloern. Tidal stirring and phytoplankton bloom dynamics in an estruary. *Marine Research*, 49:203–221, 1991.

J.E. Cloern. Phytoplankton bloom dynamics in coastal ecosystems: a review with some general lessons from sustained investigation of San Francisco Bay, California. *Reviews of Geophysics*, 34:127–168, 1996.

J.E. Cloern. The relative importance of light and nutrient limitation of phytoplankton growth : a simple index of coastal ecosystem sensitivity to nutrient enrichment. *Aquatic Ecology*, 33:3–16, 1999.

J.E. Cloern. Our evolving conceptual model of the coastal eutrophication problem. *Marine Ecology Progress Series*, 210:223–253, 2001.

J.E. Cloern, S.Q. Foster, and A.E. Kleckner. Phytoplankton primary production in the world's estuarine-coastal ecosystems. *Biogeosciences*, 11(9):2477–2501, 2014.

D.J. Conley, S. Markacer, Andersen J., T. Ellermann, and L.M. Svendsen. Coastal Eutrophication and the Danish National Aquatic Monitoring and Assessment Program. *Estuaries*, 25:848–861, 2002.

M. Davey, G.A. Tarran, M.M. Mills, C. Ridame, and R.J. Geider. Nutrient limitation of picophytoplankton photosynthesis and growth in the tropical North Atlantic. *Limnology and Oceanography*, 53:1722–1733, 2008.

W.C. Dennison, R.J. Orth, K.A. Moore, J.C. Stevenson, V. Carter, S. Kollar, P.W. Bergstrom, and R.A. Batiuk. Assessing water quality with submersed aquatic vegetation habitat requirements as barometers of Chesapeake Bay health. *Bioscience*, 43 (2):86–94, 1993.

M.J. Devlin, J. Barry, D.K. Mills, R.J. Gowen, J. Foden, D. Sivyer, and P. Tett. Relationships between suspended particulate material, light attenuation and Secchi depth in UK marine waters. *Estuarine, Coastal and Shelf Science*, 79(3):429–439, 2008.

D.M. Di Toro. vertical interactions in phytoplankton populations_ an asymptotic eigenvalue analysis.pdf. In 17^{th} *Conference Great Lakes Research*, pages 17–27, 1974.

R.C. Dugdale. Nutrient limitation in the sea: dynamics, identification, and significance. *Limnology and Oceanography*, 12:685–695, 1967.

K. Edelvang, H. Kaas, A.C. Erichsen, D. Alvarez-Berastegui, K. Bundgaard, and Peter Viskum Jø rgensen. Numerical modelling of phytoplankton biomass in coastal waters. *Journal of Marine Systems*, 57(1-2):13–29, 2005.

A.M. Edwards. Adding detritus to a nutrient – phytoplankton – zooplankton model : a dynamical-systems approach. *Journal of Plankton Research*, 23(4):389–413, 2001.

A.M. Edwards and J. Brindley. Oscillatory behaviour in a three-component plankton population model. *Dynamics and Stability of Systems*, 11(4):347–370, 1996.

P.H.C. Eilers and J.C.H. Peeters. A model for the relationship between light intensity and the rate of photosynthesis in phytoplankton. *Ecological Modelling*, 42:199–215, 1988.

R.W. Eppley. Growth rates of marine phytoplankton: correlation with light absorption by cell chlorophyll a. *Physiologia Plantarum*, 19:47–59, 1966.

R.W. Eppley. Temperature and phytoplankton growth in the sea. *Fishery Bulletin*, 70 (4):1063–1085, 1972.

R.W. Eppley. Relations between nutrient assimilation and growth in phytoplankton with a brief review of estimates of growth rate in the ocean. *Can. Bull. Fish. Aquat. Sci.*, 210:251–263, 1981.

G.T. Evans and J.S. Parslow. A model of annual plankton cycles. *Biological Oceanography*, 3:327–347, 1985.

P.G. Falkowski, D. Ziemann, Z. Kolber, and P.K. Bienfang. Role of eddy pumping in enhancing primary production in the ocean. *Nature*, 352:55–58, 1991.

M. Felip and Jordi Catalan. The relationship between phytoplankton biovolume and chlorophyll in a deep oligotrophic lake: decoupling in their spatial and temporal maxima. *Journal of Plankton Research*, 22(1):91–105, January 2000.

K. Fennel. Subsurface maxima of phytoplankton and chlorophyll : Steady-state solutions from a simple model. *Limnology and Oceanography*, 48(4):1521–1534, 2003.

J.M. Ferris and R. Christian. Aquatic primary production in relation to microalgal responses to changing light : a review. *Aquatic Sciences*, 53:187–217, 1991.

K.J. Flynn and M.J.R. Fasham. A short version of the ammonium-nitrate interaction model. *Journal of Plankton Research*, 19(12):1881–1897, 1997.

P.J S Franks. Models of harmful algal blooms. *Limnology and Oceanography*, 42(5): 1273–1284, 1997.

P.J.S. Franks. NPZ models of plankton dynamics: their construction, coupling to physics, and application. *Oceanography*, 58:379–387, 2002.

M.A.M. Friedrichs, Mary-Elena Carr, R.T. Barber, M. Scardi, D. Antoine, R.A. Armstrong, I. Asanuma, M.J. Behrenfeld, E.T. Buitenhuis, F. Chai, J.R. Christian, A.M. Ciotti, S.C. Doney, M. Dowell, John Dunne, Bernard Gentili, Watson Gregg, Nicolas Hoepffner, Joji Ishizaka, Takahiko Kameda, Ivan Lima, John Marra, Frédéric Mélin, J. K. Moore, André Morel, Robert T. O'Malley, Jay O'Reilly, Vincent S. Saba, Marjorie Schmeltz, Tim J. Smyth, Jerry Tjiputra, Kirk Waters, Toby K. Westberry, and Arne Winguth. Assessing the uncertainties of model estimates of primary productivity in the tropical Pacific Ocean. *Journal of Marine Systems*, 76(1-2):113–133, 2009.

Mingzhu Fu, Zongling Wang, Yan Li, Ruixiang Li, Ping Sun, Xiuhua Wei, Xuezheng Lin, and Jingsong Guo. Phytoplankton biomass size structure and its regulation in the Southern Yellow Sea (China): Seasonal variability. *Continental Shelf Research*, 29(18):2178–2194, 2009.

R.J. Geider and J. La Roche. Redfield revisited: variability of C:N:P in marine microalgae and its biochemical basis. *European Journal of Phycology*, 37(1):1–17, 2002.

R.J. Geider, H.L. Maclntyre, and T.M. Kana. A dynamic regulatory model of phytoplanktonic temperature acclimation to light , nutrients , and. *Limnology and Oceanography*, 43(4):679–694, 1998.

A. Gelman and D.B. Rubin. Inference from iterative simulation using multiple sequences. *Statistical Science*, 7(4):457–511, 1992.

J. Godrijan, D. Marić, I. Tomažić, R. Precali, and M. Pfannkuchen. Seasonal phytoplankton dynamics in the coastal waters of the north-eastern Adriatic Sea. *Journal of Sea Research*, 77:32–44, 2013.

J.C. Goldman and E.J. Carpenter. A kinetic approach to the effect of temperature. *Limnology and Oceanography*, 19:756–766, 1974.

J.C. Goldman, McCarthy J.J., and D.G. Peavey. Growth rate influence on the chemical composition of phytoplankton in oceanic waters. *Nature*, 279:210–215, 1979.

G. Govaert. Digital signal and image processing series: data analysis, 2009.

J.D. Haney and G.A. Jackson. Modelling phytoplankton growth rates. *Plankton Research*, 18:63–85, 1996.

Xiaoyan He, Ya Ping Wang, Qingguang Zhu, Ying Zhang, Dong Zhang, Jicai Zhang, Yang Yang, and Jianhua Gao. Simulation of sedimentary dynamics in a small-scale estuary: the role of human activities. *Environmental Earth Sciences*, 2015.

S.A. Henson, I. Robinson, J. T. Allen, and J.J. Waniek. Effect of meteorological conditions on interannual variability in timing and magnitude of the spring bloom in the Irminger Basin, North Atlantic. *Deep Sea Research Part I: Oceanographic Research Papers*, 53(10):1601–1615, 2006.

C.P. Holliday, T.C. Rasmussen, and W.P. Miller. Establishing the relationship between turbidity and total suspended sediment concentration. *Proceedings of the 2003 Georgia water resources conference*, pages 1–3, 2003.

R.W. Howarth and R. Marino. Nitrogen as the limiting nutrient for eutrophication in coastal marine ecosystems : Evolving views over three decades. *Limnology and Oceanography*, 51:364–376, 2006.

J. Huisman and F.J. Weissing. Light-limited growth and competition for light in well-mixed aquatic environments: an elementary model. *Ecology*, 75:507–520, 1994.

J. Huisman, Paul van Oostveen, and J. Weissing Franz. Critical depth and critical turbulence: Two different mechanisms for the development of phytoplankton blooms. *Limnology and Oceanography*, 44(7):1781–1787, 1999.

B.L. Hunter and E.A. Laws. ATP and chlorophyll a as estimators of phytoplankton carbon biomass. *Limnology and Oceanography*, 26(5):944–956, 1981.

Y. Huot, M. Babin, F. Bruyant, C. Grob, and M.S. Twardowski. Does chlorophyll a provide the best index of phytoplankton biomass for primary productivity studies ? *Biogeosciences Discussions*, 4:707–745, 2007.

WL|Delft Hydraulics. Mathematical simulation of algae blooms by the model BLOOM II. Technical report, 1991.

WL|Delft Hydraulics. Delft3D-WAQ users' manual. Technical report, 2003.

T. Ishige, M. Krause, M. Bott, V. F. Wendisch, and H. Sahm. The phosphate starvation stimulon of Corynebacterium glutamicum determined by DNA microarray analyses. *Journal of Bacteriology*, 185(15):4519–4529, 2003.

B.M. Jamart, D.F. Winter, and K. Banse. Sensitivity analysis of a mathematical model of phytoplankton growth and nutrient distribution in the Pacific Ocean off the northwestern U . S . coast. *Plankton Research*, 1:267–290, 1979.

Jie Jin, Su Mei Liu, Jing Ling Ren, Cheng Gang Liu, Jing Zhang, Guo Ling Zhang, and Da Ji Huang. Nutrient dynamics and coupling with phytoplankton species composition during the spring blooms in the Yellow Sea. *Deep Sea Research Part II: Topical Studies in Oceanography*, 97:16–32, 2013.

S.E. Jorgensen. Handbook of environmental data and ecological parameters, 1979.

H.F.. Kaiser. The application of electronic computers to factor analysis. *Educational and Psychological Measurement*, 20:141–151, 1960.

A.B. Kara, A.J. Wallcraft, and H.E. Hurlburt. A new solar radiation penetration scheme for use in ocean mixed layer studies: an application to the Black Sea using a fine-resolution hybrid coordinate ocean model (HYCOM)*. *Journal of Physical Oceanography*, 35(1):13–32, 2005.

D.L. Kelly and Curtis L. Smith. Bayesian inference in probabilistic risk assessment—The current state of the art. *Reliability Engineering & System Safety*, 94(2):628–643, 2009.

V.S. Kennedy, Robert R Twilley, Joan A Kleypas, James H Cowan, and Steven R Hare. Coastal and marine ecosystems. Technical report, 2002.

M. Kishi and Saburo Ikeda. Population dynamics of 'red tide' organisms in eutrophicated coastal waters — Numerical experiment of phytoplankton bloom in the East Seto Inland Sea, Japan. *Ecological Modelling*, 31(1-4):145–174, 1986.

G. Kuczera. Comprehensive at-site flood frequency analysis using Monte Carlo Bayesian inference. *Water Resources Research*, 35:1291–1312, 1999.

C. Langdon. On the causes of interspecific differences in the growth-irradiance relationship for phytoplankton . II . A general review. *Plankton Research*, 10(6):1291–1312, 1988.

Zhongping Lee, Alan Weidemann, John Kindle, Robert Arnone, Kendall L. Carder, and Curtiss Davis. Euphotic zone depth: Its derivation and implication to ocean-color remote sensing. *Journal of Geophysical Research*, 112(C3):C03009, 2007.

J. Lewis. Turbidity-controlled suspended sediment sampling for runoff-event load estimation. *Water Resources Research*, 32(7):2299–2310, 1996.

M. Lionard, Koenraad Muylaert, Dirk Van Gansbeke, and Wim Vyverman. Influence of changes in salinity and light intensity on growth of phytoplankton communities from the Schelde river and estuary (Belgium/The Netherlands). *Hydrobiologia*, 540(1-3): 105–115, 2005.

Feng Liu, Shao Jun Pang, Xiao Bo Zhao, and Chuan Ming Hu. Quantitative, molecular and growth analyses of Ulva microscopic propagules in the coastal sediment of Jiangsu province where green tides initially occurred. *Marine Environmental Research*, 74:56–63, 2012.

A. Longhurst, Shubha Sathyendranath, Trevor Platt, and Carla Caverhill. An estimate of global primary production in the ocean from satellite radiometer data. *Plankton Research*, 17(6):1245–1271, 1995.

F. J. Los. *Eco-hydrodynamic modelling of primary production in coastal waters and lakes using BLOOM.* PhD thesis, Wageningen University, 2009.

F.J. Los and J.J. Brinkman. Phytoplankton modelling by means of optimizing-a 10-year experience with BLOOM II. *Verhandlungen des Internationalen Verein Limnologie*, 23:790–795, 1988.

F.J. Los and J.W.M. Wijsman. Application of a validated primary production model (BLOOM) as a screening tool for marine, coastal and transitional waters. *Journal of Marine Systems*, 64(1-4):201–215, 2007.

F.J. Los, M.T. Villars, and M.W.M. Van der Tol. A 3-dimensional primary production model (BLOOM/GEM) and its applications to the (southern) North Sea (coupled physical–chemical–ecological model). *Journal of Marine Systems*, 74(1-2):259–294, 2008.

P.J. Luyten, J.E. Jones, R. Proctor, A. Tabor, and K. Wild-Allen. Coherens-a coupled hydrodynamic ecological model for regional and shelf seas: user documentation. Technical report, 1999.

R. Margalef. Life-forms of phytoplankton as survival alternatives in an unstable environment. *Oceanologica Acta*, 1(4):493–509, 1978.

D. Marić, Romina Kraus, Jelena Godrijan, Nastjenjka Supić, Tamara Djakovac, and Robert Precali. Phytoplankton response to climatic and anthropogenic influences in the north-eastern Adriatic during the last four decades. *Estuarine, Coastal and Shelf Science*, 115:98–112, 2012.

J.H. Martin, George A. Knauer, David M. Karl, and William W. Broenkow. VERTEX: carbon cycling in the northeast Pacific. *Deep Sea Research Part A. Oceanographic Research Papers*, 34(2):267–285, 1987.

L.W. Mays and Y.K.. Tung. *Hydrosystems Engineering and Management*. McGraw-Hill, New York, 1992.

Zhiping Mei, Zoe V Finkel, and Andrew J Irwin. Light and nutrient availability affect the size-scaling of growth in phytoplankton. *Journal of Theoretical Biology*, 259(3): 582–8, 2009.

B. Modenutti, Gonzalo Pérez, Esteban Balseiro, and Claudia Queimaliños. The relationship between light attenuation , chlorophyll a and total suspended solids in a Southern Andes glacial lake. *Verhandlungen des Internationalen Verein Limnologie*, 27:1–4, 2000.

G.K. Moore. Satellite remote sensing of water turbidity / Sonde de télémesure par satellite de la turbidité de l'eau. *Hydrological Sciences Bulletin*, 25(4):407–421, 2009.

A. Morel and Jean-Francois Berthon. Surface pigments , algal biomass profiles , and potential production of the euphotic layer : Relationships reinvestigated view of remote-sensing applications. *Limnology and Oceanography*, 34:1545–1562, 1989.

A.G. Murray and J.S. Parslow. The analysis of alternative formulations in a simple model of a coastal ecosystem. *Ecological Modelling*, 119(2-3):149–166, 1999.

L. Niu and P.H.A.J.M. Van Gelder. Probabilistic analysis of sand transport behavior at the Frisian Inlet (NL) under storm events. *Proceedings of the* 35^{th} *IAHR World Congress*, pages 1–10, 2013.

L. Niu, P H A J M Van Gelder, Yiqing Guan, and J K Vrijling. Uncertainty Analysis and Modelling of Phytoplankton Dynamics in Coastal Waters. *Environment Protection and Sustainable Development*, 1(4):193–202, 2015a.

L. Niu, P.H.A.J.M. Van Gelder, Yiqing Guan, Changkuan Zhang, and J.K. Vrijling. Probabilistic analysis of phytoplankton biomass at the Frisian Inlet (NL). *Estuarine, Coastal and Shelf Science*, 155:29–37, 2015b.

L. Niu, P.H.A.J.M. van Gelder, Changkuan Zhang, Yiqing Guan, and J.K. Vrijling. Statistical analysis of phytoplankton biomass in coastal waters: Case study of the Wadden Sea near Lauwersoog (The Netherlands) from 2000 to 2009. *Ecological Informatics*, 30:12–19, November 2015c.

G.K. Nurnberg. Prediction of phosphorus release rates from total and reductant-soluble phosphorus in anoxic lake sediments. *Journal of Fisheries Aquatic Science*, 45:453–462, 1988.

J.E. Oakley and Anthony O Hagan. Probabilistic sensitivity analysis of complex models : a Bayesian approach. *Journal of the Royal Statistical Society, Series B*, 66:751–769, 2004.

E.B. Örnólfsdóttir, S.Elizabeth Lumsden, and James L. Pinckney. Nutrient pulsing as a regulator of phytoplankton abundance and community composition in Galveston Bay, Texas. *Journal of Experimental Marine Biology and Ecology*, 303(2):197–220, 2004.

B. Paudel and Paul A. Montagna. Modeling inorganic nutrient distributions among hydrologic gradients using multivariate approaches. *Ecological Informatics*, 24:35–46, 2014.

A. Paytan and Karen McLaughlin. The oceanic phosphorus cycle. *Chemical reviews*, 107(2):563–76, 2007.

M.F. Pedersen and Jens Borum. Nutrient control of algal growth in estuarine waters. Nutrient limitation and the importance of nitrogen requirements and nitrogen storage among phytoplankton and species of macroalgae. *Marine Ecology Progress Series*, 142:261–272, 1996.

T. Platt, D. F. Bird, and S. Sathyendranath. Critical depth and marine primary production. *Proceedings of the Royal Society B: Biological Sciences*, 246:205–217, 1991.

R. Portielje, Thorkild Hvitved-Jacobsen, and Kjeld Schaarup-Jensen. Risk analysis using stochastic reliability methods applied to two cases of deterministic water quality models. *Water Research*, 34(1):153–170, 2000.

I. Primpas, George Tsirtsis, Michael Karydis, and Giorgos D. Kokkoris. Principal component analysis: Development of a multivariate index for assessing eutrophication according to the European water framework directive. *Ecological Indicators*, 10(2): 178–183, 2010.

G. Radach and Andreas Moll. Review of three-dimensional ecological modelling related to the North Sea shelf system . Part 2 : Model validation and data needs. Technical report, 2006.

T. Ramírez, D. Cortés, J.M. Mercado, M. Vargas-Yañez, M. Sebastián, and E. Liger. Seasonal dynamics of inorganic nutrients and phytoplankton biomass in the NW Alboran Sea. *Estuarine, Coastal and Shelf Science*, 65(4):654–670, 2005.

D.A. Ratkowsky, June Olley, T.A. Mcmeekin, and A. Ball. Relationship between temperature and growth rate of bacterial cultures. *Bacteriology*, 149(1):1–5, 1982.

K.H. Reckhow. A random coefficient model for chlorophyll-nutrient relationships in lakes. *Ecological Modelling*, 70(1-2):35–50, 1993.

F. Recknagel, Anita Talib, and Diederik van der Molen. Phytoplankton community dynamics of two adjacent Dutch lakes in response to seasons and eutrophication control unravelled by non-supervised artificial neural networks. *Ecological Informatics*, 1(3): 277–285, 2006.

D.S. Reis and Jery R. Stedinger. Bayesian MCMC flood frequency analysis with historical information. *Journal of Hydrology*, 313(1-2):97–116, 2005.

G. Riley. *Quantitative ecology of the plankton of the western North Atlantic*. Bingham Oceanographic Laboratory, New Haven Conn., 1949.

S. Sal and Ángel López-Urrutia. Comment: Temperature, nutrients, and the size-scaling of phytoplankton growth in the sea. *Limnology and Oceanography*, 56(5):1952–1955, 2011.

H. Sas. *Lakes restoration by reduction of nutrient loading: expectations, experiences, extrapolations*. Academia Verlag Richarz, 1989.

S. Sathyendranath and Trevor Platt. Computation of aquatic primary production: extended formalism to include effect of angular and spectral distribution of light. *Limnology and Oceanography*, 34(l):188–198, 1989.

U.M. Scharler and D. Baird. The influence of catchment management on salinity, nutrient stochiometry and phytoplankton biomass of Eastern Cape estuaries, South Africa. *Estuarine, Coastal and Shelf Science*, 56(3-4):735–748, 2003.

I.R. Schloss, Gustavo A Ferreyra, and Diana Ruiz-pino. Phytoplankton biomass in Antarctic shelf zones : a conceptual model based on Potter Cove , King George Island. *Journal of Marine Systems*, 36:129–143, 2002.

M.H. Schlüter, Agostino Merico, Karen H. Wiltshire, Wulf Greve, and Hans von Storch. A statistical analysis of climate variability and ecosystem response in the German Bight. *Ocean Dynamics*, 58(3-4):169–186, 2008.

I. Schmidt. The importance of phytoplankton biomass as an ecosystem parameter in shallow bays of the Baltic . I . Relationships between biomass and system characteristics. *Limnologyica*, 29:301–307, 1999.

J.L. Schnoor and D.M. Di Toro. Differential phytoplankton sinking and growth rates_an eigenvalue analysis.pdf. *Ecological Modelling*, 9:233–245, 1980.

T. Serra, J. Vidal, X. Casamitjana, M. Soler, and J. Colomer. The role of surface vertical mixing in phytoplankton distribution in a stratified reservoir. *Limnology and Oceanography*, 52(2):620–634, 2007.

M.K. Shukla, R. Lal, and M. Ebinger. Determining soil quality indicators by factor analysis. *Soil and Tillage Research*, 87(2):194–204, 2006.

D.A. Siegel, S.C. Doney, and J.A. Yoder. The North Atlantic spring phytoplankton bloom and Sverdrup's critical depth hypothesis. *Science (New York, N.Y.)*, 296(5568): 730–3, 2002.

M.D. Skogen. A user's guide to Norwecom: the Norwegian ecological mdoel system. Technical report, 1993.

M.D. Skogen, Einar Svendsen, Jarle Berntsen, Dag Aksnes, and Kåre B Ulvestad. Modelling the primary production in the North Sea using a coupled three-dimensional physical-chemical-biological ocean model. *Estuarine, Coastal and Shelf Science*, 41 (5):545–565, 1995.

T.J. Smayda. Harmful algal blooms : their ecophysiology and general relevance to phytoplankton blooms in the sea. *Limnology and Oceanography*, 42(5):1137–1153, 1997.

R.A. Smith. The theoretical basis for estimating phytoplankton production and specific growth rate from chlorophyll, light and temperature data. *Ecological Modelling*, 10: 243–264, 1980.

V.H. Smith. Eutrophication of freshwater and coastal marine ecosystems: a global problem. *Environment Science and Pollution Research*, 10:126–139, 2003.

Y.B. Son, Jee-eun Min, and Joo-hyung Ryu. Detecting massive green algae (Ulva prolifera) blooms in the Yellow Sea and East China Sea using Geostationary Ocean Color Imager (GOCI) data. *Ocean Science*, 47:359–375, 2012.

J.H. Steele. Environmental control of photosynthesis in the sea. *Limnology and Oceanography*, 7:137–150, 1962.

J.H. Steele and E.W. Henderson. The role of predation in plankton models. *Plankton Research*, 14(l):157–172, 1992.

G.S. Stelling and T.G.A. van Kester. On the approximation of horizonal gradients in sigma coordinates for bathymetry with steep bottom slopes. *International Journal for numerical methods in fluids*, 18:915–935, 1994.

J.G. Stockner and Naval J. Antia. Algal picoplankton from marine and freshwater ecosystems: A multidisciplinary perspective. *Canadian Journal of Fisheries and Aquatic Sciences*, 43(12):2472–2503, 1986.

E. Struyf, Adriaan Smis, Stefan Van Damme, Patrick Meire, and Daniel J. Conley. The global biogeochemical silicon cycle. *Silicon*, 1(4):207–213, 2010.

Ni Su, Jinzhou Du, Sumei Liu, and Jing Zhang. Nutrient fluxes via radium isotopes from the coast to offshore and from the seafloor to upper waters after the 2009 spring bloom in the Yellow Sea. *Deep Sea Research Part II: Topical Studies in Oceanography*, 97:33–42, 2013.

H.U. Sverdrup. On conditions for the vernal blooming of phytoplankton. 1953.

DanLing Tang, Dana R. Kester, I-Hsun Ni, YuZao Qi, and Hiroshi Kawamura. In situ and satellite observations of a harmful algal bloom and water condition at the Pearl River estuary in late autumn 1998. *Harmful Algae*, 2(2):89–99, 2003.

DanLing Tang, BaoPing Di, Guifeng Wei, I-Hsun Ni, Im Sang Oh, and SuFen Wang. Spatial, seasonal and species variations of harmful algal blooms in the South Yellow Sea and East China Sea. *Hydrobiologia*, 568(1):245–253, 2006a.

DanLing Tang, Hiroshi Kawamura, Im Sang Oh, and Joe Baker. Satellite evidence of harmful algal blooms and related oceanographic features in the Bohai Sea during autumn 1998. *Advances in Space Research*, 37(4):681–689, 2006b.

J.R. Taylor and Raffaele Ferrari. Shutdown of turbulent convection as a new criterion for the onset of spring phytoplankton blooms. *Limnology and Oceanography*, 2011.

R. Thomann and J.A. Mueller. Principles of surface water quality modeling and control, 1987.

T. Tian, H. Wei, J . Su, and C. Chung. Simulations of Annual Cycle of Phytoplankton Produc- tion and the Utilization of Nitrogen in the Yellow Sea. *Oceanography*, 61, 2005.

J.E. Truscott. Environmental forcing of simple plankton models. *Plankton Research*, 17 (12):2207–2232, 1995.

Y.K. Tung, B.C. Yen, and C.S. Melching. *Hydrosystems engineering uncertainty analysis*. Mcgraw-Hill professional engineering, New York :, 2005.

J.E.E. Van Beusekom, Christian Buschbaum, and Karsten Reise. Wadden Sea tidal basins and the mediating role of the North Sea in ecological processes: scaling up of management? *Ocean & Coastal Management*, 68:69–78, 2012.

F. Van Dolah. Marine algal toxins. *Environmental Health Perspectives*, 108(133-141), 2000.

P.H.A.J.M. Van Gelder. *Statistical methods for the risk-based design of civil structures*. PhD thesis, Delft University of Technology, 2000.

M. Villars, I. de Vries, M. Bokhorst, J. Ferreira, S. Gellers-Barkman, B. Kelly-Gerreyn, C. Lancelot, A. Menesguen, A. Moll, J. Patsch, G. Radach, M. Skogen, H. Soiland, E. Svendsen, and Vested H.J. ASMO modelling workshop on eutrophication issues. Technical report, 1996.

L. Voros and Judit Padisak. Phytoplankton biomass and chlorophyll-a in some shallow lakes in central Europe. *Hydrobiologia*, 215:111–119, 1991.

J.K. Vrijling, W. van Hengel, and R.J. Houben. Acceptable risk as a basis for design. *Reliability Engineering & System Safety*, 59(1):141–150, 1998.

Hao Wei, Jun Sun, Andreas Moll, and Liang Zhao. Phytoplankton dynamics in the Bohai Sea—observations and modelling. *Journal of Marine Systems*, 44(3-4):233–251, 2004.

F.J. Weissing and J. Huisman. Growth and competition in light gradient. *Journal of Theoretical Biology*, 168:323–336, 1994.

K. Wild-Allen, A. Lane, and P. Tett. Phytoplankton, sediment and optical observations in netherlands coastal water in spring. *Journal of Sea Research*, 47(3–4):303 – 315, 2002.

L. Woernle, H.A. Dijkstra, and H.J. Van der Woerd. Sensitivity of phytoplankton distributions to vertical mixing along a North Atlantic transect. *Ocean Science*, 10(6): 993–1011, 2014.

K.T.M. Wong, Joseph H.W. Lee, and I.J. Hodgkiss. A simple model for forecast of coastal algal blooms. *Estuarine, Coastal and Shelf Science*, 74(1-2):175–196, 2007.

J. Xuan, Feng Zhou, Da-Ji Huang, Hao Wei, Cheng-Gang Liu, and Chuan-Xi Xing. Physical processes and their role on the spatial and temporal variability of the spring phytoplankton bloom in the central Yellow Sea. *Acta Ecologica Sinica*, 31(1):61–70, 2011.

Glossary

Coastal ecosystems

Coastal ecosystems are regions of remarkable biological productivity and high accessibility, involving the interactions between all elements of flora and fauna and the physical environment, storing and cycling nutrients, filtering pollutants from inland freshwater systems, and helping to protect shorelines from erosion and storms.

Coastal eutrophication

Coastal eutrophication is formed by excess nutrients in the water column. It can cause serious problems in the coastal zone through disturbance of ecological balances and fisheries, and through interference with recreational activities and quality of life. Eutrophication is the result of an anthropogenically induced alteration of the global nitrogen cycle, and just like climate change, should be regarded as a "global change". Eutrophication is usually treated scientifically and in terms of management as a local and regional phenomenon.

Phytoplankton

Phytoplankton are microscopic floating photosynthetic organisms in aquatic environments, both freshwater and seawater. In seawater, the most common types of phytoplankton are diatoms and dinoflagellates. In the oceans, they are responsible for most of the primary production (photosynthesis). Since they need sunlight in order to photosynthesize, they are found only in the upper, sunlit layers of the water. When excessive nutrients are present, there may be excessive blooms of phytoplankton, which when they die and sink to the bottom, may use up much of the oxygen in the deeper water and create a hypoxic layer.

Euphotic depth

Euphotic zone depth reflects the depth where only 1% of the surface photosynthetic available radiation remains. It is a measure of water clarity, which is not only a quality index of an ecosystem but also an important property for primary production (Behrenfeld and Falkowski [1997]; Sathyendranath and Platt [1989]) and heat transfer (Chang [2004]; Kara et al. [2005]) in the upper layer water.

Mixed layer depth

The mixed-layer is the layer between the ocean surface and a depth usually ranging between 25 and 200m, where the density is about the same as at the surface. The mixed-layer owes its existence to the mixing initiated by waves and turbulence caused by the wind stress on the sea surface. The penetration of mixing to a certain depth (the mixed-layer depth) mostly depends on the stability of the sea water and on the incoming energy from the wind. The more stable is the surface water, the less mixing occurs, and the shallower is the mixed-layer. Many important processes occur within the mixed-layer, whether physical (e.g. direct wind-forcing of the ocean circulation), chemical (e.g. dissolution of incoming CO_2 from the atmosphere), or biological (e.g. phytoplankton production).

Acknowledgements

I would like to express my sincere gratitude to the people who made this doctoral dissertation possible.

First and foremost, I would like to thank my promotors: Professor Han Vrijling and Professor Pieter van Gelder. Many thanks are addressed to them. It is my great honour to be one of their PhD students. Prof. Vrijling, thank you for your inspiring advice and excellent guidance. My PhD study has become so much more enjoyable and inspiring by your sparkling ideas and valuable suggestions. Thanks for your time and patience in reading almost all the materials needed in our meetings. You cannot imagine how happy I was when I heard your compliment about my work and my English writing. I have not only learnt from your experience in the scientific research, but also from your attitude and wise conclusions in life. Prof. Van Gelder, you are always encouraging. I have been extremely lucky to be supervised by you who cares so much about my work. Thank you very much for putting faith in my topic and always standing by me. Thanks for everything you have done for me. I have benefitted greatly from your patient supervision and continuous encouragement.

Special thanks are addressed to Professor Changkuan Zhang. You are a very kind man and have contributed much to my study. You have always helped me when I was in a trouble. Thanks for the constructive advice in improving my research.

Many thanks are also addressed to Associate Professor Yiqing Guan and Professor Danrong Zhang. Thanks for your valuable suggestions regarding the study and my future career.

I would like to thank Professor Bas Jonkman and Professor Marcel Stive for their efforts in making the Chinese students feel at home, celebrating the Chinese New Year with us.

Thanks are extended to Ms. Mariette van Tilburg who offered me great help in correcting the writing and in translating the propositions and the summary of the dissertation. It has been a very good experience to co-organize the PhD peer group with you. Assistance provided by our secretaries, Ms. Judith Schooneveld, Ms. Agnes Groenestein, and Ms. Inge van Rooij, is greatly appreciated. Thanks for arranging everything during my PhD.

I would like to thank Cees Timmers and Franca Post in CICAT for arranging a convenient and comfortable life for me in the Netherlands.

I would like to thank my officemates: Mehdi, Wenhao, Flora, Nils, and Defne. It has been a good time to share the office with you.

The China Scholarship Council (CSC) is acknowledged for the financial support for this study.

My committee members are gratefully acknowledged for their constructive comments, which have been really important and helpful in improving the thesis.

Thanks also go to the people I met in the Netherlands, colleagues and friends, who have made my life colourful and interesting. I would like to keep you all in my memory.

Last but not the least, I would like to express my deep gratitude to my family. Thanks for always believing in me and encouraging me to do my best.

Lixia Niu

October 2015 in Delft

Curriculum Vitae

Personal Information

Name	Lixia Niu
Telephone	+31(0)684601091
E-mail	l.niu@tudelft.nl; xiaoxia3623@gmail.com
Date of Birth	15-10-1985
Nationality	Chinese

Education

2011.9-2015.11	University	Delft University of Technology
	Department	Hydraulic Engineering
	Section	Hydraulic Structures and Flood Risk
	Topic	Uncertainty Analysis of Phytoplankton Dynamics in Coastal Waters
	Degree	PhD
2008.9-2011.6	University	Hohai University
	Department	Hydrology and Water Resources
	Section	Ecological Water Environment
	Topic	Flow and Water Quality Simulation of Shallow Lakes
	Degree	MSc
2004.9-2008.6	University	North China University of Water Resources and Electric Power
	Department	Water Resources
	Section	Engineering Management
	Degree	Bachelor

Conference Papers

Yiqing Guan, Lixia Niu*, Danrong Zhang, Xiaoshuai Lv, and Li Wei, 2011. Flow and water quality simulation of Tongxiang Reservoir. The 4^{th} International Conference on Bioinformatics and Biomedical Engineering, 2048-2052.

Zhaoyue Tai, Yiqing Guan, Lixia Niu, Danrong Zhang, Mingjuan Zu, 2011. The effects of eco-environmental water demand on the power generation benefit of qinshan hydropower station. Proceedings of the 2011 IEEE International Conference on waste recycling, Ecology and Environment, 613-617.

Niu L *, and van Gelder P.H.A.J.M., 2013. Probabilistic analysis of sand transport behaviour at the Frisian Inlet (NL) under storm events. Proceedings of the 35^{th} IAHR world congress, 1-10.

Niu, L.*, Van Gelder, P.H.A.J.M., Zhang, C., Guan, Y. and Vrijling, J.K., 2015. Statistical analysis of phytoplankton biomass in the coastal waters of Lauwersoog (NL). Proceedings of the 36^{th} IAHR World Congress, 1-6.

Journal Publications

Niu L.*, Yiqing Guan, Handong Ge, Danrong Zhang, Dongmei Xia, 2011. Effect of eco-environmental water demand on electricity benefit of Qinshan Hydropower Station. Water Resources Protection, 27, 29-33.

Niu, L.*, Van Gelder, P.H.A.J.M., Guan, Y., Zhang, C. and Vrijling, J.K., 2015. Probabilistic analysis of phytoplankton biomass at the Frisian Inlet (NL). Estuarine, Coastal and Shelf Science, 155, 29-37.

Niu, L.*, Van Gelder, P.H.A.J.M., Guan, Y. and Vrijling, J.K., 2015. Uncertainty analysis and modelling of phytoplankton dynamics in coastal waters. Environment Protection and Sustainable Development, 1(4), 193-202.

Niu, L.*, Van Gelder, P.H.A.J.M., Zhang, C., Guan, Y. and Vrijling, J.K., 2015. Statistical analysis of phytoplankton biomass in coastal waters: case study of the Wadden Sea near Lauwersoog (the Netherlands) from 2000 through 2009. Ecological Informatics, 30, 12-19.

Niu, L.*, Van Gelder, P.H.A.J.M., Zhang, C., Guan, Y. and Vrijling, J.K., 2015. Physical control of phytoplankton bloom development in the coastal waters of Jiangsu (China). Ecological Modelling (Accepted). DOI: 10.1016/j.ecolmodel.2015.10.008.

Niu, L.*, Van Gelder, P.H.A.J.M., and Vrijling, J.K., 2015. Physical limitation of phytoplankton dynamics in coastal waters. Journal of Coastal Research (Accepted).